平成２４年度研究成果発表リスト

1. 論文発表

■先端表面敏感計測技術の開発と先進材料応用

国際誌

[1] A. Pratt, L. Dunne, X. Sun, M. Kurahashi and Y. Yamauchi, "Energy-level alignment at the Alq3/Fe3O4(001) interface", Appl. Phys. Vol. 111 Page 07C114 (2012).

[2] Mitsunori Kurahashi and Yasushi Yamauchi, "Huge steric effects in surface oxidation of Si(100)", Huge steric effects in surface oxidation of Si(100)", PHYSICAL REVIEW B Vol. 85 Page 161302(R) (2012).

[3] A. Pratt, M. Kurahashi, X. Sun, D. Gilks and Y. Yamauchi, "Direct observation of a positive spin polarization at the (111) surface of magnetite", PHYSICAL REVIEW B 85, 180409(R) (2012).

[4] K. Yoshino, Y. Morita, Nagatomi, Terauchi Masaharu, Tsujita Takuji, Doi Yoshihiro, Nakayama Takahito, Y. Yamauchi, M. Nishitani, Kitagawa Masaatoshi, Y. Yamauchi, Takai Yoshizo, "Changes in Ionization Potentials of MgO and CaO Films upon Heating in Air and Vacuum Investigated by Metastable De-excitation Spectroscopy", Appl. Surf. Sci. 259 Page 135 (2012).

[5] X. Sun, B. Wang and Y. Yamauchi, "Spin Splitting in a Nickel Phthalocyanine Molecule on an Fe(100) Surface by First-principles Calculations", J. Phys. Chem. C 116 Page 10976 (2012).

[6] X. Sun, B. Wang and Y. Yamauchi, "Electronic Structure and Spin Polarization of Metal (Mn Fe Cu) Phthalocyanines on an Fe(100) Surface by First-Principles Calculations", J. Phys. Chem. C 116 Page 18752 (2012).

[7] Yasuhiro YAMAUCHI, Yusuke FUKUI, Yosuke HONDA, Michiko OKAFUJI, Masahiro SAKAI, Mikihiko NISHITANI and Yasushi YAMAUCHI, "Effect of Impurity in Discharge Gas on High γ Properties of Newly Developed CeSrO Film for Novel Plasma Display Pannel", IEICE Trans. Electron. E95-C[11] Page 1761 (2012).

[8] Mitsunori Kurahashi and Yasushi Yamauchi, "Huge steric effects in surface oxidation of Si(100)", PHYSICAL REVIEW B 85, 161302(R) (2012)

[9] M. Kurahashi, X. Sun, Y. Yamauchi, "Magnetic properties of O2 adsorbed on Cu(100): A spin-polarized metastable He beam study", Phys. Rev. B 86[24] Page 245421 (2012).

[10] H. Kuwahara, Y. Yamauchi and P. Andrew, "Spin Behavior in a Quarter Rotation of the Magnetic Field", J. Korean Phys. Soc. 62[9] Page 1286 (2013).

[11] M. Kurahashi and Y. Yamauchi, "Steric effect in O2 sticking on Al(111): preference for parallel geometry", Phys. Rev. Lett. 110 Page 246102 (2013).

[12] Shiro Entani, Mitsunori Kurahashi, Xia Sun and Yasushi Yamauchi, "Spin polarization of single-layer graphene epitaxially grown on Ni(111) thin film", CARBON 61 Page 134 (2013).

[13] M. Ishii, I. Crowe, M. Halsall, A. Knights, R. Gwilliam, and B. Hamilton, "Investigation of the thermal charge ‘trapping-detrapping’ in silicon nanocrystals: Correlation of the optical properties with complex impedance spectra", Applied Physics Letters, Vol. 101, 242108 (2012).

[14] M. Ishii, B. Towlson, N. Poolton, S. Harako, X. Zhao, S. Komuro, and B. Hamilton, "Effects of oxidization and deoxidization on charge-propagation dynamics in rare-earth-doped titanium dioxide with room-temperature luminescence", Journal of Applied Physics, Vol. 111, 053514, (2012).

[15] N. Ishida, D. Fujita, "Superhydrophilic TiO_2 surfaces generated by reactive oxygen treatment", Journal of Vacuum Science and Technology A: Vacuum, Surfaces and Films, Volume 30, Issue 5, September 2012, Article number051402 (2012)

[16] N. Ishida, K. Sueoka, "Spin-polarized tunneling between optically pumped GaAs(110) surface and spin-polarized tip (Conference Paper) ", Japanese Journal of Applied Physics, Volume 50, Issue 8 PART 4, August 2011 (2011)

[17] Gao, J.-H., N. Ishida, Scott, I., D. Fujita, "Controllable growth of single-layer graphene on a Pd(1 1 1) substrate", Carbon , Volume 50, Issue 4, April 2012, Pages 1674-1680 (2012)

[18] Gao, J.-H., N. Ishida, Isaacson, S., D. Fujita, "Erratum: Controllable growth of single-layer graphene on a Pd(111) substrate (Carbon (2010) 50:4 (1674-1680)) (Erratum) ", Carbon , Volume 50, Issue 6, May 2012, Page 2375 (2012)

[19] N. Ishida, D. Fujita, "Adsorption of co-phthalocyanine on the rutile TiO 2(110) surface: A scanning tunneling microscopy/spectroscopy study", Journal of Physical Chemistry C, Volume 116, Issue 38, 27 September 2012, Pages 20300-20305 (2012)

[20] N. Ishida, D. Fujita, "Chemical-state imaging of Li using scanning Auger electron microscopy", Journal of Electron Spectroscopy and Related Phenomena, Volume 186, Issue 1, February 2013, Pages 39-43 (2013)

[21] Sahu, S., Oono, H., Ghosh, S., Bandyopadhyay, A., Fujita, D., Peper, F., Isokawa, T., Pati, R., "On Cellular Automata rules of molecular arrays (Conference Paper) ", Natural Computing, Volume 11, Issue 2, June 2012, Pages 311-321 (2012)

[22] Sahu, S., Ghosh, S., Hirata, K., Fujita, D., Bandyopadhyay, A., "Multi-level memory-switching properties of a single brain microtubule", Applied Physics Letters, Volume 102, Issue 12, 25 March 2013, Article number123701 (2013)

■先端表層領域計測技術の開発と先進材料応用

国際誌

[23] ISHIOKA Kunie, Petek H, "Raman generation of coherent phonons of anatase and rutile TiO2 photoexcited at fundamental absorption edges", PHYSICAL REVIEW B, 86 巻 (2012)

[24] Hua Jin, Shinotsuka Hiroshi, YOSHIKAWA Hideki, IWAI Hideo, ARAI Masao, TANUMA Shigeo, Sven Tougaard, "Evaluation of robustness to surface conditions of the target factor analysis method for determining the dielectric function from REELS : Application to GaAs", SURFACE AND INTERFACE ANALYSIS, 45 巻 6 号 (2012)

[25] VOROKHTAMykhailo, Ivan Khalakhan, Iwa Matolinova, KOBATA Masaaki, YOSHIKAWA Hideki, KOBAYASHI Keisuke, Vladimir Matolin, "Nanostructured Pt-CeO2 thin film catalyst grown on graphite foil by magnetron sputtering", APPLIED SURFACE SCIENCE, 267 巻 2013 号 (2012)

[26] Nagatoshi Nishiwaki, Tomoya Konishi, Shotaro Hirao, Yoshiyuki Yamashita, Hideki Yoshikawa and Masahiko Shimoda, "Hydroxylated surface of GaAs as a scaffold for a heterogeneous Pd catalyst", Chem. Chem. Phys. 14, 1424–1430 (2012).

[27] Jesse Williams, Hideki Yoshikawa, Shigenori Ueda, Yoshiyuki Yamashita, Keisuke Kobayashi, Yutaka Adachi, Hajime Haneda, Takeshi Ohgaki, Hiroki Miyazaki, Takamasa Ishigaki, and Naoki Ohashi, "Polarity-dependent photoemission spectra of wurtzite-type zinc oxide", Appl Phys. Lett. 100, 51902-1-3 (2012).

[28] I. Matolinova, R. Fiala, I. Khalakhan, M. Vorokhta, Z. Sofer, H. Yoshikawa, K. Kobayashi, V. Matolina, "Synchrotron radiation photoelectron spectroscopy study of metal-oxide thin film: catalysts: Pt-CeO_2 coated CNTs" Appl. Surf. Sci. 258, 2161-2164 (2012)

[29] T. C. Lovejoy, Renyu Chen, X. Zheng, E. G. Villora, K. Shimamura, H. Yoshikawa, Y. Yamashita, S. Ueda, K. Kobayashi, S. T. Dunham F. S. Ohuchi, and M. A. Olmstead, "Band bending and surface defects in b-Ga2O3", Appl Phys. Lett.100, 181602-1-4 (2012).

[30] M. Shimoda, T. Konishi, N. Nishiwaki, Y. Yamashita, and H. Yoshikawa, "Sulfur-mediated palladium catalyst immobilized on a GaAs surface" J. Appl. Phys. 111, 124908-1-6 (2012).

[31] Govindachetty Saravanan, Toru Hara, Hideki Yoshikawa, Yoshiyuki Yamashita, Shigenori Ueda, Keisuke Kobayashic and Hideki Abe, "Post-synthesis dispersion of metal nanoparticles by poly(amidoamine) dendrimers: size-selective inclusion, water solubilization, and improved catalytic performance", Chem. Commun. 48, 7441-7443 (2012).

[32] Hajime Wagata, Naoki Ohashi, Ken-ichi Katsumata, Hiroyo Segawa, Yoshiki Wada, Hideki Yoshikawa, Shigenori Ueda, Kiyoshi Okada and Nobuhiro Matsushita, "An aqueous solution process and subsequent UV treatment for highly transparent conductive ZnO films", J. Mater. Chem. 22, 20706–20712 (2012).

[33] T. Nagata, S. Oh, Y. Yamashita, H. Yoshikawa, R. Hayakawa, K. Kobayashi, T. Chikyow, and Y. Wakayama, "Hard x-ray photoelectron spectroscopy study on band alignment at poly(3,4-ethylen edioxythiophene):poly(styrenesulfonate)/ZnO interface", Appl. Phys. Lett. 101, 173303-1-4 (2012).

[34] Keisuke Fugane, Toshiyuki Mori, Ding Rong Ou, Pengfei Yan, Fei Ye, Hideki Yoshikawa, and John Drennan, "Improvement of Cathode Performance on Pt-CeOx by Optimization of Electrochemical Pretreatment Condition for PEFC Application", Langmuir 28, 16692 − 16700 (2012).

[35] Naoki Ohashi, Hideki Yoshikawa, Yoshiyuki Yamashita, Shigenori Ueda, Jianyong Li, Hideyo Okushi, Keisuke Kobayashi and Hajime Haneda, "Determination of Schottky barrier profile at Pt/SrTiO3:Nb junction by x-ray photoemission", Appl. Phys. Lett. 101, 251911-1-5 (2012).

国内誌

[36] 田沼繁夫 , 福島整 , 竹口雅樹 , 坂田修身 , 熊倉浩明 , 花方信孝 , 箕輪貴司 , " 物質・材料研究機構中核機能部門における計測・分析・解析技術 ", 工業材料 , 60 巻 8 号 (2012)

[37] 吉川英樹 ,"SASJ ソフトウェア勉強会の報告 ", J. Surf. Anal. 18, 190-193 (2012).

[38] 吉川英樹 ," パネルディスカッション「企業の分析部門における人材育成と SASJ への期待」 の記録 ", J. Surf. Anal. 19, 24-35 (2012).

■超先端電子顕微鏡技術の開発と先進材料応用

国際誌

[39] K. Kimoto, K. Kurashima, T. Nagai, M. Ohwada, K. Ishizuka, "Assessment of lower-voltage TEM performance using 3D Fourier transform of through-focus series", Ultramicroscopy, 121, 31-37 (2012).

[40] M. Haruta, K. Kurashima, T. Nagai, H. Komatsu, Y. Shimakawa, H. Kurata, K. Kimoto, "Visualization of hybridization states with atomic resolution using electron energy loss spectroscopy mapping", Applied Physics Letters, 100, 163107 (2012).

[41] X. Yu, N. Kanazawa, W. Zhang, T. Nagai, T. Hara, K. Kimoto, Y. Matsui, Y. Onose, Y. Tokura, "Skyrmion flow near room temperature in an ultralow current density", Nature Communications, 3, 988 (2012).

[42] N. R. Lugg, M. Haruta, M. J. Neish, S. D. Findlay, T. Mizoguchi, K. Kimoto, and L. J. Allen, "Removing the effects of elastic and thermal scattering from electron energy-loss spectroscopic data", Appl. Phys. Lett. 101, 183112 (2012).

[43] Yeong-Gi So, Masahiro Nagao, Takuro Nagai, Koji Kimoto, "HAADF-STEM study of chemical ordering in Al–Pd–Sc 1/1-crystal approximant", Journal of Alloys and Compounds Volume 543, 5 7–11 (2012).

[44] Y. G. So and K. Kimoto, "Effect of specimen misalignment on local structure analysis using annular dark-field imaging", Journal of Electron Microscopy, 61, 207-215 (2012).

[45] T. Asaka, M. Nagao, T. Yokosawa, K. Kokui, E. Takayama-Muromachi, K. Kimoto, K. Fukuda, and Y. Matsui, "Magnetocrystalline anisotropy behavior in the multiferroic $BiMnO_3$ examined by Lorentz transmission electron microscopy", Appl. Phys. Lett. 101, 052407 (2012).

[46] 西田稔 , 奥西栄治 , 西浦智博 , 河野英人 , 稲邑朋也 , 井誠一郎 , 原徹 , " Self-accommodation of B19’ martensite in Ti-Ni shape memory alloys. Part II: Characteristic interface structures between habit plane variants", PHILOSOPHICAL MAGAZINE, 92, 2234 (2012).

[47] SARAVANAN Govindachetty, 原徹 , 吉川英樹 , 山下良之 , 上田茂典 , 小林啓介 , 阿部英樹 , " Post-synthesis Dispersion of Metal Nanoparticles by Poly (amidoamine) Dendrimers: Size-selective Inclusion, Water Solubilization", CHEMICAL COMMUNICATIONS, 48, 7441 (2012).

[48] 関戸薫子 , 大村孝仁 , 原徹 , 津崎兼彰 , " Effect of dislocation density on the initiation of plastic deformation on Fe-C steels", MATERIALS TRANSACTIONS, 53, 907 (2012).

[49] 大村孝仁 , Kaoru Sekido, 原徹 , 中島清美 , 津崎兼彰 , "Dislocation character transition and related mechanical response in a body centered cubic single crystal", SCRIPTA MATERIALIA, 67, 388 (2012).

[50] 御手洗容子 , 原徹 , Maje J. Phasha, Phuti E. Ngoepe, Hilda K. Chikwanda, "Phase transformation and crystal structure of IrTi", INTERMETALLICS, 31, 26 (2012).

[51] FADILN Akmal, SARAVANAN Govindachetty, 吉川英樹 , 山下良之 , 上田茂典 , 小林啓介 , 田邉豊和 , 原徹 , G. Ramesh, 村上秀之 , N. Kazuhiko, 阿部英樹 , "Wet Chemical Synthesis of Ni-Al Nanoparticles at Ambient Condition", ADVANCED MATERIALS RESEARCH, 557-559, 442 (2012).

[52] 酒井和広 , 満田和久 , 山崎典子 , 竹井洋 , R. Yamamoto, 原徹 , 前畑京介 , 伊豫本直子 , 田中啓一 , "TEM-EDS with breakthroughs in 3D wiring and high-speed processing", JOURNAL OF LOW TEMPERATURE PHYSICS, 167, 759 (2012).

[53] 前畑京介 , 伊豫本直子 , 安宗 , 前田 , S. Matsumura, 原徹 , 満田和久 , 山崎典子 , 田中啓一 , "Development of a TES microcalorimeter with a mushroom shaped absorber deposited on an insulating layer in an overhang region", JOURNAL OF LOW TEMPERATURE PHYSICS, 167, 226 (2012).

[54] 御手洗容子 , 原徹 , 三浦誠司 , 細田秀樹 , "Phase transformation and Shape memory effect of Ti(Pt, Ir)", METALLURGICAL AND MATERIALS TRANSACTIONS A-PHYSICAL METALLURGY AND MATERIALS SCIENCE, 43A, 2901 (2012).

[55] 土谷浩一 , 原徹 , 江村聡 , MINXiaohua, 井誠一郎 , 津崎兼彰 , X.Man, K.Tanaka, A.Uemoto, "3D observation of isothermal omega phase in beta-Ti alloy by novel orthogonal FIB/SEM system" Proceedings of the 12th World Conference on Titanium, Conference place, 1, 593 (2012).

[56] T. Nagai, M. Nagao, K. Kurashima, T. Asaka, W. Zhang, K. Kimoto, "Formation of nanoscale magnetic bubbles in ferromagnetic insulating manganite $La_{7/8}Sr_{1/8}MnO_3$", Applied Physics Letters, 101, 162401 (2012).

[57] D. Paramanik, T. Suzuki, N. Ikeda, T. Nagai, C. Van Haesendonck, "Fabrication of self-masked InP nanopillars by electron cyclotron resonance ion etching", Physica E, 44, 1644-1648 (2012).

[58] J. Kikkawa, Y. Nakamura, N. Fujinoki, and M. Ichikawa, "Investigating the origin of intense photoluminescence in Si capping layer on $Ge_{1-x}Sn_x$ nanodots by transmission electron microscopy", J. Appl. Phys. 113, 074302 (2013).

[59] X. Zhang, M. Takeguchi, A. Hashimoto, K. Mitsuishi, P. Wang, P.D. Nellist, A.I. Kirkland, M. Tezuka, M. Shimojo, "Three-dimensional observation of SiO_2 hollow spheres with a double-shell structure using aberration-corrected scanning confocal", Journal of Electron Microscopy, 61, 159-169 (2012).

[60] X. Zhang, M. Takeguchi, A. Hashimoto, K. Mitsuishi, M. Tezuka, M. Shimojo," Improvement of depth resolution of ADF-SCEM by deconvolution: Effect of electron energy loss and chromatic aberration on depth resolution", MICROSCOPY AND MICROANALYSIS, 18, 603-611 (2012).

[61] A. Hashimoto, "In situ observation of Pt nanoparticles on graphene layers under high temperature using aberration-corrected transmission electron microscopy", Journal of Electron Microscopy, 61, 409-413 (2012).

[62] P. Wang, A. Hashimoto, M. Takeguchi, K. Mitsuishi, M. Shimojo, Y, Zhu, M. Okuda, A.I. Kirkland, P.D. Nellist, "Three-dimensional elemental mapping of hollow Fe_2O_3@SiO_2 mesoporous spheres using scanning confocal electron microscopy", Applied Physics Letters, 100, 213117 (2012).

[63] K. Mitsuishi, T. Onishi, Y. Tanaka, I. Sakata, K. Watanabe, N. Ishida, M. Takeguchi, D. Fujita, K. Takada, "Nazca Lines by La ordering in $La_{2/3-x}Li_{3x}TiO_3$ ion-conductive perovskite", Applied Physics Letters, 101, 073903 (2012).

[64] A. Hashimoto, P. Wang, M. Shimojo, K. Mitsuishi, P.D. Nellist, A.I. Kirkland, M. Takeguchi, "Three-dimensional analysis of nanoparticles on carbon support using aberration-corrected scanning confocal electron microscopy", Applied Physics Letters, 101, 253108 (2012).

[65] S. J. Ye, M. Song, A. Matsumoto, A, K. Togano, Y. Zhang, H. Kumakura, M. Takeguchi, R. Teranishi, and T. Kiyoshi, "Enhancing the critical current properties of internal Mg diffusion-processed MgB2 wires by Mg addition", Superconductor Science & Technology, 25, 125014 (2012).

[66] T. Mieno, S. Hasegawa, K. Mitsuishi, "Production of Various Carbon Nanoclusters by Impact Reaction Using Light-Gas Gun as Simulation of Asteroid Collisions in Space", JAPANESE JOURNAL OF APPLIED PHYSICS, 50, 125102 (2012).

[67] I. Sychugov, J. Valenta, K. Mitsuishi, J. Linnros, "Exciton localization in doped Si nanocrystals from single dot spectroscopystudies", Physical Review B, 86, 075311 (2012).

[68] K. Takazawa, J. Inoue, K. Mitsuishi, T. Kuroda, "Ultracompact Asymmetric MachZehnder Interferometers with High Visibility Constructed from Exciton Waveguides of Organic Dye Nanofibers", ADVANCED FUNCTIONAL MATERIALS, 23, 839-845 (2012).

[69] B. Shinozaki, S. Takada, N. Kokubo, K. Makise, K. Mitsuishi, K. Yamada, K. Yano, H. Nakamura, "Superconducting characteristics and microstructure of polycrystalline Zn-doped", PHYSICA C-SUPERCONDUCTIVITY AND ITS APPLICATIONS, 471, 717-720 (2012).

[70] T. Kurosu, K. Khoo, Y. Nakamura, K. Ozaki, N. Ishikawa, J. Onuki, "Reliability Enhancement of Thick AlCu Wire Bounds in IGBT Modules Using Al_2Cu Precipitates", MATERIALS TRANSACTIONS, 53, 453-456 (2012).

[71] J. Xing, M. Takeguchi, M. Tanaka, and Y. Nakayama, "Redox of NiO thin film on YSZ (111) substrate", Surface and Interface analysis, 44 , 1483-1487 (2012).

[72] E. Fujimoto, M. Sumiya, T. Ohnishi, M. Lippmaa, M. Takeguchi, Hideomi, and Y. Matsumoto, "Development of a new laser heating system for thin film growth by chemical vapor deposition", REVIEW OF SCIENTIFIC INSTRUMENTS, 83, 094701 (2012).

[73] YF. Liu, L-L. Xia, Y-N. Lu, Shen-hua Dai, Masaki Takeguchi, Hui-min Hong, and Zhi-gang Pan, "Surfactant-free microwave-assisted hydrothermal synthesis of $BaMoO_4$ hierarchical self-assemblies and enhanced photoluminescence properties", Journal of Colloid and interface Science 381, 24-29 (2012).

[74] J. Xing, M. Takeguchi, M. Tanaka and Y. Nakayama, "Reduction of a NiO thin film deposited by PLD on a single crystal YSZ (111) substrate", Journal of Materials Science 47, 5254-5262 (2012).

[75] S. Kang, D. Bae, M. Takeguchi, K. Hong, C. Chang, and M. Takeda, "Microstructural evolutions of a Cu-75-Fe-5-Ni-20 alloy depending on the isothermal annealing temperatures", Metals and Materials International, 18, 521-525 (2012).

[76] T. Moriki, S. Kang, M. Takeguchi, and M. Takeda, "Nano-Scale Precipitates Formed in Cu-Co Based Alloys and Their Magnetic Properties", Journal of Nanoscience and Nanotechnology, 12, 1688-1691 (2012).

[77] R. Kondo, R. Shimizu, N. Nomura, H. Doi, Suyalatu, Y. Tsutsumi, K. Mitsuishi, M. Shimojo, K. Noda, T. Hanawa, "Effect of cold rolling on the magnetic susceptibility of Zr-14Nb alloy", ACTA BIOMATERIALIA, 9, 5795-5801 (2013).

[78] B. Bruhn, J. Valenta, I. Sychugov, K. Mitsuishi, J. Linnros, "Transition from silicon nanowires to isolated quantum dots: Optical and structural evolution", PHYSICAL REVIEW B, 87, 045404 (2013).

[79] K. Makise, B. Shinozaki, T. Asano, K. Mitsuishi, K. Yano, K. Inoue, H. Nakamura, "Relationship between variable range hopping transport and carrier density of amorphous In_2O_3-10 wt.% ZnO thin films", JOURNAL OF APPLIED PHYSICS, 112, 033716 (2012).

[80] H. Amekura, Y. Nakayama, K. Mitsuishi, K. Kono, "Formation of metallic vanadium nanoparticles in SiO2 by ion implantation and of vanadium oxide nanoparticles by additional thermal oxidation", THIN SOLID FILMS, 520, 5528-5533 (2012).

[81] B. Zheng, N. Iketa, Y. Takeda, K. Sato, R. Sato, H. Amekura, K. Oyoshi, K. Kono, M. Edwards, M. Song, D. Ila, N. Kishimoto, "FIB fabrication and irradiation test of stencil masks for heavy-ion patterned implantation for plasmonic application", NUCLEAR INSTRUMENTS & METHODS IN PHYSICS RESEARCH SECTION B-BEAM INTERACTIONS WITH MATERIALS AND ATOMS, 272, 183-187 (2012).

[82] M. Tanaka, "Structural and Morphological Study of Ni Clusters Deposited on $SrTiO_3$ Surfaces Studied by UHV-TEM/STM", e-J. Surf. Sci. Nanotechnol. 10, 459-462 (2012).

[83] M. Tanaka, "Growth behavior and field-induced diffusion of Ni clusters / particles on $SrTiO_3$ (001) observed by UHV-TEM/STM", Appl. Phys. A, DOI:10.1007/s00339-013 -7690-7 (2013).

国内誌

[84] 田沼繁夫 , 福島整 , 竹口雅樹 , 坂田修身 , 熊倉浩明 , 花方信孝 , 箕輪貴司 , " 物質・材料研究機構中核機能部門における計測・分析・解析技術 ", 工業材料 ,60, 18-23 (2012).

解説

[85] 木本浩司 , "STEM による結晶構造観察 ", 顕微鏡 , 47 , 98-103 (2012).

著書

[86] K. Mitsuishi, "Monte Carlo Method in FEBID Process Simulations (chapter8)." Nanofabrication Using Focused Ion and Electron Beams, Page 321-346 (2012).

■強磁場固体ＮＭＲ計測技術の開発と先進材料応用

国際誌

[87] Mutsuo Igarashi, Takehito Nakano, Pham Tan Thi, Yasuo Nozue, GOTO Atsushi, HASHI Kenjiro, OHKI Shinobu, SHIMIZU Tadashi, Andraz Krajnc, Peter Jeglic, Denis Arcon, "NMR study of thermally activated paramagnetism in metallic low-silica X zeolite filled with sodium atoms", PHYSICAL REVIEW B, Vol.87, No.7, 075138-1 ～ 075138-7

[88] Mariko Ando, Itaru Oikawa, OHKI Shinobu, TANSHO Masataka, SHIMIZU Tadashi, Hideki Maekawa, Hajime Kiyono, "Oxygen-17NMR Study of Defects in LnO1.5CeO2 (Ln = La and Nd)", CHEMISTRY LETTERS, Vol.42, No.1, 57 ～ 59

[89] Kazuma Gotoh, Toru Ishikawa, Saori Shimazu, Naoaki Yabuuchi, Shinichi Komaba, Kazuyuki Takeda, GOTO Atsushi, DEGUCHI Kenzo, OHKI Shinobu, HASHI Kenjiro, SHIMIZU Tadashi, Hiroyuki Ishida, "NMR study for electrochemically inserted Na in hard carbon electrode of sodium ion battery," JOURNAL OF POWER SOURCES, Vol.225, 137 ～ 140

[90] Hajime Kiyono, Yuuya Matsuda, Toshihiro Shimada, Mariko Ando, Itaru Oikawa,haideki Maekawa , Susumu Nakayama, OHKI Shinobu, TANSHO Masataka, SHIMIZU Tadashi, Pierre Florian, Dominuqie Massiot, "Oxygen-17 nuclear magnetic resonance measurements on apatite-type lanthanum silicate (La9.33(SiO4)6O2)", SOLID STATE IONICS, Vol.228, No.1, 64 ～ 69

[91] Ryutaro OHASHI, Masayoshi Saito, Takashi Fujita, Toshihito Nakai, Hiroaki Utsumi, DEGUCHI Kenzo, TANSHO Masataka, SHIMIZU Tadashi, "Observation of ^{47,49}TiNMR Spectra of $TiCl_4/MgCl_2$ Catalysts under an Ultrahigh Magnetic Field", CHEMISTRY LETTERS, Vol.141, No.12, 1563 ～ 1565

[92] Keiji Shimoda, Koichi Doi, Tessui Nakagawa, Yu Zhang, Hiroki Miyaoka, Takayuki Ichikawa, TANSHO Masataka, SHIMIZU Tadashi, Anthony K. Burrell, Yoshitsugu Kojima," Comparative Study of Structural Changes in NH3BH3, LiNH2BH3, and KNH2BH3 During Dehydrogenation Process", JOURNAL OF PHYSICAL CHEMISTRY C, Vol.116, No.9, 5957 ～ 5964

[93] Yuichi Hasegawa, Yoshio Inoue, DEGUCHI Kenzo, OHKI Shinobu, TANSHO Masataka, SHIMIZU Tadashi, Koji Yazawa, "Molecular Dynamics of a Polyaniline/ β -Cyclodextrin Complex Investigated by 13C Solid-State NMR", JOURNAL OF PHYSICAL, Vol.116, No.6, 1758 ～ 17604

■強力中性子線計測技術の開発と先進材料応用

国際誌

[94] Genki ANO, Mitsuhiro AKATSU, Koji ARAKI, Kazuo MATSUO, Yoshiaki TACHIKAWA, Keisuke MITSUMOTO, Takashi YAMAGUCHI, Yuichi NEMOTO, Terutaka GOTO, Naoya TAKEDA, Andreas DOENNI, and Hideaki KITAZAWA, "Quadrupole Ordering and Rattling Motion of Clathrate Compound $Pr_3Pd_{20}Ge_6$", J. Phys. Soc. Jpn. 81, 0347101-1-10 (2012).

[95] Hitoshi Yamaoka, Patrik Thunstrom, Ignace Jarrige, Kenya Shimada, Naohito Tsujii, Masashi Arita, Hideaki Iwasawa, Hirokazu Hayashi, Jian Jiang, Takafumi Habuchi, Daisuke Hirayama, Hirofumi Namatame, Masaki Taniguchi, Urara Murao, Shingo Hosoya, Akira Tamaki, and Hideaki Kitazawa, "High-resolution photoelectron spectroscopy study of Kondo metals: $SmSn_3$ and $Sm_{0.9}La_{0.1}Sn_3$", Phys. Rev. B 85, 115120-1-7 (2012).

[96] Seisuke Nigo, Masato Kubota, Yoshitomo Harada, Taisei Hirayama, Seiichi Kato, Hideaki Kitazawa, and Giyuu Kido, "Conduction band caused by oxygen vacancies in aluminum oxide for resistance random access Memory", J. Appl. Phys. 112, 033711-1-6 (2012).

[97] Y. Hu, C. N. Borca, E. Kleymenov, M. Nachtegaal, B. Delley, M. Janousch, A. Doenni, M. Tachibana, H. Kitazawa, E. Takayama-Muromachi, M. Kenzelmann, C. Niedermayer, T. Lippert, A. Wokaun, and C. W. Schneider, "Experimental and ab initio investigations of the x-ray absorption near edge structure of orthorhombic $LuMnO_3$", Appl. Phys. Lett. 100 , 252901-1-4 (2012).

[98] M. Garganourakis, Y. Bodenthin, R. A. de Souza, V. Scagnoli, A. Doenni, M. Tachibana, H. Kitazawa, E. Takayama-Muromachi, and U. Staub, "Magnetic and electronic orderings in orthorhombic $RMnO_3$ (R=Tm, Lu) studied by resonant soft x-ray powder diffraction", Phys. Rev. B 86, 054425-1-5 (2012).

[99] Noriki Terada, Dmitry D. Khalyavin, Pascal Manuel, Yoshihiro Tsujimoto, Kevin Knight, Paolo G. Radaelli, Hiroyuki S. Suzuki, and Hideaki Kitazawa, "Spiral-Spin-Driven Ferroelectricity in a Multiferroic Delafossite $AgFeO_2$", Phys. Rev. lett. 109, 097203-1-4 (2012).

[100] Jana Poltierová Vejpravová, Jan Prokleška, Jirí Pospíšil, Hideaki Kitazawa, Antonio Pereira Gonçalves, Takemi Komatsubara, Clemens Ritter, Olivier Isnard, Vladimír Sechovský, "Magnetic and transport properties of $CePt_3Ge$ Kondo lattice in crystalline and sub-micron state", J. Alloys and Comp. 520, 22-26 (2012).

[101] Hitoshi Yamaoka, Yumiko Zekko, Akio Kotani, Ignace Jarrige, Naohito Tsujii, Jung-Fu Lin, Jun'ichiro Mizuki, Hideki Abe, Hideaki Kitazawa, Nozomu Hiraoka, Hirofumi Ishii, and Ku-Ding Tsuei, "Electronic transitions in $CePd_2Si_2$ studied by resonant x-ray emission spectroscopy at high pressures and low temperatures", Phys. Rev. B 86 (2012) p.235131-1-8 (2012).

[102] M. Hase, V. Yu Pomjakushin, V. Sikolenko, L. Keller. A Dönni and H. Kitazawa, "Negative magnetization of $Li_2Ni_2Mo_3O_{12}$ including two spin subsystems, distorted honeycomb lattice and linear chain", Journal of Physics: Conference Series 400, 032017-1-4 (2012).

[103] H. Ono, T. Nakano, N. Takeda, G. Ano, M. Akatsu, Y Nemoto, T. Goto and H. Kitazawa, "Specific heat of $Ce_3Pd_{20}Si_6$ single crystal in magnetic fields", Journal of Physics: Conference Series 391, 012054-1-4 (2012).

[104] Taro NAKAJIMA, Setsuo MITSUDA, Keiichiro TAKAHASHI, Keisuke YOSHITOMI, Kazuya MASUDA, Chikafumi KANEKO, Yuki HONMA, Satoru KOBAYASHI, Hideaki KITAZAWA, Masashi KOSAKA, Naofumi ASO, Yoshiya UWATOKO, Noriki TERADA, Shuichi WAKIMOTO, Masayasu TAKEDA, and Kazuhisa KAKURAI, "Uniaxial-Pressure Control of Magnetic Phase Transitions in a Frustrated Magnet $CuFe_{1-x}Ga_xO_2$ (x=0, 0.018)", Journal of the Physical Society of Japan 81, 094710-1-8 (2012).

[105] Masashi Hase, Vladimir Yu. Pomjakushin, Andreas Dönni, and Hideaki Kitazawa, "Magnetic Structure of $SrCo_3P_4O_{14}$ Determined from Neutron Powder Diffraction Results", Journal of the Physical Society of Japan 81, 064702-1-4 (2012).

[106] M. Hase, A. Dönni, K. Ozawa, H. Kitazawa, O. Sakai, V. Yu Pomjakushin, L. Keller, K. Kaneko, N. Metoki, K. Kakurai, M. Matsuda, T. Yang, R. Cong, J. Lin, "Neutron scattering studies of the spin-5/2 antiferromagnetic linear trimer substance $SrMn_3P_4O_{14}$", Journal of Physics: Conference Series 340, 0120661-1-7 (2012).

[107] H.Ohtuka, V.A.Dinh, T.Ohno, K.Tsuzaki, H.Suzuki and H.Kitazawa, "Effects of carbon on magnetic properties and transformed structures in Fe-based alloys", Proc. of The 3rd Int. Symp. On Steel Science ISSS2012, p.247 (2012).

[108] T. Hosaka, S. Hachiuma, H. Kuroe, T. Sekine, M. Hase, K. Oka, T. Ito, H. Eisaki, M. Fujisawa, S. Okubo, and H. Ohta, "Magnetic and Electric Properties in the Distorted Tetrahedral Spin Chain System $Cu_3Mo_2O_9$", J. Phys.: Conference Series, 400, 032022 1-4 (2012).

[109] K. Misoka, K. Doi, T. Hamasaki, H. Kuroe, T. Goto, T. Sekine, T. Sasaki, M. Hase, K. Oka, T. Ito, and H. Eisaki, "Cu-NMR study on dimer-chain complex quantum spin system $Cu_3Mo_2O_9$", J. Phys.: Conference Series, 400, 032055 1-4 (2012).

[110] Oba Yojiro, Ohnuma Masato, Ohnuma Shigehiro, Furusaka Michihiro, Koppoju Suresh, Takeda Shin, "Nanostructure characterization of Co-Pd-Si-O soft magnetic nanogranular film using small-angle X-ray and neutron scattering", J. Magn Magn Mater., 334, 45-51(2013)

[111] Iwase Hiroki, Sawada Shin-ichi, Yamaki Tetsuya, Koiszumi Satoshi, Ohnuma Masato, Maekawa Yasunari, "Hierarchical Structure Analysis of Graft-Type Polymer Electrolyte Membranes Consisting of Cross-Linked Polytetrafluoroethylene by Small-Angle Scattering in a Wide-Q Range", Macromolcules, 45, 9121-9127(2012)

[112] Kozikowski Pawel, Ohnuma Masato, Herzer Giselher, Polak Christian, Budinsky Viktoria, Koppoju Suresh, Lewandowska Malgorzata, Kurzydlowski Krzysztof J., "Relaxation studies of amorphous alloys with creep induced magnetic and structural anisotropy", Scripta Mater., 67, 767-766(2012)

[113] Sato Rodrigo, Momida Hiroyoshi, Ohnuma Masato, Sasase Masato, Ohno Takahisa, Kishimoto Naoki, Takeda Yoshihiko, "Experimental dispersion of the third order optical susceptibility of Ag nanoparticles", J. THE OPTICAL SOCIETY OF AMERICA B-OPTICAL PHYSICS, 29, 2410-2413(2012)

[114] Seishi Abe, Ping De Hai, Nakamura Shintaro, Ohnuma Masato, Ohnuma Shigehiro, "Metal-Doped Magnetite Thin Films", J. NANOSCIENCE AND NANOTECHNOLOGY, 12, 5087-5090(2012)

[115] T. Machida, K. Kosuge, T. Kato, H. Nakamura, H. Takeya, T. Mochiku, S. Ooi, Y. Mizoguchi, Y. Takano, K. Hirata, H. Sakata, "Unidirectional electronic structure in the parent state of iron-chalcogenide superconductor $Fe_{1+\delta}Te$", J. Phys. Soc. Jpn. 81 (2012) 074714.

[116] H. Nakamura, T. Machida, T. Kato, M. Fujimoto, H. Funahashi, M. Iguchi, K. Kosuge, T. Yamasaki, S. Ooi, T. Mochiku, S. Nakano, K. Hirata, T. Hasegawa, H. Sakata, "Impurity resonance states in $Bi_2Sr_{1.6}La_{0.4}CuO_{6+\delta}$", J. Supercond. Novel Mag. 25 (2012) 1263.

[117] T. Machida, K. Kosuge, T. Kato, H. Nakamura, H. Takeya, T. Mochiku, S. Ooi, Y. Mizoguchi, Y. Takano, H. Sakata, K. Hirata, "One-dimensional electronic order in $Fe_{1.07}Te$ probed by scanning tunneling spectroscopy", J. Supercond. Novel Mag. 25 (2012) 1273.

[118] K. Hirata, A. Thakur, S. Ooi, T. Mochiku, "Vortices in superconducting nano-networks with anti-dots array", Central Euro. J. Phys. 10 (2012) 576.

[119] K. Ozawa, Y. Nakano, T. Mochiku, Z. X. Cheng, L. Z. Wang, H. Iwai, Y. Tsuchiya, H. Fujii, N. Igawa, "Electrochemical characteristics of layered $Li_{1.95}Mn_{0.9}Co_{0.15}O_3$ (C2/m) as a lithium-battery cathode", J. Electrochem. Soc. 159 (2012) A300.

[120] C. Enachescu, M. Nishino, S. Miyashita, L. Stoleriu, and A. Stancu, "Monte Carlo Metropolis study of cluster evolution in spin-crossover solids within the framework of a mechanoelastic model", Phys. Rev. B. , 86, 054114-(1-7) (2012)

[121] T. Nakada, T. Mori, S. Miyashita, M. Nishino, S. Todo, W. Nicolazzi, and P. A. Rikvold, "Critical temperature and correlation length of an elastic interaction model for spin-crossover materials", Phys. Rev. B. 85, 054408-(1-8) (2012).

[122] H. Mamiya, "Recent advances in understanding magnetic nanoparticles in AC magnetic fields and optimal design for targeted hyperthermia," J. Nanomater., 査読有 vol. 2013, (2013) 752973

[123] H. Mamiya and B. Jeyadevan, " Magnetic hysteresis loop in a superparamagnetic state ", IEEE Transactions on Magnetics 査読有 in press.

[124] H. Mamiya and S. Nimori, "Memory effects in Heisenberg spin glasses: Spontaneous restoration of the original spin configuration rather than preservation in a frozen state", Journal of Applied Physics 査読有 Vol.111 (2012) 07E147-1-3

[125] H. Mamiya and B. Jeyadevan, "Formation of non-equilibrium magnetic nanoparticle structures in a large alternating magnetic field and their influence on magnetic hyperthermia treatment", IEEE Transactions on Magnetics 査読有 Vol. 48 (2012) 3258.

[126] Naohito Tsujii and Hideaki Kitazawa,, "Ferromagnetic ordering with Heavy Fermion behavior in YbPdSi", Solid State Communications 159, 65 (2013).

[127] Hitoshi Yamaoka, Patrik Thunstrom, Naohito Tsujii, I. Jarrige, K. Shimada, M. Arita, H. Iwasawa, H. Hayashi, J. Jiang, H. Namatame, M. Taniguchi, N. Hiraoka, H. Ishii, K.D. Tsuei, M. Giovannini, Ernst Bauer, "Electronic structure and the valence state of Yb2Pd2Sn and

YbPd2Sn studied by photoelectron and resonant x-ray emission spectroscopies", Phys. Rev. B 86, 085137 (2012).

[128] Y. Tanaka, N. Terada, T. Nakajima, T. Kojima, Y. Takata, S. Mitsuda, M. Oura, Y. Senba, H. Ohashi and S. Shin, "Incommensurate Orbital Modulation Behind Ferroelectricity in $CuFeO_2$", Phys. Rev. Lett. 109 127205 (2012)

[129] R. D. Johnson, N. Terada and P. G. Radaelli, "Comment on "Spin-canting-induced improper ferroelectricity and spontaneous magnetization reversal in $SmFeO_3$", Phys. Rev. Lett. 108 219701 (2012)

[130] T. Nakajima, S. Mitsuda, J. T. Haraldsen, R. S. Fishman, T. Hong, N. Terada and Y. Uwatoko, "Magnetic interactions in the multiferroic phase of $CuFe_{1-x}Ga_xO_2$ (x=0.035) refined by inelastic neutron scattering with uniaxial-pressure control of domain structure", Phys. Rev. B 85 144405 (2012)

[131] S. Mitsuda, K. Yoshitomi, T. Nakajima, C. Kaneko, H. Yamazaki, M. Kosaka, N. Aso, Y. Uwatoko, Y. Noda, M. Matsuura, N. Terada, S. Wakimoto, M. Takeda, K. Kakurai, "Uniaxial-stress enhancement of spin-driven ferroelectric polarization in a multiferroic $CuFe_{1-x}Ga_xO_2$", J. Phys. Conference Series 340 012062 (2012)

[132] S. Kimura, K. Watanabe, T. Fujita, M. Hagiwara, H. Yamaguchi, T. Kashiwagi, N. Terada, "Electromagnon Excitation of the Triangular Lattice Antiferromagnet $CuFeO_2$ in High Magnetic Field", J. Low Temp. Phys. 1-5 (2012)

[133] N. Terada, D. D. Khalyavin, P. Manuel, Y. Tsujimoto, K. Knight, P. G. Radaelli, H. S. Suzuki, and H. Kitazawa, "Ferroelectricity and lattice distorition associated with spin orderings in a multiferroic delafossite $AgFeO_2$", EPJ Web of Conferences 40 15008 (2013)

[134] A. Senyshyn, H. Boysen, R. Niewa, J. Banys, M. Kinka, Y. Burak, V. Adamiv, F. Izumi, I. Chumak, and H. Fuess, J. Phys. D: Appl. Phys., 45, 175305 (2012).

[135] J. Han, J. Zhu, Y. Li, X. Yu, S. Wang, G. Wu, H. Xie, S. C. Vogel, F. Izumi, K. Momma, Y. Kawamura, Y. Huang, J. B. Goodenough, and Y. Zhao, "Experimental visualization of lithium conduction pathways in garnet-type $Li_7La_3Zr_2O_{12}$," Chem. Commun., 48, 9840 (2012).

国内誌

[136] 門馬綱一 , 泉 富士夫 , " 次世代三次元可視化プログラム VESTA 3", 日本結晶学会誌 , 54, 119(2012).

[137] 河村幸彦 , 門馬綱一 , 泉 富士夫 , " 粉末回折データの MEM 解析・三次元可視化用ソフトウェアの開発 ", 波紋 , 23, 66 (2013).

解説

[138] 大沼正人 " 小角散乱法によるナノサイズ不均質の評価 " 表面科学 , 33, 278-283(2012)

[139] 間宮広明 " 磁性ナノ粒子の交流磁場応答と選択的がん温熱療法 " マテリアルインテグレーション, Vol. 25, (2012) 11.

著書

[140] C. Enachescu, M. Nishino, S. Miyashita, "Theoretical Descriptions of Spin-Transitions in Bulk Lattice", in "Spin-crossover materials - properties and applications" M.A.Halcrow (ed) John Wiley & Sons, Chichester, UK, 2013, 455-474.

■放射光を利用した先進計測技術の開発と先進材料応用

国際誌

[141] M.Vysinka, M. Mizusawa and K. Sakurai, "Growth and Characteristics of Liesegang Rings in Cu--Cr System: Optical and XRF Study", WDS'11 Proceedings of Contributed Papers: Part III -- Physics (eds. J. Safrankova and J. Pavlu), Charles University, Prague, Matfyzpress, p.147-154 (2011).

[142] Vallerie Ann Samson and Kenji Sakurai, "Non-equilibrium swelling in spin-coated methylcellulose ultra-thin films: effect on surface topography and film structure", Soft Matter, 8, 7351-7356 (2012).

[143] Vallerie Ann Innis-Samson and Kenji Sakurai, "Swelling in spin-coated methylcellulose ultra-thin films: effect on film structure, surface topography, and temperature-response property", Soft Matter, 2012, 8, 7351

国内誌

[144] Vallerie Ann Innis-Samson, Mari Mizusawa and Kenji Sakurai, "X-Ray Reflection Tomography Reconstruction for Surface Imaging: Simulation Versus Experiment", Adv. X-Ray Chem Anal. Jpn, 43, 391-400 (2012) (in English)

2. 口頭発表

■先端表面敏感計測技術の開発と先進材料応用

国際会議（招待）

[145] Oscar Custance,"Characterization of pentacene molecules adsorbed on the TiO2(101) anatase surface by means of bimodal atomic force microscopy and simultaneous scanning tunneling microscopy" International Workshop on Soft Interface Sciences for Young Scientists (SISYS2012), Tsukuba (Japan), (2012/11/21-2012/11/22).

[146] T. Suzuki, Y. Yamauchi and S. Hishita, "Scattering of spin-polarized 4He+ ions at surfaces" 19th International Workshop on Inelastic Ion-Surface Collisions, Frauenchiemsee Germany (2012/09/16-21).

[147] M. Ishii, "Nano-probing of the surface excited by keV photon: What should we detect for high spatial resolution?", The 13th edition of Trends in Nanotechnology International Conference (TNT2012), Madrid, Spain, (September 10-14, 2012)

[148] M. Ishii, "Surface Dielectric Relaxation (SDR) toward electromechanical analyses of polymer brushes", Max-Planck Institute seminar", Mainz, Germany,(August, 2012)

[149] FUJITA Daisuke, Mingsheng XU, "Characterization of Functional Nanomaterials for Nanorisk Assessment and Social Acceptance", IUMRS-ICEM 2012, パシフィコ横浜 , 横浜市 , 2012/09/23-2012/09/28

[150] FUJITA Daisuke, ISHIDA Nobuyuki, "Decontamination and Superhydophilicity on TiO2 Surfaces", 13th International Symposium on Biomimetic Materials Processing, ホテルアソシア高山リゾート , 高山 , 2013/01/22-2013/01/25

国内学協会会議（招待・依頼）

[151] 藤田大介 , " 走査型プローブ顕微鏡法の国際標準化とロードマップ ", ナノプローブテクノロジー第 167 委員会第 67 回研究会 , 物質・材料研究機構千現地区 , つくば , 2012/07/17 - 2012/07/18

[152] 藤田大介 , " マテリアルイノベーションのための NIMS 先端微細構造解析プラットフォーム / マテリアルイノベーションのための NIMS 先端微細構造解析プラットフォーム ", 第 1 回微細構造解析プラットフォームワークショップ, 九州大学　伊都キャンパス　伊都ゲストハウス , 福岡 , 2012/10/12

[153] 藤田大介, "TC201: 走査プローブ顕微鏡法（SPM）の国際標準化 ", 表面化学分析国際標準化セミナー「表面分析における国際標準化の現状」, 幕張メッセ　国際会議場, 千葉市, 2012/09/04

[154] 藤田大介, " 最先端計測共用基盤の構築とマテリアルイノベーションの加速 ", 文部科学省ナノテクノロジープラットフォームシンポジウム , 東京大学生産技術研究所総合研究実験棟 An 棟 2F コンベンションホール, 東京 , 2012/10/10

[155] 藤田大介, " 最先端極限計測装置群によるナノテク・材料研究開発の高度支援 ", 文部科学省ナノテクノロジープラットフォームシンポジウム , 東京大学生産技術研究所総合研究実験棟 An 棟 2F コンベンションホール, 東京 , 2012/10/10

[156] 藤田大介, "NIMS の目指す先端計測技術の開発と共用による イノベーションの推進 ", 共用・計測 合同シンポジウム 2013, 物質・材料研究機構千現地区 , つくば , 2013/02/28-2013/03/01

[157] 藤田大介, " 微細構造解析プラットフォームの概要と先端ナノ計測設備群の紹介 ", 日本化学会第 93 春季年会 (2013), 立命館大学 , 草津（滋賀県), 2013/03/22-2013/03/25

国際会議（一般）

[158] GAOJian-Hua, SAGISAKA Keisuke, ISHIDA Nobuyuki, FUJITA Daisuke, "Epitaxial Growth of Single- and Few-layer Graphene on Pt(111) and Pd(111) Surfaces by Surface Segregation", Graphene 2012 International Conference, Brussels44Center,Brussels,Belgium, 2012/04/10 - 2012/04/13

[159] ISHIDA Nobuyuki, FUJITA Daisuke, "Adsorption of Co-phthalocyanine on the rutile TiO2(110) surface: an STM/STS study", International Conference on Nanoscience + Technology (ICN+T2012), The Sorbonne grand amphitheatre,Paris,France, 2012/07/23 - 2012/07/27

[160] GAOJian-Hua, SAGISAKA Keisuke, ISHIDA Nobuyuki, FUJITA Daisuke, "Epitaxial Growth of Single- and Few-layer Graphene on Pt(111) and Pd(111) Surfaces by Surface Segregation", Graphene 2012 International Conference, Brussels44Center,Brussels, 2012/04/10 - 2012/04/13

[161] GUOHongxuan, FUJITA Daisuke, "In-situ surface observation by using stress fields scanning probe microscopy", 20th International Colloquium on Scanning Probe Microscopy, Kariyushi Urban Resort,Okinawa, 2012/12/17 - 2012/12/19

[162] GUOHongxuan, GAOJian-Hua, FUJITA Daisuke, "Characterization of graphene and BN nano sheet by helium ion microscopy", Microscopy & Microanalysis 2012 Meeting, Phoenix Convention Center ,Phoenix,US, 2012/07/27 - 2012/08/02

[163] GUOHongxuan, NAGANO Shoko, ONISHI Keiko, FUJITA Daisuke, "Application of helium ion microscope on processing and Characterization of nano wires", AVS 59th International Symposium and Exhibition, Tempa Conventional Center,Tempa,US, 2012/10/28 - 2012/11/02

国内学協会会議（一般）

[164] 藤田大介, 石田暢之 , GUOHongxuan, "Nanoscale Interface and Surface Characterization for GREEN Research", 第 4 回ナノ材料科学環境拠点シンポジウム , 物質•材料研究機構並木地区, つくば市 , 2012/06/26

[165] 石田暢之 , 藤田大介, " 走査型オージェ電子顕微鏡によるリチウムの検出 ", 第 73 回応用物理学会学術講演会 , 松山大学 , 愛媛大学 , 松山市 , 2012/09/11 - 2012/09/14

■先端表層領域計測技術の開発と先進材料応用

国際会議（招待）

[166] YOSHIKAWA Hideki, "Database of Optical Constants of Semiconductors for Surface Chemical Analysis", IUVSTA Workshop for Surface Analysis and Standardization 2013,Okinawa,Japan(2013/01/15-2013/01/19)

[167] TANUMA Shigeo, "Present Status of Standardization of Quantitative Surface Chemical Analysis by AES and XPS", iSAS13,Okinawa,Japna(2013/01/15-2013/01/19)

[168] FUKUSHIMA Sei, "An introduction of High-resolution characteristic X-ray spectroscopy -double-crystal type spectrometer and its application-", Open seminar of CEA,Paris,France(2013/02/04-2013/02/05)

[169] H. Yoshikawa,"Bulk Sensitive Analysis by Hard X-ray Photoelectron Spectroscopy", Korean symposium on surface analysis (KoSSA), Korea, (Oct. 10-12, 2012).

国内学協会会議（招待・依頼）

[170] 田沼繁夫 , " ナノ計測と標準化 , ナノテクノロジー社会受容特論 ", 大阪大学 , 大阪市 , 日本 (2012/06/30)

[171] 岩井秀夫 , " オージェ電子分光法（AES）", 第 53 回　表面科学基礎講座　表面・界面の基礎と応用 , 東京 , 日本 (2012/07/10-2012/07/12)

[172] 岩井秀夫 , " 高エネルギー分解能 AES　元素分析のためのエネルギー軸目盛の校正 ", 表面分析実用化セミナー , 東京 , 日本 (2012/07/31)

[173] 伊藤嘉昭 , 福島整 , 寺澤倫孝 , " 挿入光源による高分解能 X 線結晶分光器を用いた X 線発光スペクトル ", SPring-8 シンポジウム 2012, 大阪大学コンベンションセンター , 大阪市 , 日本 (2012/08/25-2012/08/26)

[174] 岩井秀夫 , " 超高真空装置の取り扱い , 初心者のための実用表面分析講座 ", JASIS コンファレンス 2012, 幕張メッセ , 千葉 , 日本 (2012/09/04-2012/09/07)

[175] 田沼繁夫 , " モノづくりを支える表面分析技術 : 表面分析の現状とその課題 ", 第 13 回真空シンポジウム , 東京ビックサイト , 東京 , 日本 (2012/10/18)

[176] 田沼繁夫 , " 電子の非弾性散乱データベースの現状と展望 ", 第 32 回表面科学学術講演会 , 東北大学 , 仙台市 , 日本 (2012/11/20-2012/11/22)

[177] 永富隆清 , 田沼繁夫 , " オージェ電子分光法分析における電子線誘起試料損傷の 標準化とデータベース化 ー SiO2 薄膜表面の損傷過程ー ", 第 32 回表面科学学術講演会 , 東北大学 , 仙台市 , 日本 (2012/11/20-2012/11/22)

[178] 吉川英樹 , 田沼繁夫 " 電子分光シミュレーターとそのデータベースの現状と展望 ", 第 32 回表面科学学術講演会 , 東北大学　仙台 , (2012/11/20-22)

[179] 岩井秀夫 , " 飛行時間型二次イオン質量分析装置の紹介と応用例 ", NIMS 微細構造解析プラットフォーム　第1回地域セミナー , 物質・材料研究機構 , つくば市 , 日本 (2012/11/27)

国際会議（一般）

[180] FUKUSHIMA Sei, TANAKA Akihiro, GOTO Keisuke, "A Basic Concept of Standard Noise Database for Spectro-chemical Analysis", The 3rd Asian Materials Data Symposium (AMDS2012), Okinawa,Japan,(2012/04/15-2012/04/19).

[181] FUKUSHIMA Sei, Yoshiaki Ito, Tatsunori Tochio, Tatsuo Fujii, Michitaka, Kenji Yoshii, Yasuhiro Yoneda, "Quantitative Determination of the Oxidation state of Fe in Fe3O4 by High-resolution X-ray Fluorescence Spectroscopy", European Conference on X-Ray Spectrometry (EXRS-2012),Vienna,Austria,(2012/06/18-2012/06/22)

[182] FUKUSHIMA Sei, Kenji Uchida, Yoshiaki Ito, Mitsuaki Huruya, Tatsuo Fujii, Tatsunori Tochio, Masugu Sato, Toshio Ninomiya, Michitaka, "The Observation of The Profile Change of

Fe Ka1,2 spectra using excitation energy around K-absorption Edge", European Conference on X-Ray Spectrometry (EXRS-2012) ,Vienna,Austria,(2012/06/18-2012/06/22)

[183] Yoshiaki Ito, Nobuyuki Shigeoka, Hirofumi Ohashi, Tatsunori Tochio, FUKUSHIMA, "Determination of Co and Fe K absorption edge using the high-resolution X-ray fluorescence emission spectra", European Conference on X-Ray Spectrometry (EXRS-2012) ,Vienna,Austria,(2012/06/18-2012/06/22)

[184] Kenji Yoshii, Ignace Jarrige, Daiju Matsumura, Yasuo Nishihata, Chikashi Suzuki, Yoshiaki Ito, Takeshi Mukoyama, Tatsunori Tochio, Shinotsuka Hiroshi, FUKUSHIMA Sei, "Probing the Ba 5d states in BaTiO3 and BaSO4: A resonant x-ray emission study at the Ba-L3 edge", European Conference on X-Ray Spectrometry (EXRS-2012) ,Vienna,Austria,(2012/06/18-2012/06/22)

[185] OKUI Masato, FUKUSHIMA Sei, Michiru Yamashita, VLAICUAUREL MIHAI, Maya Yasui, "Oxidation State Analysis of Fe in Volcanic Rocks", European Conference on X-Ray Spectrometry (EXRS-2012) ,Vienna,Austria,(2012/06/18-2012/06/22)

[186] Takayuki Hasegawa, Masaharu Uemura, Touko Tanigawa, Takafumi Tsurui, Masayoshi Shimizu, Shinsei Yokoi, Toshiaki Ohta, Kenta Amemiya, Noboru Fukada, Muneyuki Motoyama, Kazuhiro Kanda, FUKUSHIMA Sei, "K and L-edge Spectra of Several Sulfur Compounds, European Conference on X-Ray Spectrometry (EXRS-2012)", Vienna,Austria,(2012/06/18-2012/06/22)

[187] Masaharu Uemura, Takayuki Hasegawa, Takafumi Tsurui, Masayoshi Shimizu, Shinsei Yokoi, Toshiaki Ohta, Kenta Amemiya, Noboru Fukada, Muneyuki Motoyama, Kazuhiro Kanda, FUKUSHIMA Sei, "L-edge for the 1st period transition elements, European Conference on X-Ray Spectrometry (EXRS-2012)", Vienna,Austria,(2012/06/18-2012/06/22)

[188] FUKUSHIMA Sei, Yoshiaki Ito, Yukihito Nagashima, Chihiro Sakai, "Oxidation State Analysis of Sulfur in Glass Samples by high-resolution X-ray Fluorescence spectroscopyFe3O4 by High-resolution X-ray Fluorescence Spectroscopy", European Conference on X-Ray Spectrometry (EXRS-2012) ,Vienna,Austria,(2012/06/18-2012/06/22)

[189] Yoshikazu Nakanishi, FUKUSHIMA Sei, Yoshiaki Ito, Sei-kou Tou, Hirotoshi Honda, Masayuki Iso, Souta Hashimoto, Makoto Koyama, Shinzou Yoshikado, "The Change of high-resolution Nb L-alpha spectra of LiNbO3", European Conference on X-Ray Spectrometry (EXRS-2012) ,Vienna,Austria,(2012/06/18-2012/06/22)

[190] FUKUSHIMA Sei, KIMURA Takashi, IWAI Hideo, TANAKA Akihiro, "Oxidation State Analysis of Cr in the Oxide Layer between Stainless Steel and Metallic Tin by AES, the 29th European Conference on Surface Science (ECOSS-29)", Edinburgh International Conference Centre, Edinburgh,United Kingdom(2012/09/03-2012/09/07)

[191] TANUMA Shigeo, Shinotsuka Hiroshi, C.J. Powell, D.R. Penn, "Database of electron stopping powers in elemental solids for surface analysis", The 3rd Asian Materials Data Symposium (AMDS2012), Okinawa,Japan,(2012/04/15-2012/04/19).

[192] ISHIOKA Kunie, "Spatially Inhomogeneous Coherent Phonon-Plasmon Dynamics in n-type GaAs, -XVIIIth International Conference on Ultrafast Phenomena", Lausanne, Switzerla nd,(2012/07/08-2012/07/13)

[193] ISHIOKA Kunie, "Coherent Phonons in Anatase and Rutile TiO2 Excited at Fundamental Absorption Edge", 14th International Conference on Vibrations at Surfaces,Kobe,Jap an(2012/09/24-2012/09/28)

国内学協会会議（一般）

[194] 荻原俊弥 , 永富隆清 , 田沼繁夫 , " 傾斜ホルダーを利用した極低角度入射ビームによるデルタドープ多層薄膜のオージェ深さ方向分析 ", 第 72 回分析化学討論会 , 鹿児島大学 , 鹿児島市 , 日本 (2012/05/19-2012/05/20).

[195] 伊藤嘉昭 , 福島整 , 杤尾達紀 , 藤井達生 , 吉井賢資 , 米田安宏 , 寺澤倫孝 , " 高分解能 2 結晶分光器による化学状態分析 ", 第 72 回分析化学討論会 , , 鹿児島大学 , 鹿児島市 , 日本 (2012/05/19-2012/05/20).

[196] 杤尾達紀 , 大橋弘史 , 伊藤嘉昭 , 福島整 , 山下満 , 寺澤倫孝 , " 価数混合した Cr 化合物の定量分析について ", 第 72 回分析化学討論会 , , 鹿児島大学 , 鹿児島市 , 日本 (2012/05/19-2012/05/20).

[197] 伊藤嘉昭 , 藤井達生 , 福島整 , 林直顕 , 蔭山博之 , 寺澤倫孝 , 吉井賢資 , "Fe(II), Fe(III), Fe(IV) の K-alpha,beta スペクトルと ,Fe3O4 の K-alpha スペクトルに関する考察 ", 第 72 回分析化学討論会 , , 鹿児島大学 , 鹿児島市 , 日本 (2012/05/19-2012/05/20).

[198] 石岡邦江 , Hrvoje Petek, " アナターゼおよびルチル TiO2 単結晶のコヒーレントフォノン生成機構 ", 日本物理学会 2012 秋季講演大会 , 日本 (2012/09/18-2012/09/21)

[199] 吉川英樹 , 吉原一紘 , 田沼繁夫 , "「データ解析ソフトウェア COMPRO の新機能」―角度分解 XPS を使った半導体バンド曲りの定量評価―", 第 39 回表面分析研究会 , 古河電気工業株式会社　横浜研究所講堂 , 横浜市 , 日本 (2012/06/25-2012/06/26)

[200] 荻原俊弥 , 永富隆清 , 田沼繁夫 , " 極低角度入射ビームを用いた高感度 , 高深さ分解能オージェ深さ方向分析による極薄膜多層試料の分析 ", 日本分析化学会第 61 年会 , 金沢市 , 日本 (2012/09/19-2012/09/21)

[201] 福島整 , " X 線励起と電子線励起の Cr Auger スペクトルの比較 ", 第 39 回表面分析研究会 , 古河電気工業株式会社　横浜研究所講堂 , 横浜市 , 日本 (2012/06/25-2012/06/26)

[202] 松本凌 , 上本光太 , 田中博美 , 吉川英樹 , 吉原一紘 , "X 線光電子分光スペクトルの数学関数表現 ", 高専シンポジウム , 仙台市 , 日本 (2013/01/26)

[203] 上本光太 , 松本凌 , 田中博美 , 吉川英樹 , 吉原一紘 , " 表面分析支援ソフトウェアの開発 ", 高専シンポジウム , 仙台市 , 日本 (2013/01/26)

[204] 田中博美 , 吉川英樹 , 岸田悟 , " 水素還元処理法による固有ジョセフソントンネルデバイスの新規作製法 ", 平成 25 年電気学会全国大会 , 名古屋市 , 日本 (2013/03/20-2013/03/22)

[205] 永富隆清 , 柳内克昭 , 田沼繁夫 , " 表面分析及び標準化に関する IUVSA ワークショップ ", 学術振興会第 141 委員会第 151 回研究会 , 東京 , 日本 (2013/02/06-2013/02/07)

[206] 田沼繁夫 , 吉川英樹 , 篠塚寛志 , 上田隆一 , "Calculations of Mean Escape Depths of Photoelectrons in Elemental Solids Excited by Linearly Polarized X-ray for High Energy Photoelectron Spectroscopy", 表面分析研究会第 40 回研究会 , 東京 , 日本 (2013/02/21-2013/02/22)

[207] 福島整 , " X 線励起と電子線励起の Cr Auger スペクトルの比較（その後） ", 第 40 回表面分析研究会 , 東京 , 日本 (2013/02/21-2013/02/22)

[208] 後藤敬典 , 山内幸彦 , 田沼繁夫 , " 金属とその酸化物のオージェ・2 次電子放射特性 : ", 第 40 回表面分析研究会 , 東京 , 日本 (2013/02/21-2013/02/22)

[209] 岩井秀夫 , 小畠雅明 , 吉川英樹 , 田沼繁夫 , 小林啓介 , " 実験室系硬 X 線光電子分光装置の開発と応用 ", 共用・計測　合同シンポジウム 2013, つくば市 , 日本 (2013/02/28-2013/03/01)

■超先端電子顕微鏡技術の開発と先進材料応用

国際会議（招待）

[210] K. Kimoto, "Spatially-Resolved Diffractometry with Atomic-Column Resolution", Microscopy and Microanalysis 2012, Arizona, USA, (2012/7/29-8/2).

[211] K. Kimoto, M. Haruta, K. Kurashima, T. Nagai, H. Kurata, "Atomic-resolution characterization of oxides using electron microscopy", IUMRS-ICEM 2012 , Yokohama (Japan), (2012/9/23-28).

[212] M. Shimojo, K. Mitsuishi, M. Takeguchi, "Deposition of magnetic and photoconductive nanostructures." Focused electron beam induced processing (FEBIP) 4th workshop, University of Zaragoza, Spain, (2012/6/20-21).

[213] M. Takeguchi, "Electron Holography Researches for Energy & Environment Materials in NIMS." Electron Holography Symposium, National Nanofab Center, Daejeon, Korea, (2012/6/6-8).

国内学協会会議（招待・依頼）

[214] 木本浩司 , " 球面収差補正装置による高分解能観察の実際 ", 日本顕微鏡学会　第 68 回学術講演会 , つくば , (2012/05/14-16).

[215] 木本浩司 , " 電子顕微鏡におけるモノクロメーターの利点と実際 ", 日本顕微鏡学会　第 68 回学術講演会 , つくば , (2012/05/14-16).

[216] 木本浩司 , "STEM 入門 ", 第 28 回分析電子顕微鏡討論会 , 幕張 , (2012/09/4-5).

[217] 原徹 ," 三次元再構築像観察に適した直交配置型 FIB-SEM の特徴とその応用 ",SCANTECH2012, 日本顕微鏡学会走査電子顕微鏡分科会 , 東京都市大学 , (2012/09/14).

[218] 松村晶 , 前畑京介 , 田中啓一 , 原徹 , 満田和久 ," 超伝導マイクロカロリーメーター (TES) 分析電子顕微鏡への期待 ", 第 60 回応用物理学会春季学術講演会 , 神奈川 ,(2013/03/27-30)

[219] K. Mitsuishi, A. Hashimoto, M. Shimojo, M. Takeguchi, K. Ishizuka, " 共焦点電子顕微鏡法による３次元観察の可能性 ", 荷電粒子ビームの工業への応用第 132 委員会第 199 回研究会 , 弘済会館 ,(2012/1/20).

[220] M. Shimojo, K. Mitsuishi, M. Takeguchi, " 電子顕微鏡を利用したナノ構造作製 ", 表面技術協会ナノテク部会第 46 回研究会 , 芝浦工業大学 ,(2012/8/7).

[221] 橋本綾子 , 竹口雅樹 , "Protochips 社製試料ホルダーを用いた触媒ナノ粒子の高温観察 " JASIS2012, 幕張メッセ国際展示場 ,(2012/9/5-7).

[222] 橋本綾子 , " 実動環境対応物理分析 TEM によるグラフェン上の触媒ナノ粒子の高温 TEM 観察 " NIMS・AIST 微細構造解析プラットフォーム合同地域セミナー ,(独) 産業総合技術研究所 ,(2012/12/06).

国際会議（一般）

[223] H. Kamioka, R. Hosaki, N. Nagaoka, T.Hara, T.Nishida, H.Mori, T.Yamashiro, "Bone Collagen Production Revealed by UHVEM Tomography and FIB-SEM", The IADR/AADR/CADR General Session & Exhibition, Int'l. Assoc. for Dental Research., Seattle, USA., (2013/03/20-22).

[224] K. Sawada, T. Hara, H. Kushima, M. Tabuchi, K. Kimura, "Effects of minor element and creep deformation on Z phase formation in Gr.91 steel", Energy Materials Conf. 2012, Loughborouch, GB., (2012/10/16-19).

[225] 于秀珍 , 金澤直也 , 張偉珠 , 長井拓郎 , 原徹 , 木本浩司 , 松井良夫 , 小野瀬佳文 , 十倉好紀 , " 低消費電力磁気メモリ素子 ― スキルミオン素子 ", 第 12 回国際ナノテクノロジー総合展・技術会議 (nano tech 2013) , 東京（日本）, (2013/1/30 -2/1).

[226] M. Haruta, K. Kurashima, T. Nagai, H. Kurata, K. Kimoto, "Atomic-resolution characterization of oxides using electron energy loss spectroscopy mapping", 19th WIEN2k WORKSHOP, Tokyo (Japan), (2012/9/4).

[227] M. Haruta, K. Kurashima, T. Nagai, H. Kurata, K. Kimoto, "Visualization of Hybridization States with Atomic Resolution Using STEM-EELS", Microscopy & Microanalysis 2012 Meeting , Phoenix (USA), (2012/7/29 -8/2).

[228] A. Hashimoto, M. Takeguchi, "Transmission Electron Microscopy Observation of Pt nanoparticles on Graphene Layers at High Temperature." AMTC3, 長良川国際会議場 , 岐阜市 ,(2012/5/9-11).

[229] M. Shimojo, K. Mitsuishi, M. Takeguchi : "Deposition of magnetic and photoconductive nanostructures" Focused electron beam induced processing (FEBIP) 4th workshop, (2012/620-21).

[230] J. Cao, J. Xing, Y. Zhang, H. Tong, Y. Bi, T. Kako, M. Takeguchi, J. Ye, "The Photoelectrochemial properties of p-CaFe204/n-ZnFe204 junction based photo-electrodes." 2012 Chinese Materials Conference, 太原理工大学 , 山西省太原市 , 中国 ,(2012/7/13-18).

[231] M. Takeguchi, X. Zhang, A. Hashimoto, K. Mitsuishi, M. Shimojo, P. Wang, P. Nellist, A. Kirkland, "Scanning Confocal Electron Microscopy (SCEM) Combined with Deconvolution Technique." Microscopy and Microanalysis 2012, Phoenix Convention Center, Phoenix, AZ, USA, (2012/7/29-8/2).

[232] M. Song, N. Ogawa, S. Samitsu, I. Ichinose, "Quantitative analysis of porosity of nanoporous polymer with TEM tomography.", Int. Union of Mater. Res. Soc. – Int. conf. on electronic materials 2012 (IUMRS-ICEM2012), Pacifico Yokohama, Yokohama, Japan, (2012/9/23-28).

[233] M. Song, S. Ye, M. Takeguchi, A. Matsumoto, H. Kumakura, K. Togano, R. Teranishi, T. Kiyoshi, "Correlation between microstructure and high critical current of MgB2 Superconductor wires fabricated with internal magnesium dif.", IUMRS-ICEM 2012, Pacifico Yokohama, Yokohama, Japan, (2012/9/23-28).

[234] S. J. Ye, A. Matsumoto, K. Togano, Y. Zhang, H. Kumakura, M. Song, R. Teranishi, T. Kiyoshi, "Critical current properties and structure of internal Mg diffusion-processed filamentary MgB_2 wires", Int. Union of Mater. Res. Soc. – Int. conf. on electronic materials 2012 (IUMRS-ICEM 2012), Yokohama, Japan, (2012/9/23-28).

[235] H. Amekura, N. Ishikawa, N. Okubo, D.K. Avasthi, S.A. Khan, U.B. Singh, K. Mitsuishi, Y. Nakayama, "Critical Evaluation of the Synergy Model for Elongation of Embedded Nanoparticles by Swift Heavy Ion Irradiation." IUMRS-ICEM2012, Yokohama, Japan, (2012/9/23-28).

[236] K. Takazawa, J. Inoue, K. Mitsuishi, "Ultra-Compact Photonic Circuit Components Based on Propagation of Exciton Polaritons in Organic Dye Nanofibers." PRiME 2012, Hawai Convention Center, Honolulu, USA, (2012/10/7-12).

[237] N. Ishikawa, M. Takeguchi, S.Watanabe, T. Inami, "Dynamic TEM observation of Fe production from FeO which includes Si at the high temperature", 6th International Congress on the Science and Technology of Ironmaking (ICSTI2012), Hotel Royal Tulip, Rio de Janeiro, Brazil, (2012/10/14-18).

[238] H. Amekura, N. Okubo, N. Ishikawa, D. Tsuya, Y. Nakayama, K. Mitsuishi, "Embedded Zn0 nanoparticles irradiated with swift heavy ions: Irradiation-induced formation of metal phase and elongation." 25th International Conference of Atomic Collisions in Solids, 京都大学, 京都府, 日本 ,(2012/10/21-25).

[239] H. Amekura, N. Okubo, N. Ishikawa, S.A. Khan, U.B. Singh, D.K. Avasthi, Y. Nakayama, K. Mitsuishi, "Critical Evaluation of the Synergy Model for Elongation of Embedded Nanoparticles by Swift Heavy Ion Irradiation." 8th International Symposium on Swift Heavy Ions in Matter, 京都大学 , 京都府 , 日本 ,(2012/10/24-27).

[240] M. Song, H. Araki, S. Kuroda, K. Sakaki, "Bonding of Cold Sprayed Aluminum on Glass – A Study with Transmission Electron Microscopy. 5th Asian thermal Spray Conference (ATSC2012), つくば国際会議場 , つくば市 , 日本 ,(2012/11/26-28).

[241] N. Ishikawa, M. Takeguchi, T. Inami, "In-situ observation of Fe precipitate in FeO which includes Si at elevated temperature" IUVSTA Workshop for Surface Analysis and Standardization 2013, 沖縄自治会館 , 那覇市 , 日本 ,(2013/1/15-1/19).

国内学協会会議（一般）

[242] 原徹 , 澤田浩太 , 井誠一郎 , 田中啓一 , 大柿真毅 , 松村晶 , 椎山謙一 , 藤昇一 , " マイクロカロリメータ型 EDS による金属材料中の微量添加元素の検出下限値の評価 ", 日本顕微鏡学会第 68 回学術講演会 , つくば , (2012/5/14-16).

[243] 澤田浩太 , 九島秀昭 , 原徹 , 田淵正明 , 木村一弘 , " ASME Gr.91 鋼の Z 相析出挙動に及ぼす微量添加元素およびクリープの影響 ", 日本鉄鋼協会第 164 回秋季講演大会 , 愛媛 , (2012/9/17-19).

[244] 澤田浩太 , 九島秀昭 , 原徹 , 小林覚 , 田淵正明 , 木村一弘 , "ASME Gr.91 鋼の長時間クリープ強度のヒート間差と組織安定性 ", 第 50 回記念高温強度シンポジウム , 日本材料学会 , 京都 ,(2012/12/6-7).

[245] 鴨田紀一 , 長田俊郎 , 高橋宏治 , 原　徹 , " セラミックスの自己き裂治癒における改変機構の解明 ", 第 152 回日本金属学会春季大会 , 東京 ,(2013/03/27-29).

[246] 伊藤仁彦 , 原徹 , 久保佳実 , " リチウム空気 2 次電池の可逆的充放電過程における正極反応生成物の分析 ", 第 53 回電池討論会 , 福岡 ,(2012/11/14-16).

[247] 御手洗容子 , 原徹 , 川喜多磨美子 , 高橋円 , 高橋聡 , 細田秀樹 , "TiPdZr における相変態と形状記憶効果の合金組成依存性 ", 日本金属学会 2012 年秋期講演大会 , 愛媛 ,(2012/09/17-19).

[248] 倪浩天 , MIN Xiaohua, 江村聡 , 原徹 , 土谷浩一 , " Precipitation Kinetics of omega Phase in beta titanium alloys", 日本金属学会 2012 年秋期 (第 151 回) 講演大会 , 愛媛 ,(2012/09/17-19).

[249] L.Zhang, T.Ohmura, K.Sekido, T.Hara, K.Nakajima, K.Tsuzaki, "Application of in-situ nanoindentation in TEM", 日本顕微鏡学会第 68 回学術講演会 , つくば , (2012/5/14-16).

[250] 長井拓郎 , 長尾全寛 , 倉嶋敬次 , 浅香透 , 張偉珠 , 竹口雅樹 , 木本浩司 , " ローレンツ電顕法による強磁性マンガン酸化物におけるナノスケール磁気バブルの観察 ", 日本顕微鏡学会第 68 回学術講演会 , つくば ,　(2012/5/14-16).

[251] 治田充貴 , 倉嶋敬次 , 長井拓郎 , 小松寛 , 島川祐一 , 倉田博基 , 木本浩司 , " 混成軌道を区別した原子分解能酸素マッピング ", 日本顕微鏡学会第 68 回学術講演会 , つくば ,　(2012/5/14-16).

[252] 吉川純 , 橘田晃宜 , 香山正憲 , " バインダーフリー二次電池電極の作製と評価 ", 第 68 回日本顕微鏡学会 , 茨城県つくば市 ,(2012/5/14–16).

[253] 吉川純 , 寺田尚平 , 軍司章 , 治田充貴 , 長井拓郎 , 倉嶋敬次 , 木本浩司 , " モノクロメータ搭載 TEM-EELS による $LiCoO_2$ 正極材料の電子構造解析 ", NIMS 先端計測シンポジウム 2013, 茨城県つくば市 , (2013/2/28–3/1)

[254] 橋本綾子 , 竹口雅樹 , " グラフェン上の白金ナノ粒子の高温その場観察 ", 日本顕微鏡学会第 68 回学術講演会 , つくば .　(2012/5/14 -16).

[255] 田中美代子 , "$SrTiO_3$ 上 Ni クラスターの形態及び構造観察 ", 日本顕微鏡学会第 68 回学術講演会 , つくば市 ,(2012/05/14-16).

[256] 長谷川明 , 葉術軍 , 竹口雅樹 , 松本明善 , 熊倉浩明 , 戸叶一正 , 寺西亮 , 木吉司 , "IMD 法で製作した MgB_2 超伝導線材の分析透過電子顕微鏡による評価 ", 日本顕微鏡学会第 68 回学術講演会 , つくば国際会議場 , つくば市 ,(2012/5/14-16).

[257] 石川信博 , 竹口雅樹 , 稲見隆 , " ウスタイト還元に対するシリカ添加効果の動的観察 ", 日本顕微鏡学会第 68 回学術講演会 , 筑波国際会議場 , つくば市 , 日本 ,(2012/5/13-16).

[258] 助台榮一 , 横山隆 , 長谷川明 , "Weak beam 法と HREM 法による Al-Mg-Si 合金の摩擦撹拌接合部の内部組織観察 ", 日本顕微鏡学会第 68 回学術講演会 , つくば国際会議場 , つくば市 ,(2012/5/14-16).

[259] 長谷川明 , 小川展弘 , 佐光貞樹 , 一ノ瀬泉 , " ナノポーラスポリマーの TEM トモグラフィー観察 ", 日本顕微鏡学会第 68 回学術講演会 , つくば国際会議場 , つくば市 ,(2012/5/14-16).

[260] T. Nagai, M. Nagao, K. Kurashima, T. Asaka, W. Zhang, M. Takeguchi, K. Kimoto, " ローレンツ電顕法による強磁性マンガン酸化物におけるナノスケール磁気バブルの観察 ", 日本顕微鏡学会第 68 回学術講演会 , つくば国際会議場 , つくば市 , 日本 ,(2012/5/14-16).

[261] Z. Xiaobin, M. Takeguchi, A. Hashimoto, K. Mitsuishi, P. Wang, P. D. Nellist, A. I. Kirkland, M. Tezuka, M. Shimojo, "Improvement in depth resolution of Cs-corrected SCEM by deconvolution technique." 日本顕微鏡学会第 68 回学術講演会 , つくば国際会議場 , つくば市 , 日本 ,(2012/5/14-16).

[262] 橋本綾子 , "High temperature TEM observation of Pt nanoparticles on graphene layers.", 第 4 回ナノ材料科学環境拠点シンポジウム ,(独) 物質・材料研究機構並木地区 , つくば市 , 日本 ,(2012/06/26).

[263] 下条雅幸 , 三石和貴 , 竹口雅樹 : " 電子顕微鏡を利用したナノ構造作製 ", 表面技術協会ナノテク部会第 46 回研究会 , (2012/8/7).

[264] 田中美代子 , "$SrTi0_3$ 上 Ni クラスターのエピタキシーと特性評価 ", 2012 年秋期　第 73 回応用物理学会学術講演会 , 愛媛大学・松山大学 , 松山市 , 日本 ,(2012/09/11-14).

[265] L. Dan, K. Mitsuishi, K. Harada, M. Shimojo, D. Ju, M. Takeguchi, "Direct phase acquisition in electron holography with a atage-scanning system.", 日本金属学会 2012 秋期大会 , 愛媛大学 , 松山市 , 日本 ,(2012/9/17-19).

[266] 石川信博 , 竹口雅樹 , 稲見隆 , " シリカ添加ウスタイトにおける高温下での析出現象 ", 日本鉄鋼協会平成 24 年度秋期講演大会 , 愛媛大学 , 松山市 , 日本 ,(2012/9/17-19).

■強磁場固体ＮＭＲ計測技術の開発と先進材料応用

国内学協会会議（招待・依頼）

[267] 清水禎 , 端健二郎 , 大木忍 , 野口隆志 , " 極低温空間での目視・画像化を可能にする技術の開発 ", 2012 年秋季低温工学・超電導学会 , 岩手県情報交流センターアイーナ , 盛岡市 , 2012/11/07- 2012/11/09

[268] 清水禎 , " NMR の被災 , 復旧の現状 , 今後の課題 ", 超伝導科学技術研究会 , 第 79 回ワークショップ , 全日通霞が関ビルディング 大会議室Ｂ , 東京 , 2012/07/19

国際会議（一般）

[269] Hideto Imai, HASHI Kenjiro, Takashi Sanada, Kazuhiro Kamiguchi, Atsushi Ito, Manabu Watanabe, Kei Kubobuchi, Masato Mogi, Masashi Matsumoto, Nobutaka Chiba, OHKI Shinobu, SHIMIZU Tadashi, Masaharu Hatano, Takashi Matsumoto, "6Li NMR spectroscopic investigation on local structures and battery properties of Li2MnO3 cathode materials", 222th Electrochemical Society Meeting, Hawaii Convention Center,Honolulu, Hawaii, 米国 , 2012/10/07- 2012/10/12

[270] HASHI Kenjiro, SHIMIZU Tadashi, OHKI Shinobu, NOGUCHI Takashi, KIYOSHI Tsukasa, "Damage of a 930MHz NMR magnet in NIMS caused by the Tohoku earthquake", ICEC 24 - ICMC 2012, Fukuoka International Congress Center, 福岡市 , 2012/05/14- 2012/05/18

[271] Mutsuo Igarashi, Takehito Nakano, GOTO Atsushi, HASHI Kenjiro, SHIMIZU Tadashi, Hanazawa Atsufumi, Yasuo Nozue, "NMR property of rubidium loaded sodalite", 16th International Symposium on Intercalation Compounds, Jezerka Congress Hotel,Sec-Ustupky,Czech Republic

国内学協会会議（一般）

[272] 清水禎 , 端健二郎 , 大木忍 , 野口隆志 , " 極低温空間での目視・画像化を可能にする技術の開発 ", 2012 年秋季低温工学・超電導学会 , 岩手県情報交流センターアイーナ , 盛岡市 , 2012/11/07- 2012/11/09

[273] 端健二郎 , 後藤敦 , 大木忍 , 清水禎 , " 四極子核の磁場掃引 NMR 測定 ", 第 51 回 固体ＮＭＲ・材料フォーラム , 産業技術総合研究所　臨海新都心センター , 東京都 , 2012/05/12

[274] 大橋竜太郎 , 川村祐史 , 熊谷翼秀 , 井田朋智 , 水野元博 , 大木忍 , 丹所正孝 , 清水禎 , " 酸化インジウムの 115In NMR スペクトル解析 ", 第 52 回固体ＮＭＲ・材料フォーラム , 大阪大学吹田キャンパス , 大阪市 , 2012/10/17

[275] 齋藤雅由 , 魚住俊也 , 菅野利彦 , 梅林秀年 , 清水禎 , "13C- 固体ＮＭＲ緩和時間によるチーグラー・ナッタ触媒中の電子供与体の運動性の研究 ", 第 61 回高分子討論会 , 名古屋工業大学 , 名古屋市 , 2012/09/19- 2012/09/21

[276] 飯島隆広 , 山瀬利博 , 丹所正孝 , 清水禎 , " 常磁性ポリ酸の固体 95Mo NMR", ウインクあいち , 愛知県名古屋市 , 2012/11/08- 2012/11/10

[277] 後藤和馬 , 石川徹 , 嶋津沙織 , 藪内直明 , 駒場慎一 , 武田和行 , 後藤敦 , 出口健三 , 大木忍 , 端健二郎 , 清水禎 , 石田祐之 , " ナトリウムイオン電池負極炭素中の Na についての固体 Na NMR による解析 ", 第 39 回炭素材料学会年 , 長野市生涯学習センター TOiGO, 長野市 , 2012/11/28- 2012/11/30

[278] 安東真理子 , 及川格 , 前川英己 , 丹所正孝 , 清水禎 , 清野肇 , "Y, Ca および Sc をドープしたセリアおよびジルコニア系酸化物イオン伝導体の O・タ 17 NMR による欠陥構造解析 ", 第 146 回日本金属学会 , 筑波大学

[279] 及川格 , 安東真理子 , 丹所正孝 , 清水禎 , 前川英己 , "NMR によるペロブスカイト型プロトン伝導体の欠陥の解 ", 第 148 回日本金属学会 , 東京都市大学

[280] 垣木智行 , 鋤柄宜 , 丹所正孝 , 清水禎 , 徳武輝征 , 篠原正樹 , 松本哲也 , 木村基哲 , 遠藤守信 , " 高アルカリイオン吸蔵炭素材料の分子構造及び吸蔵メカニズム ", 第 53 回電池討論会 , ヒルトン福岡シーホーク , 福岡市 , 2012/11/14 - 2012/11/16

■強力中性子線計測技術の開発と先進材料応用

国内学協会会議（招待）

[281] Hideaki Kitazawa, Yukihiko KAWAMURA, Hiroaki MAMIYA Hiroaki, Noriki TERADA, Hiroyuki SUZUKI, Naohito TSUJII, Andreas DOENNI, Koji Kaneko, Naoto Metoki, Naoki Igawa, Akinori Hoshikawa, Toru Ishigaki, "Neutron scattering study toward to development of energy-efficient environment-friendly refrigeration technology",IUMRS-ICEM 2012, パシフィコ横浜 , (2012/09/23-27).

[282] 大　沼　正　人 , KOZIKOOWSKIPawel Marek, KOPPOJUSuresh, Vacuumschmelze, Vacuumschmelze, "Structural Anisotropy of Amorphous Ribbons Annealed under the Stress", IUMRS-ICA 2012, 韓国（釜山）, (2012/08/26-31)

[283] 大沼正人 , 大場洋次郎 , KOZIKOOWSKIPawel Marek, KOPPOJUSuresh, "Study on the Early Stage of Precipitation in Steels by Combined use of SANS and SAXS", アメリカ結晶学会年会 , 合衆国（ボストン）, (2012/07/28-08/01)

[284] M.Ohnuma, Y.Oba, S.Koppoju, "Combined Use of Small-Angle X-Ray and Neutron Scattering: SAS in Color", TMS2012(アメリカ材料系３学会１４１回年会),合衆国(テキサス), (2013/3/11-15)

[285] Masamichi Nishino (invited), " Macroscopic nucleation and dynamical features caused by spin and lattice degrees of freedom in spin crossover systems", PDSTM2012 , CNRS campus of Meudon-Bellevue,Paris, (2012/05/23)

国内学協会会議（招待・依頼）

[286] 北澤英明," 中性子散乱法による環境・エネルギー材料のマルチスケール解析 ", 第1回 TIA ナノグリーンセミナー , 物質・材料研究機構 ,(2012/07/20)

[287] 北澤英明 , 櫻井健次 , 武田良彦 , 加藤誠一 , 虫明磨毅 , 藤田大介 , "SIMS 等を用いた吸着挙動の検討 ", 廃棄物減容のための Cs 動態研究に関する JAEA-NIMS 共同研究ミーティング, 電中研　大手町会議室 ,(2012/07/30)

[288] 北澤英明 , 河村幸彦 , 門馬綱一 , 加藤誠一 , 辻井直人 , 茂筑高士 , Andreas DOENNI, Lukas Keller, Jiri Prchal, Pavel Javorsky, Junrong Zhang, 鳥居周輝 , 米村雅雄 , 神山　崇 , " 希土類 3 元系化合物の同相構造相転移 ", 第 4 回 J-PARC/MLF シンポジウム・茨城県ビームライン平成 23 年度成果報告会 , 日本科学未来館 ,(2012/10/10-11)

[289] 北澤英明 , 虫明磨毅 , 岩井秀夫 , 山田裕久 , 藤田大介 , " 微量分析技術による Cs の粘土層への吸着挙動 ", 第 10 回環境研究シンポジウム , 学術総合センター一橋記念講堂 ,(2012/11/14)

[290] 北澤英明 , 櫻井健次 , 河野健一郎 , 武田良彦 , 虫明磨毅 , 岩井秀夫 , 藤田大介 , 山田裕久 , "TOF-SIMS による Cs- バーミキュライトの検討 ", 第三回 JAEA-NIMS「Cs 脱離機構解明と脱離法の開発」会合 ,NBF ユニックスビル ,(2013/02/06)

[291] 北澤英明 , " 中性子散乱法による環境・エネルギー材料のマルチスケール解析 ", 第９３回 NIMS セミナー , 物質・材料研究機構 ,(2012/11/08)

[292] 間宮広明 , " がん温熱治療中に生じる磁性ナノ粒子の非平衡定常配向構造と発熱特性 ", 第 43 回ナノバイオ磁気工学専門研究会 東京 (2012/06/01)

[293] 泉 富士夫 , " 粉末X線・中性子回折による構造精密化と電子・核密度分布の決定 ", 第 60 回固体イオニクス研究会 , つくば市 (2012/5/31).

国際会議（一般）

[294] Hideaki Kitazawa, Yukihiko KAWAMURA, Noriki TERADA, Hiroaki Mamiya, Hiroyuki SUZUKI, Andreas DOENNI, Koji Kaneko, Naoto Metoki, Naoki Igawa, "Neutron diffraction study of rare-earth compound Ho_5Pd_2 with a large magnetocaloric effect", The 19th International Conference on Magnetism (ICM2012) , Busan (Korea), (July 8 – 13, 2012).

[295] H.Ohtuka, V.A.Dinh, T.Ohno, K.Tsuzaki, H.Suzuki and H.Kitazawa, "Effects of carbon on magnetic properties and transformed structures in Fe-based alloys", The 3rd Int. Symp. On Steel Science ISSS2012, Kansai Seminar House, Kyoto (May 27-30, 2012).

[296] H. Ohtsuka, V.A. Dinh, T. Ohno, K. Tsuzaki, H. Suzuki and H. Kitazawa, "Effects of Carbon on Magnetic Properties and Structures in Fe-Based Alloys", NIMS conference 2012, Epocal Tsukuba, Japan (June4-6,2012).

[297] M. Hase, V. Yu. Pomjakushin, L. Keller, A. Dönni, O. Sakai, T. Yang, R. Cong, J. Lin, K. Ozawa, and H. Kitazawa, Magnetism of $SrM_3P_4O_{14}$ (M^{2+}=3d ions) investigated using neutron-scattering measurements, The 19th International Conference on Magnetism 2012 (ICM2012), Busan, Korea, (July 8 – 13, 2012).

[298] H. Kuroe, R. Kino, R. Itoh, T. Hosaka, T. Hasegawa, T. Sekine, T. Kihara, M. Tokunaga, M. Hase, T. Takehana, H. Kitazawa, K. Oka, T. Ito, and H. Eisaki, "High field phase diagram in multiferroic $Cu_3Mo_2O_9$", The 19th International Conference on Magnetism 2012 (ICM2012), Busan, Korea, (July 8 – 13, 2012).

[299] H. Kuroe, K. Aoki, R. Itoh, T. Hosaka, T. Hasegawa, S. Hachiuma, M. Akaki, H. Kuwahara, T. Sekine, M. Hase, K. Oka, T. Ito, and H. Eisaki, "Zn-substitution effects in multiferroic $Cu_3Mo_2O_9$", The 19th International Conference on Magnetism 2012 (ICM2012), Busan, Korea, (July 8 – 13, 2012).

[300] R. Itoh, T. Hosaka, T. Hasegawa, H. Kuroe, T. Sekine, M. Hase, K. Oka, T. Ito, and H. Eisaki, "Cross-correlation effects in multiferroic $Cu_3Mo_2O_9$", The 19th International Conference on Magnetism 2012 (ICM2012), Busan, Korea, (July 8 – 13, 2012).

[301] T. Mochiku, Y. Hata, K. Yamaguchi, Y. Tsuchiya, A. Hoshikawa, K. Iwase, D. Sulistyanintyas, T. Ishigaki, H. Yasuoka, K. Hirata, "Annealing effect on structure and superconductivity in $FeSr_2YCu_2O6_{+\delta}$ magnetic superconductor", 25th International Symposium on Superconductivity (ISS2012), Tokyo, Japan, (Nov. 3-5, 2012).

[302] K. Yamaguchi, K. Kinoshita, Y. Hata, T. Mochiku, H. Yasuoka, "Superconductivity of $FeSr_2YCu_2O_{+\delta}$", 3rd International Conference on Superconductivity and Magnetism, Istanbul, Turkey, (April 29-May 4, 2012).

[303] S. Ooi, T. Mochiku, M. Tachiki, K. Hirata, "Vortex states of exfoliated $Bi_2Sr_2CaCu_2O_{8+y}$ thin film with and without micro-hole array", 25th International Symposium on Superconductivity (ISS2012), Tokyo, Japan, (Nov 3-5, 2012).

[304] H.S. Suzuki, N. Terada, A. Kikkawa, K. Kaneko, N. Metoki,"Magnetic structure transition in $PrPd_3$", The 19th international conference on Magnetism, Busan Korea, (July 8 – 13, 2012).

[305] H. Mamiya and B. Jeyadevan, "Formation of non-equilibrium magnetic nanoparticle structures in a large alternating magnetic field and their influence on magnetic hyperthermia treatment", INTERMAG2012, Vancouver, (May7-11, 2012)

[306] H. Mamiya and S. Nimori, "A new approach to the characterization of aging, rejuvenation, and memory effects in magnetic systems", 19th International Conference on Magnetism, Busan, (July 8 – 13, 2012)

[307] H. Mamiya and B. Jeyadevan, "Non-equilibrium steady states of magnetic nanoparticles in alternating magnetic fields and the biomedical applications", 2nd International Conference Asian Union of Magnetics Societies, Nara, (Oct 2 -5, 2012)

[308] H. Mamiya, N. Terada, N. Tujii, H. Kitazawa, A. Hoshikawa, T. Ishigaki, "Re-examination of dilute spinel ferrites for eco-friendly refrigerants", IUMRS-ICEM2012, Yokohama, (Sep 23 – 28,2012)

[309] N. Terada, D. D. Khalyavin, P. Manuel, Y. Tsujimoto, K. Knight, P. G. Radaelli, H. S. Suzuki and H. Kitazawa, "Ferroelectric polarization induced by magnetic ordering in delafossite $AgFeO_2$", Join Eutropean Magnetic Symposia 2012 (JEMS2012) Parma, Italy (Sep 9-14, 2012)

[310] S. Kimura, K. Watanabe, T. Fujita, M. Hagiwara, H. Yamaguchi, T. Kashiwagi, N. Terada, "Electromagnon Excitation of the Triangular Lattice Antiferromagnet $CuFeO_2$ in High Magnetic Fields", 10th International Conference on Research in High Magnetic Field (RHMF2012) Wuhan, China (Jul 3-6, 2012)

国内学協会会議（一般）

[311] 北澤英明 , " 巨大磁気熱量効果を示す GdCo2B2 単結晶の磁気相図 ", 日本物理学会 2012 年秋季大会 ,(2012/09/18 ~ 2012/09/21).

[312] 北澤英明 , " 希土類3元系化合物 TbXAl(X=Ni, Cu, P d) の同相構造相転移 ", 日本中性子科学会第 12 回年会 , 京都大学百周年時計台記念館 , (2012/12/10 ~ 2012/12/11).

[313] 北澤英明 , 河村幸彦 , Lukas Keller, 豊泉沙織 , 寺田典樹 , 間宮広明 , AndreasDOENNI, Seongsu Lee, 目時直人 , 金子耕士 , 井川直樹 , 田巻明 , " 磁気冷凍材料 R5Pd2（R=Tb,Ho）

の中性子回折 II", 日本物理学会第 68 回年次大会 , 広島大学東広島キャンパス , (2013/03/26 - 2013/03/29).

[314] 北澤英明 , Jiri Pospisil, Ajeya Gupta, 虫明磨毅 , 辻井直人 , 柳町治 , " 巨大磁気熱量効果を示す $GdCo_2B_2$ 単結晶の磁気相図 ", 日本物理学会 2012 年秋季大会 , 横浜国立大学 , (2012/09/18 - 2012/09/21).

[315] 大塚秀幸 ,V.A.Dinh, 大野隆央 , 津崎兼彰 , " 第一原理計算を用いた侵入型元素を含む bcc-Fe の磁気モーメントおよび軸比の計算 ", 日本金属学会　2012 年秋期講演大会　愛媛大学　城北キャンパス　(2013.9.17-19)

[316] 大塚秀幸 ,V.A.Dinh, 大野隆央 , 津崎兼彰 , "BCC-Fe における炭素位置と軸比・磁気モーメントに及ぼす炭素の効果の第一原理計算 ", 日本鉄鋼協会　第 164 回秋季講演大会　愛媛大学　城北キャンパス　(2013.9.17-19)

[317] 大塚秀幸 ,V.A.Dinh, 大野隆央 , 津崎兼彰 , 北澤英明 , 中村照美 , 土谷浩一 , " 第一原理計算によるマルテンサイトの軸比と磁気モーメント ", 共用・計測　合同シンポジウム (2013) 低炭素研究ネットワーク研究成果報告会 / 微細構造解析プラットフォーム・ワークショップ /NIMS 先端計測シンポジウム (2013)

[318] 大塚秀幸 ,V.A.Dinh, 大野隆央 , 津崎兼彰 , 北澤英明 , 中村照美 , 土谷浩一 , " 第一原理計算を用いた bcc-Fe の軸比 ", 日本金属学会 2013 年春期講演大会 , 東京理科大学神楽坂キャンパス　(2013.3.27-29)

[319] 青木謙人 , 佐藤輔 , 木野亮 , 保坂朋宏 , 伊藤龍亮 , 長谷川卓哉 , 黒江晴彦 , 関根智幸 , 長谷正司 , 岡邦彦 , 伊藤利充 , 永崎洋 , " マルチフェロイック物質 $(CuZn)_3Mo_2O_9$ の Zn 置換効果 II", 2012 年秋季大会 , 横浜国立大学 ,(2012.9.18-21)

[320] 長谷川卓哉 , 木野亮 , 佐藤輔 , 青木謙人 , 伊藤龍亮 , 保坂朋宏 , 黒江晴彦 , 関根智幸 , 木原工 , 徳永将史 , 長谷正司 , 竹端寛治 , 北澤英明 , 岡邦彦 , 伊藤利充 , 永崎洋 , 松本正茂 , " マルチフェロイック物質 $Cu_3Mo_2O_9$ の強磁場磁化・分極測定 ", 2012 年秋季大会 , 横浜国立大学 ,(2012.9.18-21)

[321] 保坂朋宏 , 木野亮 , 佐藤輔 , 青木謙人 , 伊藤龍亮 , 長谷川卓哉 , 黒江晴彦 , 関根智幸 , 長谷正司 , 岡邦彦 , 伊藤利充 , 永崎洋 , " マルチフェロイック物質 $(CuZn)_3Mo_2O_9$ の磁場 - 温度相図 ", 2012 年秋季大会 , 横浜国立大学 ,(2012.9.18-21)

[322] 佐藤輔 , 木野亮 , 青木謙人 , 保坂朋宏 , 伊藤龍亮 , 長谷川卓哉 , 黒江晴彦 , 関根智幸 , 長谷正司 , 岡邦彦 , 伊藤利充 , 永崎洋 , " マルチフェロイック物質 $(CuZn)_3Mo_2O_9$ のラマン散乱 ", 2012 年秋季大会 , 横浜国立大学 ,(2012.9.18-21)

[323] 伊藤龍亮 , 木野亮 , 佐藤輔 , 青木謙人 , 保坂朋宏 , 長谷川卓哉 , 黒江晴彦 , 関根智幸 , 長谷正司 , 岡邦彦 , 伊藤利充 , 永崎洋 , " マルチフェロイック物質 $Cu_3Mo_2O_9$ の交差相関 ", 2012 年秋季大会 , 横浜国立大学 ,(2012.9.18-21)

[324] 木野亮 , 佐藤輔 , 青木謙人 , 保坂朋宏 , 伊藤龍亮 , 長谷川卓哉 , 黒江晴彦 , 関根智幸 , 長谷正司 , 岡邦彦 , 伊藤利充 , 永崎洋 , " マルチフェロイック物質 $(CuZn)_3Mo_2O_9$ の比誘電率及び電気分極測定 ", 2012 年秋季大会 , 横浜国立大学 ,(2012.9.18-21)

[325] 安井幸夫 , 岡崎竜二 , 寺崎一郎 , 長谷正司 , 萩原雅人 , 益田隆嗣 , 榊原俊朗 , "CuO_2 リボン鎖を持つ $Rb_2Cu_2Mo_3O_{12}$ の特異な基底状態と磁場効果 ", 2012 年秋季大会 , 横浜国立大学 ,(2012.9.18-21)

[326] 萩原雅人 , 益田隆嗣 , 榊原俊朗 , 安井幸夫 , 岡崎竜二 , 寺崎一郎 , 長谷正司 , " 一次元量子スピン磁性体 $Rb_2Cu_2Mo_3O_{12}$ の磁場誘起相 ", 2012 年秋季大会 , 横浜国立大学 ,(2012.9.18-21)

[327] 星野侑宏 , 新聡一郎 , 後藤貴行 , 長谷正司 , 佐々木孝彦 , " 擬一次元競合鎖 $Cs_2Cu_2Mo_3O_{12}$ における ^{133}Cs-NMR", 2012 年秋季大会 , 横浜国立大学 ,(2012.9.18-21)

[328] 星野侑宏 , 新聡一郎 , 後藤貴行 , 長谷正司 , 佐々木孝彦 , " 擬一次元競合鎖 $Rb_2Cu_2Mo_3O_{12}$ における ^{87}Rb-NMR", 2012 年秋季大会 , 横浜国立大学 ,(2012.9.18-21)

[329] 晦日慶太, 土井憲一, 浜崎智彰, 黒江晴彦, 後藤貴行, 関根智幸, 佐々木孝彦, 長谷正司, 岡邦彦, 伊藤利充 , 永崎洋 , 一次元鎖とダイマーからなる磁性 $Cu_3Mo_2O_9$ の Cu-NMR V", 2012 年秋季大会 , 横浜国立大学 ,(2012.9.18-21)

[330] 益田隆嗣 , 安井幸夫 , 長谷正司 , 萩原雅人 , 河村聖子 , 中島健次 , 富安啓輔 , 寺崎一郎 , 菊地龍弥 , 稲村泰弘 , 左右田稔 , " 強磁性フラストレート鎖 $Rb_2Cu_2Mo_3O_{12}$ の磁気励起 ", 第 68 回年次大会 (2013 年) , 広島大学 ,(2013.3.26-29)

[331] 成瀬晃樹 , 川股隆行 , 大野真澄 , 松岡禎知 , 長谷正司 , 黒江晴彦 , 関根智幸 , 佐々木孝彦 , 岡邦彦 , 伊藤利充 , 永崎洋 , 小池洋二 , " 擬 1 次元反強磁性体 $Cu_3Mo_2O_9$ 単結晶における熱伝導と磁気秩序 ", 第 68 回年次大会 (2013 年) , 広島大学 ,(2013.3.26-29)

[332] 青木謙人, 佐藤輔, 木野亮, 保坂朋宏, 伊藤龍亮, 長谷川卓哉, 黒江晴彦, 関根智幸, 長谷正司, 岡邦彦 , 伊藤利充 , 永崎洋 , " マルチフェロイック物質 $(CuZn)_3Mo_2O_9$ の Zn 置換効果 Ⅲ ", 第 68 回年次大会 (2013 年) , 広島大学 ,(2013.3.26-29)

[333] 木野亮, 佐藤輔, 青木謙人, 保坂朋宏, 伊藤龍亮, 長谷川卓哉, 黒江晴彦, 関根智幸, 長谷正司, 岡邦彦 , 伊藤利充 , 永崎洋 , " マルチフェロイック物質 $(CuZn)_3Mo_2O_9$ の比誘電率及び電気分極測定Ⅱ ", 第 68 回年次大会 (2013 年) , 広島大学 ,(2013.3.26-29)

[334] 佐藤輔, 木野亮, 青木謙人, 保坂朋宏, 伊藤龍亮, 長谷川卓哉, 黒江晴彦, 関根智幸, 長谷正司, 岡邦彦 , 伊藤利充 , 永崎洋 , " マルチフェロイック物質 $(CuZn)_3Mo_2O_9$ のラマン散乱Ⅱ ", 第 68 回年次大会 (2013 年) , 広島大学 ,(2013.3.26-29)

[335] 黒江晴彦, 小池秀弥, 工藤吉喜, 青木謙人, 佐藤輔, 木野亮, 保坂朋宏, 伊藤龍亮, 長谷川卓哉, 関根智幸 , 長谷正司 , 川崎郁斗 , 渡邊功雄 , 岡邦彦 , 伊藤利充 , 永崎洋 , "$(CuZn)_3Mo_2O_9$ の μSR 測定 ", 第 68 回年次大会 (2013 年) , 広島大学 ,(2013.3.26-29)

[336] 星野侑宏 , 新聡一郎 , 後藤貴行 , 長谷正司 , 佐々木孝彦 , " 擬一次元競合鎖 $A_2Cu_2Mo_3O_{12}$ (A = Rb or Cs) における ^{87}Rb-NMR および ^{133}Cs-NMR", 第 68 回年次大会 (2013 年) , 広島大学 ,(2013.3.26-29)

[337] 長谷正司 , " 低次元スピン系とフラストレーションスピン系の中性子散乱研究 ", 物性研究所客員所員講演会 , 東京大学物性研究所柏の葉キャンパス (2012.4.19)

[338] 安井幸夫 , 長谷正司 , 富安啓輔 , 河村聖子 , 中島健次 , 加倉井和久 , 益田隆嗣 , " 強磁性フラストレート鎖 $Rb_2Cu_2Mo_3O_{12}$ の非弾性中性子散乱 ", JAEA-CROSS プロジェクト研究「機能性物質の構造と電子物性」 ミニ研究会 ,T's 横浜パシフィック ホール 2, (2012.9.21-22)

[339] 安井幸夫, 寺崎一郎 , 長谷正司 , 萩原雅人 , 左右田稔 , 益田隆嗣 , 富安啓輔 , 河村聖子, 中島健次 , 加倉井和久 , "CuO_2 リボン鎖を持つ $Rb_2Cu_2Mo_3O_{12}$ の中性子磁気非弾性散乱 ", 第 4 回 J-PARC/MLF シンポジウム , 日本科学未来館 , (2012.10.10-11)

[340] 安井幸夫, 寺崎一郎 , 長谷正司 , 萩原雅人 , 左右田稔 , 益田隆嗣 , 富安啓輔 , 河村聖子, 中島健次 , 加倉井和久 , "CuO_2 リボン系 $Rb_2Cu_2Mo_3O_{12}$ の中性子磁気非弾性散乱 ", 日本中性子科学会・第１２回年会 , 京都大学 、(2012.12.10-11)

[341] 長谷正司 , " 中性子散乱測定を利用した 3d 金属酸化物の磁性の研究 ", 第 6 回三機関連携 量子複雑現象」 研究会 ,NIMS, (2013.1.21)

[342] 亀山太一 , 小間香保里 , 松葉健 , 吉澤俊介 , 小関泰二 , 金子真一 , 竹屋浩幸 , 茂筑高士 , 平田和人 , 西田信彦 ," 超伝導量子磁束ダイナミクスの実空間高速測定 ", 日本物理学会第 68 回年次大会 , 広島大学 , (2013.3.26.-29)

[343] 町田理 , 藤澤唯太 , 五十嵐圭 , 大井修一 , 茂筑高士 , 立木実 , 小森和範 , 平田和人 , 坂田英明 , "$IrTe_2$ における走査トンネル分光 ", 日本物理学会第 68 回年次大会 , 広島大学 ,(2013.3.26-29)

[344] 藤澤唯太 , 町田理 , 五十嵐圭 , 大井修一 , 茂筑高士 , 立木実 , 小森和範 , 平田和人 , 坂田英明 , "$IrTe_2$ の単結晶育成とその評価 ", 日本物理学会第 68 回年次大会 , 広島大学 , (2013.3.26-29)

[345] 大井修一 , 茂筑高士 , 立木実 , 平田和人 , " メゾスコピック Bi2212 高温超伝導体における渦糸状態 ", 日本物理学会第 68 回年次大会 , 広島大学 , (2013.3.26-29)

[346] 平田和人 , 大井修一 , 茂筑高士 , " アンチドット格子を有する Bi-2212 系の c 軸方向抵抗 ", 日本物理学会第 68 回年次大会 , 広島大学 ,(2013.3.26-29)

[347] 鈴木悠介 , 茂筑高士 , 柏木隆成 , 吉崎亮造 , 門脇和男 , "Bi 系トホポロシジカル絶縁体の磁場中輸送特性 ", 日本物理学会第 68 回年次大会 , 広島大学 ,2013.3.26-29)

[348] 茂筑高士 , 鈴木悠介 , 松下能孝 , 土屋佳則 , 藤井宏樹 , 小林剛 , 勝矢良雄 , 田中雅彦 , 坂田修身 , 門脇和男 , "$Cu_xBi_2Se_3$ の結晶構造解析 ", 日本物理学会第 68 回年次大会 , 広島大学 ,(2013.3.26-29)

[349] 茂筑高士 , 鈴木悠介 , 松下能孝 , 土屋佳則 , 藤井宏樹 , 小林剛 , 勝矢良雄 , 田中雅彦 , 坂田修身 , 門脇和男 , "Cu をドープしたトポロジカル絶縁体 Bi_2Se_3 の結晶構造 ", 日本結晶学会平成 24 年度年会 , 東北大学 , (2012.10.25-26)

[350] 山口和宏 , 畑慶明 , 茂筑高士 , 安岡宏 , "$FeSr_2YCu_2O_{6+\delta}$ の超伝導特性 II", 日本物理学会 2012 年秋季大会 , 横浜国立大学 , (2012.9.18-21)

[351] 茂筑高士 , 畑慶明 , 山口和宏 , 土屋佳則 , 星川晃範 , 岩瀬謙二 , Dyah Sulistyanintyas, 石垣徹 , 安岡宏 , 平田和人 , "$FeSr_2YCu_2O_{6+\delta}$ におけるアニール効果 ", 日本物理学会 2012 年秋季大会 , 横浜国立大学 , (2012.9.18-21)

[352] 山口和宏 , 木下和樹 , 畑慶明 , 茂筑高士 , 安岡宏 , "$FeSr_2LnCu_2O_{6+y}$ の希土類元素の置換効果", 粉体粉末冶金協会平成 24 年度春季大会 , 京都工芸繊維大学 , (2012.5.22-24)

[353] 鈴木博之 , 寺田典樹 , 目時直人 , 金子耕士 ,"$PrPd_3$ の磁気構造 ", 日本物理学会第 68 回年次大会 , 広島大学　東広島市 , (2013/3/26 –29)

[354] 西野正理 , " 弾性的長距離相互作用系における界面成長　非平衡系の物理 ",　京大基礎研究会 , 湯川記念館 , (2012.8.2)

[355] 西野正理 , 宮下精二 ,K. Boukheddaden, F. Varret, " スピンクロスオーバー系におけるドメイン成長 ", 日本物理学会 2012 年秋季大会 , 横浜国大 , (2012.9.18)

[356] 西野正理 , 宮下精二 ,K. Boukheddaden, F. Varret, " スピンクロスオーバー系の臨界現象における短距離相互作用の効果 ",　日本物理学会 2013 年年次大会 , 広島大 , (2013.3.26)

[357] 間宮広明 , 二森茂樹 , 寺田典樹 , 北澤英明 , 星川晃範 , 石垣徹 , " 幾何学的にフラストレートした磁性体 ZnFe2O4 におけるスピン秩序の成長と破壊 , そして再生 ", 第 4 回 MLF シンポジウム 東京　(2012.10.10- 11)

[358] 間宮広明 , バラチャンドランジャヤデワン , " がんの新しい温熱治療の際に生じる強磁性ナノ粒子の非平衡配向状態 ", 日本物理学会 2012 年秋季大会 横浜　(2012.9.18 -21)

[359] 間宮広明 , 二森茂樹 , 寺田典樹 , 北澤英明 , 星川晃範 , 石垣徹 , " 幾何学的にフラストレートした磁性体におけるスピン秩序の再生 ", 日本中性子科学会第 12 回年会 京都　(2012.12.10 -11)

[360] 間宮広明 , " 磁性粒子イメージングにおける大振幅交流磁場への非線形非平衡応答 ", 平成 24 年度　磁性流体連合講演会 京都　(2012.11.29)

[361] 間宮広明 , 二森茂樹 , 寺田典樹 , 北澤英明 , 星川晃範 , 石垣徹 , " フラストレートした反強磁性体 ZnFe2O4_ におけるスピン秩序の成長と若返り、そして再生 ", 日本物理学会第 68 回年次大会 東広島　(2013.3.26 – 29)

[362] 辻井直人 , " カゴ状構造を持つ Yb 化合物の合成と物性 ", 日本物理学会　第 68 回年次大会 , 広島大学 (2013/03/26 - 29).

[363] 鳴海康雄 , 森岡貴之 , 齋藤康太 , 野尻浩之 , 中村哲也 , 広野等子 , 木下豊彦 , 寺田典樹 , 北澤英明 , 金道浩一 , " 強磁場軟 X 線 MCD による三角格子反強磁性体 $CuFeO_2$ のスピン・軌道状態の解明 ", 2012 年日本物理学会秋季大会 , 横国大 (2012/09/18 - 21)

[364] 玉造博夢 , 満田節生 , 中島多朗 , 金子周史 , 保坂翔太 , 竹端寛治 , 高増正 , 寺田典樹 , 北澤英明 " 磁性誘電性マルチフェロイック $CuFeO_2$ の強誘電相における磁場掃引による分極誘起 (その 2)", 2012 年日本物理学会秋季大会 , 横国大 (2012/09/18 -21)

[365] 中村真一 , 小林康浩 C, 北尾真司 , 瀬戸誠 , 不破章雄 , 寺田典樹 , " マルチフェロイック酸化物 $CuFeO_2$ 系のメスバウアー分光 II", 2012 年日本物理学会秋季大会 , 横国大 (2012/09/18 - 2012/09/21)

[366] 木村尚次郎 , 渡邊和雄 , 藤田崇仁 , 萩原政幸 , 山口博則 , 柏木隆成 , 寺田典樹 , " 三角格子反強磁性体 $CuFeO_2$ の円偏光 ESR", 2013 年日本物理学会年次大会 , 広島大 (2013/03/26 - 29).

[367] 金子周史 , 中島多朗 , 満田節生 , 田中良和 , 寺田典樹 , 脇本秀一 , 武田全康 , 加倉井和久 , "3 次元中性子偏極解析及び共鳴 X 線散乱を用いたマルチフェロイック $CuFe_{1-x}Ga_xO_2$ のらせん磁気相における磁気・結晶構造の精密探査（その 2） ", 2013 年日本物理学会年次大会 , 広島大 (2013/03/26 - 29).

[368] 玉造博夢 , 金子周史 , 堀川哲 , 鈴木主翼 , 保坂翔太 , 中島多朗 , 満田節生 , 竹端寛治 , 高増正 , 寺田典樹 , 北澤英明 , " マルチフェロイック $CuFeO_2$ における多段磁場誘起磁気秩序に固有な誘電緩和の Hybrid-Magnet(28T) を用いた探査 ", 2013 年日本物理学会年次大会 , 広島大 (2013/03/26 - 29).

■放射光を利用した先進計測技術の開発と先進材料応用

国内学協会会議（招待・依頼）

[369] 桜井健次 , " イントロダクトリートーク ",「薄膜・多層膜の埋もれた界面の解析　一高度な量子ビーム源による新しい研究の方向性研究会」, 高エネルギー加速器研究機構 (つくば市),2012.6.26 ～ 28

国際会議（一般）

[370] Kenji Sakurai, Vallerie Ann Innis-Samson, Hiromi Eba and Mari Mizusawa, "XAFS imaging by projection-type X-ray fluorescence microscope, 15th International Conference on X-Ray Absorption Fine Structure", Beijing, China, July 22-28, 2012,

[371] V.A. Innis-Samson, M. Mizusawa, K. Sakurai, "Synchrotron Micro-XRF Elemental Analysis of the Mussel Shell Perna Viridis from Manila Bay", Philippines, Denver Marriott Tech Center Hotel,Denver, Colorado, USA, August 6-10, 2012

[372] V.A. Innis-Samson and K. Sakurai, "Thickness Dependence of the Hydrophilic-Hydrophobic Switching Function of Methylcellulose Thin Films: An X-ray Reflectivity Study", Denver Marriott Tech Center Hotel,Denver, Colorado, USA, August 6-10, 2012

[373] K. Stoev and K. Sakurai, "Quick X-ray Reflectivity of Spherical Samples", Denver Marriott Tech Center Hotel,Denver, Colorado, USA, August 6-10, 2012

[374] K. Sakurai and M. Mizusawa, "X-ray Fluorescence Imaging of Growing Chemical Patterns", Denver Marriott Tech Center Hotel,Denver, Colorado, USA, August 6-10, 2012

[375] K. Sakurai, V. A. I.-Samson, M. Mizusawa and H. Eba, "Non-Scanning Type X-Ray Fluorescence and X-Ray Diffraction Imaging and the Applications", IUMRS-International Conference on Electronic Materials (IUMRS-ICEM 2012), Pacifico Yokohama, Yokohama, Japan, September 23-28, 2012

[376] V. A. I.-Samson, M. Mizusawa and K. Sakurai, "High resolution distribution of major and trace elements in the calcite shell layer of the Mussel shell Perna Viridis from Manila Bay", Philippines: A synchrotron micro-XRF study, IUMRS-International Conference on Electronic Materials (IUMRS-ICEM 2012), Pacifico Yokohama, Yokohama, Japan, September 23-28, 2012

[377] K. Sakurai and K. Stoev, "Computer modeling of convex and concave samples for q-XRR setups", International Grazing-Incidence Small Angle Scattering Meeting, Kyoto Institute of Technology, Japan, November 14-15, 2012,

[378] V. A. I.- Samson, M. Mizusawa, K. Sakurai, "Probing Heterogeneous Structures on Surfaces by X-ray and Neutron Reflection Tomography", International Grazing-Incidence Small Angle Scattering Meeting, Kyoto Institute of Technology, Japan, November 14-15, 2012,

国内学協会会議（一般）

[379] 桜井健次 , 水沢まり , " 成長する化学パターンの蛍光X線イメージング ", 日本顕微鏡学会 第 68 回学術講演会 , エポカルつくば (つくば市),2012..5.14 〜 16

[380] Vallerie Samson, 水沢まり , 桜井健次 , "X 線反射トモグラフィ ", 日本顕微鏡学会 第 68 回学術講演会 , エポカルつくば (つくば市),2012..5.14 〜 16

[381] Vallerie Samson, 水沢まり , 桜井健次 , "Recent quick reflectivity measurements with laboratory X-ray source",「薄膜・多層膜の埋もれた界面の解析　ー高度な量子ビーム源による新しい研究の方向性」研究会 , 高エネルギー加速器研究機構 (つくば市),2012.6.26 〜 28

[382] 桜井健次 ,Vallerie Ann Innis-Samson, 水沢まり , " クイックX線反射率装置の開発 ", 第４８回Ｘ線分析討論会 , 名古屋大学 野依記念学術交流館 , 2012.10.31 〜 11.2

[383] 水沢まり , 桜井 健次 , " 投影型 X 線顕微鏡による多結晶 X 線回折イメージング ", 第４８回X線分析討論会 , 名古屋大学 野依記念学術交流館 , 2012.10.31 〜 11.2

[384] Vallerie Ann Innis Samson and Kenji Sakurai, "Surface Property and X-ray Reflectivity Evaluation of the Thickness Dependence of the Hydrophobic Switching Nature of Methylcellulose Ultra-Thin Films", 第４８回X線分析討論会 , 名古屋大学 野依記念学術交流館 , 2012.10.31 〜 11.2

[385] Krassimir Stoev and Kenji Sakurai, "Sample Curvature Effects in Quick X-Ray Reflectivity", 第４８回X線分析討論会 , 名古屋大学 野依記念学術交流館 , 2012.10.31 〜 11.2

[386] Vallerie Ann Innis Samson, Mari Mizusawa and Kenji Sakurai, "X-ray and Neutron Reflection Tomography: New Complementary Techniques for Surface Imaging", 第４８回X線分析討論会, 名古屋大学 野依記念学術交流館 , 2012.10.31 〜 11.2

[387] Vallerie Ann Innis Samson, Mari Mizusawa and Kenji Sakurai, Synchrotron μ -XRF characterization of the Mussel shell Perna Viridis from Manila Bay, Philippines, 第４８回X線分析討論会 , 名古屋大学 野依記念学術交流館 , 2012.10.31 〜 11.2

[388] 桜井健次 ,Vallerie Ann Innis-Samson, 江場宏美 , 水沢まり , " 投影型蛍光Ｘ線顕微鏡によるＸＡＦＳイメージング ", 第４８回Ｘ線分析討論会 , 名古屋大学 野依記念学術交流館 , 2012.10.31 〜 11.2

[389] 桜井健次 , 水沢まり , " 成長する化学パターンの蛍光X線イメージング ", 第４８回X線分析討論会 , 名古屋大学 野依記念学術交流館 , 2012.10.31 〜 11.2

[390] 桜井健次 , 水沢まり , " 成長する化学パターンの蛍光X線イメージング ", 物構研サイエンスフェスタ , エポカルつくば ,2013.3.14-15

[391] 桜井健次 ,Vallerie Ann Innis-Samson, 水沢まり , " Ｘ線反射率のリアルタイム計測 ", 2013 年応用物理学会春季学術講演会 , 神奈川工科大学 ,2013.3.27-30

[392] Vallerie Ann Innis-Samson, Mari Mizusawa and Kenji Sakurai, "Probing Heterogeneous Structures on Surfaces by X-ray and Neutron Reflection Tomography", 2013 年応用物理学会春季学術講演会 , 神奈川工科大学 ,2013.3.27-30

[393] 桜井健次 , 水沢まり , "X 線投影顕微鏡による化学反応の蛍光 X 線動画イメージング ", 2013 年応用物理学会春季学術講演会 , 神奈川工科大学 ,2013.3.27-30

3. プレス発表

■先端表面敏感計測技術の開発と先進材料応用

[1] 倉橋光紀 , 山内泰 ,「分子軸とスピンの向きを指定した酸化反応を世界で初めて実現」(2012.4.26)

[2] 倉橋光紀 , 山内泰 ,「酸化鉄表面スピン特性の解明と大幅な改善に成功」 (2012.5.25)

■先端表層領域計測技術の開発と先進材料応用

[3] 阿部英樹 , 吉川英樹 , 原徹「燃料電池電極触媒活性 15 倍向上 : 金属ナノ粒子可溶化技術の開発に成功」(平成 24 年 4 月 23 日)

■超先端電子顕微鏡技術の開発と先進材料応用

[4] 日刊工業新聞「「スキルミオン結晶」微小電力駆動に成功」（2012.8.8）理研・東大との共同研究。

[5] 日経産業新聞「スピン , 低電流で変化 , 省電力メモリー開発に道」（2012.8.23）理研・東大との共同研究。

■強力中性子線計測技術の開発と先進材料応用

[6] 日刊工業新聞等「非磁性原子を置換することで磁性・誘電特性の制御に成功」一次世代メモリデバイスの開発に新しいアイディアー (2012.8.8)

4．特許

■先端表面敏感計測技術の開発と先進材料応用

[1] 特願 2012-132445, 山内泰 , プラットアンドリュー , 倉橋光紀 , オゾンビーム発生装置 , 2012/6/12

[2] 特願 2012-141133, 石井真史 , 高温インピーダンス測定装置 , 2012/6/22

[3] 特願 2012-149031 ザンハン , 唐捷 , 秦禄昌 , ユエンジンシ , 新谷紀雄 , 山内泰 , 六ホウ化金属冷電界エミッター、その製造方法及び電子銃 , 2012/7/3

[4] 特願 2012-168532 ザンハン , 唐捷 , 秦禄昌 , ユエンジンシ , 新谷紀雄 , 山内泰 , 金属ホウ化物フィールドエミッター作製方法 , 2012/7/30

[5] 登録 5051634 鈴木拓 , 山内泰 , イオンビーム発生方法とそれを実施する為のイオンビーム発生装置 , 2012/8/3

■先端表層領域計測技術の開発と先進材料応用

[6] 登録 5207271 田中博美 , 吉川英樹 , 高温超電導単結晶上での面内型ジョセフソン接合形成法 , 2013/3/1

[7] 特願 2012-090413 阿部英樹 , サラバナンゴバンダッチャリ , 原徹 , 吉川英樹 , 山下良之 , 上田茂典 , 小林啓介 , ナノ粒子包摂デンドリマー集積電極触媒及びその製造方法 , 2012/4/11

[8] 特願 2012-136453 大橋直樹 , 吉川英樹 , 廣瀬左京 , 抵抗スイッチングデバイス , 2012/6/16

[9] 特願 2012-256243 阿部英樹 , ノールアクマルファディル , 村上秀之 , 吉川英樹 , 山下良之 , 上田茂典 , 田邊豊和 , グバラベンカタラメッシュ , サラバナンゴビンダッチャリ , 有賀克彦 , 石原伸輔 , 小径 Ni_3C ナノ粒子及びその製造方法 , 小径 Ni_3C ナノ粒子含有電極触媒及びその製造方法 , 2012/11/22

[10] 特願 2012-287587 阿部英樹 , ノールアクマルファディル , 村上秀之 , 吉川英樹 , 山下良之 , 上田茂典 , 田邊豊和 , グバラベンカタラメッシュ , サラバナンゴビンダッチャリ , 耐酸化性 NiAl ナノ粒子及びその製造方法 , 耐酸化性 NiAl ナノ粒子含有ボンドコート層 , 2012/12/28

[11] 特願 PCT/JP2013-053457 抵抗スイッチングデバイスおよびその製造方法 , 2013/2/14

■超先端電子顕微鏡技術の開発と先進材料応用

[12] 特願 2012-090413 阿部英樹 , サラバナンゴヴィンダッチャリ , 原徹 , 吉川英樹 , 山下良之 , 上田茂典 , 小林啓介 , ナノ粒子包摂デンドリマー集積電極触媒及びその製造方法 , 2012/04/11

[13] 特願 2012-115599 阿部英樹 , フランシスマーラーオキシリア , 石原伸輔 , 田邊豊和 , サラバナンゴヴィンダチェティ , グバラベンガタラメシュ , 原徹 , 許亜 , 菱田俊一 , 有賀克彦 , ナノ単結晶板材集積触媒及びその製造方法 , 2012/05/21

[14] 登録 5077943 御手洗容子 , 原徹 , 細田秀樹 , 三浦誠司 , PtTi 高温形状記憶合金 , 2012/09/07

[15] 特願 PCT/JP2012/067988 御手洗容子 , 川喜多麻美子 , 平徳海 , 原徹 , 高温形状記憶合金 , 2012/7/13

[16] 登録 5187844 平野敏幸 , 原徹 , 出村雅彦 , 楊君友 , 許亜 , CO 酸化触媒 , 2013/02/01

[17] 登録 5187845 平野敏幸 , 原徹 , 出村雅彦 , 楊君友 , 許亜 , メタノール分解触媒 , 2013/02/01

[18] 特願 2012-041460 サラバナンゴヴィンダッチャリ , 山下良之 , 原徹 , 吉川英樹 , 小林啓介 , 阿部英樹 , 上田茂典 , ナノ粒子包接デンドリマー蛍光体及びその製造方法 , 2012/3/1

[19] 特願 2012-101654 竹口雅樹 , 三石和貴 , 原田研 , 透過型電子顕微鏡及び電子線干渉法 , 2012/4/26

■強力中性子線計測技術の開発と先進材料応用

[20] 特願 2013-000652 加藤誠一 , 原田幸明 , セシウム除染法 , 2013/1/7

[21] 特願 2013-000681 加藤誠一 , 原田幸明 , セシウム抽出法 , 2013/1/7

[22] 特願 2013-003068 原田幸明 , 加藤誠一 , セシウム除去方法及びこれに用いるセシウム除去装置 , 2013/1/11

■放射光を利用した先進計測技術の開発と先進材料応用

[23] 特願 2012-178025, 桜井健次 , サムソン・ヴァレリー・アン・イニス , 水沢多鶴子 , X線撮像装置及びその使用法、中性子線撮像装置及びその使用法 , 2012/8/10

5. 主要論文別刷り

■先端表面敏感計測技術の開発と先進材料応用

[1] Mitsunori Kurahashi and Yasushi Yamauchi, "Huge steric effects in surface oxidation of Si(100)", PHYSICAL REVIEW B 85, 161302(R) (2012)

■先端表層領域計測技術の開発と先進材料応用

[2] Hua Jin, Shinotsuka Hiroshi, YOSHIKAWA Hideki, IWAI Hideo, ARAI Masao, TANUMA Shigeo, Sven Tougaard, "Evaluation of robustness to surface conditions of the target factor analysis method for determining the dielectric function from REELS : Application to GaAs", SURFACE AND INTERFACE ANALYSIS, 45 巻 6 号 (2012)

■超先端電子顕微鏡技術の開発と先進材料応用

[3] M. Haruta, K. Kurashima, T. Nagai, H. Komatsu, Y. Shimakawa, H. Kurata, K. Kimoto, "Visualization of hybridization states with atomic resolution using electron energy loss spectroscopy mapping", Applied Physics Letters, 100, 163107 (2012).

■強磁場固体ＮＭＲ計測技術の開発と先進材料応用

[4] Ryutaro OHASHI, Masayoshi Saito, Takashi Fujita, Toshihito Nakai, Hiroaki Utsumi, DEGUCHI Kenzo, TANSHO Masataka, SHIMIZU Tadashi, "Observation of ^{47,49}TiNMR Spectra of $TiCl_4$/$MgCl_2$ Catalysts under an Ultrahigh Magnetic Field", CHEMISTRY LETTERS, Vol.141, No.12, 1563 ～ 1565

■強力中性子線計測技術の開発と先進材料応用

[5] Noriki Terada, Dmitry D. Khalyavin, Pascal Manuel, Yoshihiro Tsujimoto, Kevin Knight, Paolo G. Radaelli, Hiroyuki S. Suzuki, and Hideaki Kitazawa, "Spiral-Spin-Driven Ferroelectricity in a Multiferroic Delafossite $AgFeO_2$", Phys. Rev. lett. 109, 097203-1-4 (2012).

■放射光を利用した先進計測技術の開発と先進材料応用

[6] Vallerie Ann Innis-Samson and Kenji Sakurai, "Swelling in spin-coated methylcellulose ultra-thin films: effect on film structure, surface topography, and temperature-response property", Soft Matter, 2012, 8, 7351

PHYSICAL REVIEW B **85**, 161302(R) (2012)

Huge steric effects in surface oxidation of Si(100)

Mitsunori Kurahashi and Yasushi Yamauchi
National Institute for Materials Science, 1-2-1 Sengen, Tsukuba, Ibaraki 305-0047, Japan
(Received 5 October 2011; revised manuscript received 13 January 2012; published 19 April 2012)

We report an experimental evidence that the initial sticking probability (S_0) of O_2 on a clean Si(100) surface depends strongly on the alignment of O_2 molecules. S_0 was measured with a single spin-rotational state [$(J,M) = (2,2)$] selected O_2 ($^3\Sigma_g^-$) beam. The temperature and translational energy dependence of S_0 indicate that oxidation via the direct process gives a sticking probability ratio of 1.7 between "helicopter" and "cartwheel" geometries, while the indirect process dominant at low temperatures and translational energies exhibits no appreciable steric effects. The present experiment reveals that oxidation via the direct process occurs only when the molecular axis is nearly parallel to the surface.

DOI: 10.1103/PhysRevB.85.161302 PACS number(s): 68.49.Df, 34.50.Lf, 68.47.Fg, 79.20.Rf

Reactions with molecular oxygen are of vital importance in many fields of natural science such as combustion, atmospheric chemistry, and surface science. Since an O_2 molecule has an anisotropic shape, the final product and/or the rate of oxidation could depend on its relative geometry. However, how such steric effects appear in individual oxidation reactions is not clear at all. For instance, the O_2 adsorption on clean metallic surfaces, although the preference of the geometry in which the O_2 axis is parallel to the surface has been theoretically predicted,[1–3] no such preference has been detected for clean Pd(100)[4,5] and Ag(100)[5] surfaces. The same questions may arise for clean semiconductor surfaces like Si. Indeed, the initial stage of Si oxidation has been studied extensively[6–15] due to its importance in semiconductor technology. No experimental observations, however, have been reported for the steric effects in the Si oxidation. Instead it is known that the O_2 dissociation on Si is quite inefficient and therefore the rate-determining step in the oxide growth.[6] Actually, the initial sticking probability (S_0) of O_2 on Si(100) is <0.2 even at the translational energy (E_{TE}) of 0.3 eV and at the substrate temperature (T_S) of 1000 K.[8] However, the origin of this inefficiency is not understood well. Narrowness of the barrierless channels leading to the O_2 dissociation has been suggested to be one of the origins,[9] but the recent calculation[11] does not support this. The inefficiency in the triplet-singlet conversion of an O_2 molecule moving at a finite velocity has also been considered as another factor.[9,11] It might be reasonable to expect that the low S_0 is associated with the stringent geometrical requirement for the O_2 dissociation, but this is not clear because recent calculations[10,11] have predicted rather low activation barriers (0.1–0.2 eV) for the perpendicular geometry.

In the present study, using a single spin-rotational state-selected O_2 beam developed recently by the authors,[16] we have found that in the case of the direct process, O_2 reacts with a Si(100) surface only when the molecular axis is nearly parallel to the surface. This tendency persists even at $E_{TE} > 0.3$ eV, indicating that the activation barrier for the perpendicular geometry is much higher than 0.3 eV. The present study indicates that an O_2 beam with a definite rotational state permits a quantitative analysis of directionality in O_2-surface interactions.

To investigate the steric effect in oxidation, we need an O_2 beam with a well defined rotational state. A magnetic deflection technique permits the production of such a beam because the magnetic moment of O_2, which originates from its spin, depends also on the rotational angular momentum (K).[16–18] The quantum states of O_2 are represented with the total angular momentum (J) and its field projection (M).[17–19] In the state $(J,M) = (2,2)$, since the rotational state is nearly specified to be $K = 1$ and $M_K = 1$,[16,19] the probability distribution for the O_2 axis direction is approximately equal to the square of the spherical harmonic function $|Y_1^1|^2$ ($\propto \sin^2\theta$),[20] where θ is the polar angle relative to the magnetic field (H) direction [see Fig. 1(a)]. If we prepare an O_2 beam in the (2,2) state and transport it adiabatically to the sample position, we can realize the so-called helicopter/cartwheel geometries by directing H perpendicular/parallel to the surface [see Fig. 1(b)]. Because the molecular axis tends to be parallel to the surface for the helicopter geometry while both parallel and perpendicular configurations occur in the cartwheel geometry, the comparison of these two geometries enables us to discuss the steric effects in O_2-surface interactions. We note that the effect of the rotational motion can be neglected because the rotational energy for the O_2 $K = 1$ state ($\sim$0.3 meV, see Ref. 17) is much smaller than the O_2 translational energies discussed in this study. In the present experiment, the O_2 molecules in the (2,2) state selected by a hexapole magnet[16] were adiabatically transported to the analysis chamber, and the H direction at the sample position was controlled with three pairs of Helmholtz coils. Similar control of the quantization axis with H was successfully conducted for measuring the surface spin polarization with a triplet metastable He beam.[21] The velocity of the (2,2) beam, which was controlled by changing both the ratio of the O_2/He gas mixture in the nozzle and the number of the hexapole magnet elements, was determined with a Stern-Gerlach analysis.[16]

The sticking measurement was performed using the King-Wells method[22] at normal incidence. An ion gauge (IG) was used to monitor the O_2 pressure during the sticking because of its high collection efficiency compared to a quadrupole mass spectrometer (QMS). Measurement with an IG was enabled because of the focusing effect of O_2 by the hexapole magnet, which allows O_2 to be the main content of the gas in the analysis chamber even at a low O_2/He mixing ratio of $<5\%$. The sequence of measurement is illustrated in Fig. 1(c). The O_2 beam was introduced to the analysis chamber at $t = t_1$ with the shutter closed. Both O_2 and He contributed to the pressure rise

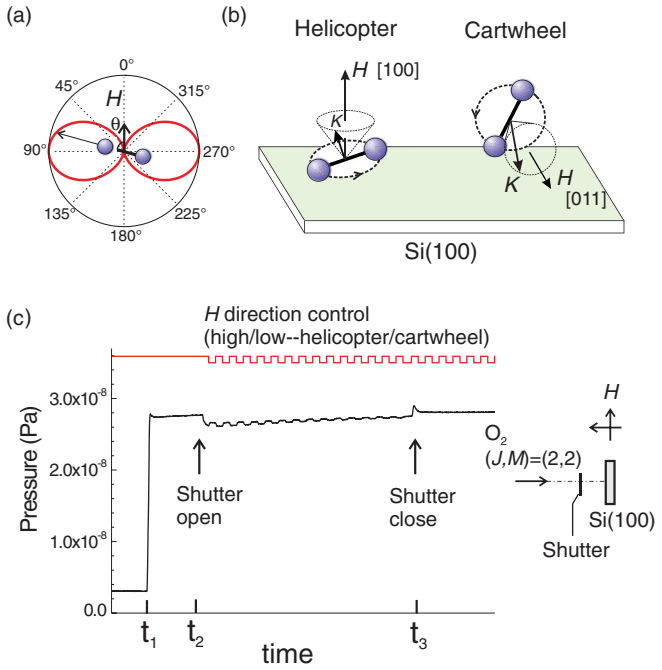

FIG. 1. (Color online) (a) Polar plot of the probability distribution for the angle between the molecular axis of O_2 $[(J,M) = (2,2)]$ with respect to the magnetic field direction. (b) Control of the helicopter and cartwheel geometries by the magnetic field direction. (c) Illustration for the sticking probability measurement and the raw data.

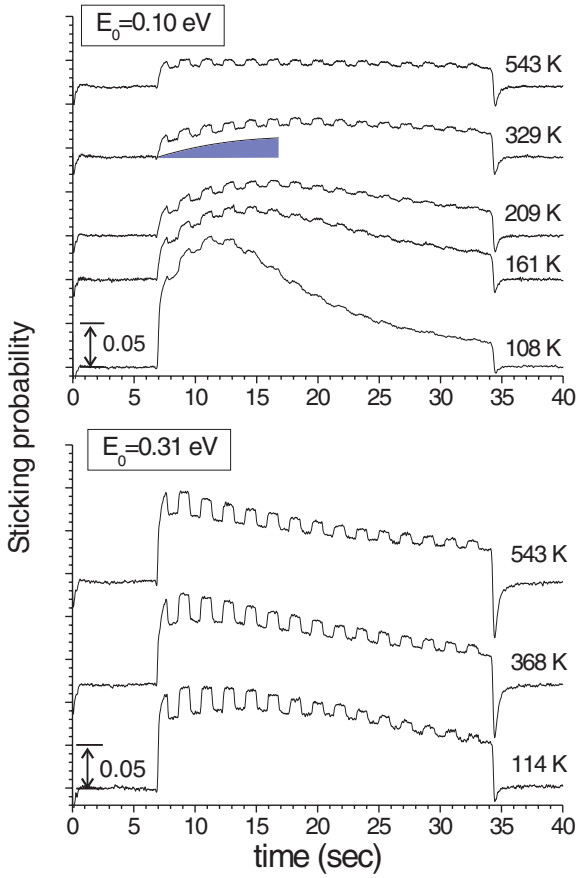

FIG. 2. (Color online) The time evolution of the sticking probability (S) measured at various substrate temperatures. The results for two different translational energies of 0.10 and 0.31 eV are presented.

at $t = t_1$, but the contribution of O_2 $[P(O_2)]$ was determined using a QMS after the sticking measurement. After opening the shutter at $t = t_2$, the pressure decreased by ΔP due to sticking onto the surface. Here, the sticking probability (S) is given by $\Delta P/P(O_2)$. The helicopter/cartwheel geometries [see Fig. 1(b)] were switched by changing the H direction ($|H| = 1$ G) every second following the control signal shown in Fig. 1(c). The IG was shielded with permalloy plates to eliminate the effects of the magnetic field on the ion current. The modulations observed in the IG signal reflect the difference in S between the two geometries. Figure 1(c) shows that the helicopter geometry, which exhibits larger ΔP, results in higher S, indicating that O_2 molecules parallel to the surface are more reactive than those perpendicular to the surface. The pressure recovered when the reaction was stopped by closing the shutter at $t = t_3$. The IG signal showed no modulations after $t = t_3$ although the field switching continued, indicating that the effect of the field change on the IG signal was almost completely removed. The beam flux was set to be $\sim 5 \times 10^{13}$ molecules/cm^2/sec ($\sim$0.04 monolayers/sec) by adjusting the position of the O_2 beam source.

A piece of n-type Si wafer (resistivity <0.02 Ω cm) with a size of $25 \times 5 \times 0.5$ mm was used as a sample. The sample surface was cleaned by direct resistive heating at 1473 K for 10 seconds followed by a gradual cool to 300 K. After this treatment, the low-energy electron diffraction pattern of the surface showed sharp spots corresponding to a clean Si(100) surface. The base pressure of the analysis chamber was better than 5×10^{-9} Pa.

The sticking curves measured at two different E_{TE} show different T_S dependencies similar to previous studies (see Fig. 2).[8,12,13] S decreases drastically with T_S at $E_{TE} = 0.10$ eV, while it is less sensitive to T_S at $E_{TE} = 0.31$ eV [see Figs. 2 and 3(a)]. This behavior has been explained as the coexistence of the precursor-mediated process and the direct process.[8,12,13] The former depends largely on T_S and dominates at lower E_{TE} and T_S, while the latter is insensitive to T_S and dominates at higher E_{TE} and T_S.[8,12,13] Recent molecular dynamics simulations have, however, suggested that the efficient sticking at low E_{TE} and T_S is due to the dynamical steering mechanism in which the low velocity molecules tend to be redirected to preferred orientations at lower T_S.[1,23] In the following, we denote the process mediated by a precursor or the dynamic steering mechanism as the indirect process.

It is necessary to clarify how the indirect and direct processes contribute to the observed difference in S between the helicopter $[S(H)]$ and cartwheel $[S(C)]$ geometries. Note that, although both $S(H)$ and $S(C)$ show definite T_S dependencies especially at $E_{TE} = 0.10$ eV [see Figs. 2 and 3(a)], their difference is nearly temperature independent at $T_S < 300$ K [see Fig. 3(b)]. This indicates that the temperature-independent process, i.e., the direct process, is the main cause of the observed steric effects. In contrast, the ratio $S_0(H)/S_0(C)$ approaches to unity with decreasing $T_S < 300$ K [see Fig. 3(c)], indicating that the indirect process, which becomes dominant at lower T_S, has no appreciable steric effects. If the precursor mechanism is operating, the present results mean that the

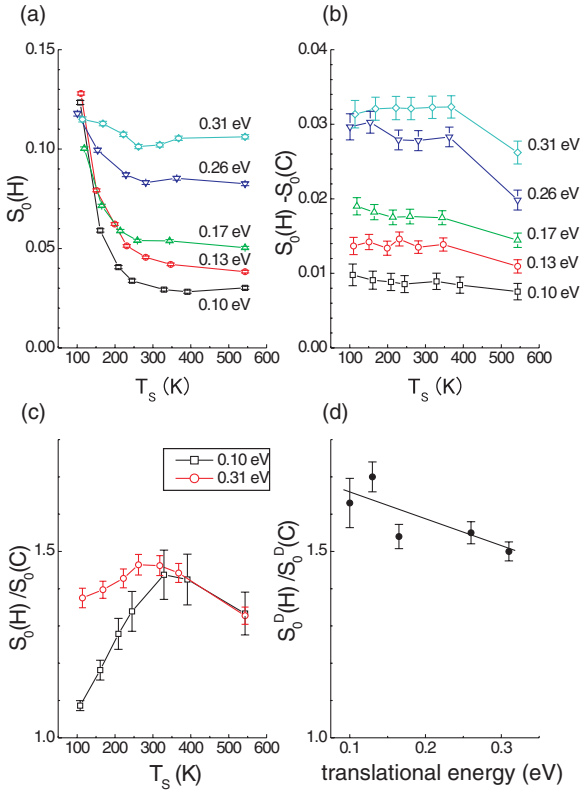

FIG. 3. (Color online) The temperature dependence of (a) S_0 for the helicopter geometry, (b) the difference in S_0 between the helicopter [$S_0(H)$] and cartwheel geometries [$S_0(C)$], and (c) their ratio. (d) The ratio in S_0 estimated for the direct process at various translational energies. The sticking probabilities measured at T_S = 320–360 K were used for the estimate. The line is a guide to the eye.

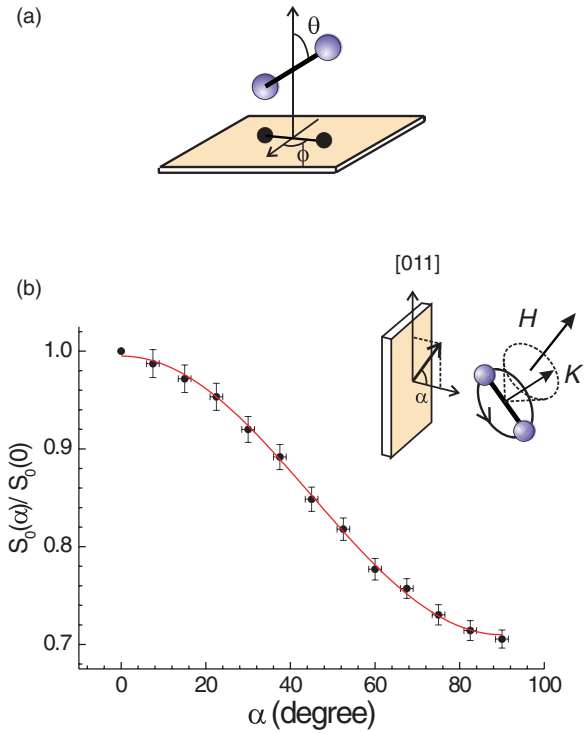

FIG. 4. (Color online) (a) The coordinate of an O_2 molecule relative to the surface. (b) The normalized initial sticking probability measured at E_{TE} = 0.31 eV and T_S = 340–350 K as a function of the polar angle α. The solid curve is a fit to the $\sin^2\alpha$ dependence described in the text.

steric effect in the O_2 trapping process is negligibly weak. Considerable steric effects have been detected in the trapping probability of heteronuclear molecules,[24,25] but such effect might be weaker in homonulear molecules like O_2 because the anisotropy in the molecule-surface interaction potential would be much smaller.

Figure 2 shows that S initially increases, exhibits a broad peak, and then decreases with the exposure time. This means that the surface becomes more reactive to O_2 by adsorbing a small amount of O_2. This tendency is remarkable when the indirect process is dominant, i.e., at lower E_{TE} and T_S. In addition, Fig. 2 shows that S(H)-S(C), which may reflect the contribution of the direct process, decays slowly and monotonically without showing any peaks. Considering these results, the broad peak in S is expected to originate from the indirect process. To the best of our knowledge, there have been no reports on such an initial increase in the oxidation rate of Si(100). It has, however, been reported that Si atoms are ejected toward the surface[14] and that the surface work function decreases at the early stage of oxidation.[15] These phenomena, which have been ascribed to oxygen occupation of the dimer backbond site,[14,15] might be associated with the observed initial increase in the oxidation rate. We note that the S_0 values reported previously[8,13] are larger than those shown in Fig. 3(a). This might originate from the shape of the sticking curve (see Fig. 2). Although our S_0 values are those taken just after opening the shutter, the reported values[8,13] are close to those at the peak. Previous studies[8,13] might be unable to resolve the initial increase in S and took the peak value as S_0.

The steric factor for the direct process [$S_0^D(H)/S_0^D(C)$] can be estimated as follows. Since the sticking curves in Fig. 2 involve the contribution of the indirect process, we need to subtract its contribution (S^I) to derive $S_0^D(H)/S_0^D(C)$. As noted above, the broad peak in the sticking curve can be assigned to the indirect process. A background resulting in the broad peak is shown with a shaded area in the sticking curve measured at T_S = 329 K and E_{TE} = 0.10 eV (see Fig. 2). This corresponds to the lowest estimate for S^I obtained by assuming $S^I = 0$ at the moment of the shutter opening. The steric factor obtained after subtracting S^I estimated in this way [see Fig. 3(d)] can therefore be regarded as the lower limit of $S_0^D(H)/S_0^D(C)$.

How does the chemisorption rate of an incident O_2 molecule (R) depend on the direction of its axis relative to the surface? R may depend on the polar and azimuth angles of θ and ϕ relative to the surface [see Fig. 4(a)]. In the following, however, we neglect the ϕ dependence and later show the validity of this assumption. Considering the probability distribution of the molecular axis direction for the O_2 (2,2) state, the ratio of R averaged over the helicopter (R_H) and cartwheel (R_C) geometries, which is equal to the ratio $S(H)/S(C)$, is given by

$$\frac{R_H}{R_C} = \frac{\int_0^{\frac{\pi}{2}} R(\theta)\sin^3\theta d\theta}{\int_0^{\frac{\pi}{2}} R(\theta)\sin\theta d\theta - \frac{1}{2}\int_0^{\frac{\pi}{2}} R(\theta)\sin^3\theta d\theta}. \quad (1)$$

If the quantization axis for the (2,2) state has a polar angle α relative to the surface normal, the analytical expression for the averaged reaction rate R_α is reduced to $R_\alpha = R_H + (R_C - R_H)\sin^2\alpha$. This relation was verified by measuring S as a function of α [see Fig. 4(b)]. This is also an experimental proof that the quantization axis is successfully controlled using the H direction. We changed the H direction within the surface plane and measured the variation of S to detect the ϕ dependence in R. However, the difference in S between H//[001] and [011] was <1% of S_0. The ϕ dependence can therefore be neglected in the present case.

The characteristics of $R(\theta)$ are analyzed as follows for the direct process. Following Eq. (1), R_H/R_C is equal to 1 when $R(\theta)$ is a constant, while it has a higher limit of 2 when $R(\theta) = \delta(\theta - \pi/2)$. To reproduce the experimental value of $S_0^D(H)/S_0^D(C) \sim 1.7$ [see Fig. 3(d)], $R(\theta)$ therefore needs to have a larger value at around $\theta = \pi/2$. If we assume $R(\theta) = 0$ and 1 at $\theta = 0 - \chi$ and $\chi - \pi/2$, respectively, $\chi = \pi/3$ gives $R_H/R_C \sim 1.7$. This means that in the case of the direct process, only those molecules tilting to the surface plane within 30° react with the Si(100) surface. As mentioned above, because the steric factor shown in Fig. 3(d) gives a lower limit of $S_0^D(H)/S_0^D(C)$, the angular range within which the reaction occurs should be narrower than this. This almost exclusive preference for the parallel geometry is one of the origins for the inefficient O_2 dissociation on Si(100).

We note the followings as to the oxidation mechanism discussed in recent theoretical studies. First, Fig. 3(d) shows that the steric factor doesn't change largely with $E_{TE} < 0.3$ eV, indicating that the activation barrier for the perpendicular ($\theta = 0$) geometry is much higher than 0.3 eV. The activation barrier estimated by recent simulations (0.1–0.2 eV)[10,11] cannot explain this. Second, the E_{TE} dependence of the steric factor in S_0 [see Fig. 3(c)] does not support the triplet-singlet (T-S) conversion model[9,11] suggested for explaining the decrease in S_0 with E_{TE} at <0.1 eV. The decrease of S_0 with E_{TE} has been attributed to the decrease in the T-S conversion rate with the increase of the O_2 velocity based on the Landau-Zener-Stueckelberg theory.[9,11] If this is true, $S_0(H)/S_0(C)$ would not depend on E_{TE} because both S_0(H) and $S_0(C)$ should be proportional to $E_{TE}^{-\frac{1}{2}}$.[9,11] Recent calculations of the O_2 dissociation on Al(111) have indicated that the activation barriers for both the parallel and perpendicular geometries substantially increase by implementing the locally spin-constrained density functional theory.[3,26] Si has no free electrons unlike Al, but similar increase in the activation barrier might occur because Si surfaces have metallic dangling bonds extending toward vacuum. A calculation including both the nonadiabatic effect and the spin selection rule might resolve the inconsistency between the experiment and the theory for the O_2 sticking on Si(100).

In summary, we have clarified the almost exclusive preference for the parallel geometry in the Si(100) oxidation via the direct process. Since the direct process is dominant at high-temperature conditions,[8,12,13] the alignment control of O_2 might be effective for controlling the thermal oxidation of Si used for fabricating high performance devices. The present study has also established a precision method enabling analytical evaluation of the directionality in O_2-surface interactions. Steric effects may play important roles in oxidation processes in which the O_2 dissociative adsorption is inefficient. The present method would be useful to analyze the mechanism of such processes.

The authors are thankful to Masanori Yata and Andrew Pratt for fruitful discussions. This research was supported by the Ministry of Education, Science, Sports and Culture, Grant-in-Aid for Scientific Research (B) (Grant No. 22360021).

[1] A. Groß, A. Eichler, J. Hafner, M. J. Mehl, and D. A. Papaconstantopoulos, Surf. Sci. **539**, L542 (2003).
[2] M. Alatalo, S. Jaatinen, P. Salo, and K. Laasonen, Phys. Rev. B **70**, 245417 (2004); K. Moritani, M. Tsuda, Y. Teraoka, M. Okada, A. Yoshigoe, T. Fukuyama, T. Kasai, and H. Kasai, J. Phys. Chem. C **111**, 9961 (2007).
[3] J. Behler, K. Reuter, and M. Scheffler, Phys. Rev. B **77**, 115421 (2008).
[4] A. Gerbi, L. Savio, L. Vattuone, F. Pirani, D. Cappelletti, and M. Rocca, Angew. Chem. Int. Ed. **45**, 6655 (2006).
[5] L. Vattuone, L. Savio, F. Pirani, D. Cappelletti, M. Okada, and M. Rocca, Prog. Surf. Sci. **85**, 92 (2010).
[6] T. Engel, Surf. Sci. Rep. **18**, 91 (1993).
[7] M. L. Yu and L. A. DeLouise, Surf. Sci. Rep. **19**, 285 (1994).
[8] B. A. Ferguson, C. T. Reeves, and C. B. Mullins, J. Chem. Phys. **110**, 11574 (1999).
[9] K. Kato, T. Uda, and K. Terakura, Phys. Rev. Lett. **80**, 2000 (1998).
[10] X. L. Fan, Y. F. Zhang, W. M. Lau, and Z. F. Liu, Phys. Rev. Lett. **94**, 016101 (2005).
[11] A. Hellman, Surf. Sci. **603**, 173 (2009).
[12] T. Miyake, S. Soeki, H. Kato, T. Nakamura, A. Namiki, H. Kamba, and T. Suzaki, Phys. Rev. B **42**, 11801 (1990).
[13] M. Yata, Y. Uesugi-Saitow, M. Kitajima, A. Kubo, and V. E. Korsukov, Phys. Rev. Lett. **91**, 206103 (2003); M. Yata, Phys. Rev. B **81**, 205402 (2010).
[14] D. G. Cahill and P. Avouris, Appl. Phys. Lett. **60**, 326 (1992).
[15] S. Ogawa and Y. Takakuwa, Surf. Sci. **601**, 3838 (2007).
[16] M. Kurahashi and Y. Yamauchi, Rev. Sci. Instrum. **80**, 083103 (2009).
[17] N. A. Kuebler, M. B. Robin, J. J. Yang, A. Gedanken, and D. R. Herrick, Phys. Rev. A **38**, 737 (1988).
[18] V. Aquilanti, D. Ascenzi, D. Cappelletti, and F. Pirani, Nature (London) **371**, 399 (1994).
[19] M. Tinkham and M. W. P. Strandberg, Phys. Rev. **97**, 937 (1955).
[20] H. W. Kroto, *Molecular Rotation Spectra* (Dover, New York, 2003).
[21] M. Kurahashi, T. Suzuki, X. Ju, and Y. Yamauchi, Phys. Rev. B **67**, 024407 (2003).
[22] D. A. King and M. G. Wells, Surf. Sci. **29**, 454 (1972).
[23] A. Gross, S. Wilke, and M. Scheffler, Phys. Rev. Lett. **75**, 2718 (1995).
[24] T. J. Curtiss, R. S. Mackay, and R. B. Bernstein, J. Chem. Phys. **93**, 7387 (1990).
[25] U. Heinzmann, S. Holloway, A. W. Kleyn, R. E. Palmerk, and K. J. Snowdon, J. Phys.: Condens. Matter **8**, 3245 (1996).
[26] J. Behler, B. Delley, S. Lorenz, K. Reuter, and M. Scheffler, Phys. Rev. Lett. **94**, 036104 (2005).

Research article

SURFACE and INTERFACE ANALYSIS

Received: 25 September 2012 Revised: 8 November 2012 Accepted: 10 November 2012 Published online in Wiley Online Library: 8 January 2013

(wileyonlinelibrary.com) DOI 10.1002/sia.5196

Evaluation of robustness to surface conditions of the target factor analysis method for determining the dielectric function from reflection electron energy loss spectra: Application to GaAs

H. Jin,[a] H. Shinotsuka,[a] H. Yoshikawa,[a]* H. Iwai,[a] M. Arai,[a] S. Tanuma[a] and S. Tougaard[b]

Target factor analysis (TFA) of a series of angle-resolved reflection electron energy loss spectra (REELS) was recently demonstrated to be a useful method to determine bulk energy loss functions (ELFs), which by the TFA are separated from the surface-loss structures of REELS. The dielectric function is then readily derived by Kramers–Kronig analysis of the ELF. The advantage of the method compared with other methods, which are also based on the analysis of REELS, is that the condition of the outermost surface region is unimportant because the excitations that occur there are removed by the TFA and ideally a pure bulk component is determined. Our method is thus particularly useful for determining the ELF from compound materials that are hard to clean without modifying the outermost atomic layers. In this paper, the robustness of the method was studied by applying it to three GaAs samples with different surface compositions caused by different surface cleaning methods. The results showed that when electrons of energy 3000–4500 eV were used, the resulting bulk ELFs were essentially identical except for small differences for the sample that had the largest thickness of the modified surface layer. It is concluded that this is a useful method, provided that the thickness of the modified layer is kept to a minimum by using shallow angle sputtering and by using REELS electrons at a sufficiently high energy that a major part of the electron trajectories are at a depth larger than the thickness of the modified surface layer.

Keywords: REELS; factor analysis; dielectric function; energy loss function; GaAs

Introduction

Dielectric functions or optical constants (OCs) are essential for describing interactions between electrons and materials.[1,2] Furthermore, energy loss functions (ELFs), which are calculated from dielectric functions or OCs, are fundamental physical quantities needed to obtain the electron inelastic mean free paths (IMFP) and stopping powers in solids.[3–7] There are several ways to determine the dielectric functions of materials. The most common method is based on optically measured data. However, optical data tables found in handbooks usually consist of a combination of various data sets from different publications, and for many materials, there are no data in the 20–50 eV energy range.[8]

Different methods are currently applied to determine the dielectric function from analysis of reflection electron energy loss spectra (REELS).[9–13] Because REELS is very surface sensitive, these methods require a clean surface and for compound materials a stoichiometric composition of the outermost few atomic layers of the material. For elemental solids, it is usually not a problem to produce clean surfaces. However, for compounds and oxides, it is very difficult because traditional cleaning methods, which involve either chemical cleaning or ion bombardment of the surface to remove surface contaminants, are likely to alter the composition of the outermost layers. In addition, ion bombardment will produce damage of the crystal lattice and cause atomic mixing in a surface region. Compounds and oxides are therefore likely to either have a surface contamination layer or a changed composition in the outermost few atomic layers. It is therefore questionable if these REELS-based methods can be applied to determine the dielectric function of compounds and oxides.

In a previous paper,[14] we proposed a simple and efficient method for determining the OCs of a target material with target factor analysis (TFA) of angle-resolved REELS (AR-REELS). This method was applied to the analysis of AR-REELS of Si and SiO_2 specimens and was superior to other methods because it did not require theoretical information about the surface excitation effect or surface ELF and was less sensitive to the exact conditions in the outermost few nanometers of the sample than REELS

* *Correspondence to: H. Yoshikawa, National Institute for Materials Science, 1-2-1 Sengen, Tsukuba, Ibaraki 305-0047, Japan. E-mail: YOSHIKAWA.Hideki@nims.go.jp*

a *National Institute for Materials Science, 1-2-1 Sengen, Tsukuba, Ibaraki 305-0047, Japan*

b *Department of Physics and Chemistry, University of Southern Denmark, DK-5230 Odense M, Denmark*

analyses by electron beam with an energy much less than 2 keV. This method enables us to determine experimentally the bulk ELF from a series of AR-REELS. In the present paper, we investigate the extent to which this method is able to produce the same dielectric function when applied to REELS from three GaAs samples that have different surface-altered layers.

The altered layer may be expected to be 1–5 nm thick, and for the method to be applicable, it is necessary that the electrons in the REELS experiment reach sufficiently large depths to make sure that they have spent a significant part of their total trajectory in the bulk region of the sample. For a 4000 eV electron, the IMFP in GaAs is approximately 7 nm, as estimated by the TPP-2M predictive IMFP formula.[15] Thus, electrons in this energy range should ensure that the electrons will carry information on the energy loss processes in the bulk of the material. For this method to be valid, the determined bulk ELF must be independent of the surface condition of the specimen. One of the purposes of this paper is to investigate to what extent this assumption is true.

To this end, we have investigated the effect of surface cleaning on the determination of the ELF for a GaAs specimen with AR-REELS. We used two cleaning procedures. One method is the commonly used Ar^+ sputtering method. However, its use is likely to result in crystal defects and compositional changes in the near-surface region. The other cleaning method we used involves washing the GaAs specimen with running deionized water with ultrasonic vibrations. This method was previously shown to produce a damage-free surface.[16–18]

To minimize the problems, we want to use low-energy Ar^+ sputtering at a shallow incident angle to reduce the depth of the damaged layer. Therefore, we used the TFA method to derive the ELFs and OCs from a series of AR-REELS for GaAs samples cleaned by Ar^+ sputtering and by the damage-free deionized-water cleaning method, respectively, and compared the results to investigate the possibility of using ion-sputter cleaning at a low-energy and shallow incident angle. The primary energies of the electron beam were 3000, 4000, and 4500 eV, which are higher than for a conventional REELS measurement. They were chosen to ensure that part of the electron trajectory was in a range beyond the depth at which the surface was damaged. At low primary electron energies, the coupling between surface and bulk excitations has a strong effect even for an undamaged surface, and an accurate description of this requires a more involved model.[9,12,19] This is another reason why we used a higher-energy electron beam to obtain bulk ELFs as simply as possible.

Experiments and analysis procedures

Commercial single-crystal *p*-type GaAs(100) (doped with Zn) specimens were cleaned by Ar^+ sputtering or ultrasonic running deionized water (URDIW), because an untreated GaAs surface includes native oxides. Ar^+ sputtering was performed for 15 and 50 min, respectively under two sets of conditions for the incident energy and angle: a normal condition (2000 eV, 30°) and a mild condition (1200 eV, 7°). The incident angles of Ar^+ ion beam were measured with respect to the surface plane. The ion beam energy of 1200 eV was the lower limit of our equipment. For comparison, another specimen was cleaned using URDIW, which is a promising procedure for cleaning III–V semiconductor compounds.[16–18] It can produce an oxide-free and damage-free GaAs surface within 1 h. The oxygen dissolved in the deionized water plays an important role, and the Ga and As oxide removal rates are greatly increased by reducing the dissolved oxygen concentration in the deionized water. This deoxygenation was achieved by N_2 gas bubbling. First, the sample was chemically etched in $NH_4OH : H_2O_2 : H_2O = 1 : 1 : 50$ solution for 1 min and then rinsed with deionized water. Next, the etched sample was placed in a vessel and immersed for 1 h in running deionized water with ultrasonic vibration. The deionized water was deoxygenated in a container by bubbling N_2 gas through it. The URDIW cleaning was undertaken in a glove box filled with N_2 gas. Quantitative XPS analysis showed that the composition of the GaAs surface after URDIW cleaning was stoichiometric. On the other hand, the atomic composition of the GaAs specimen after ion sputtering was slightly Ga rich in the surface region. Ga oxide and As oxide XPS peaks were not detected for the GaAs samples cleaned by URDIW and ion sputtering.

The angle-resolved and primary-energy-dependent REELS measurements were performed for GaAs specimens cleaned by normal Ar^+ sputtering, mild Ar^+ sputtering, and URDIW. The electron incident angle for REELS was fixed at 30° to the surface normal. The emission angles were changed from 15° to 75° with respect to the surface normal by rotating the inclined specimen holder. The primary electron beam energies were varied from 3000 to 4500 eV. The geometry and details of the REELS measurements are reported in our previous work.[20,21]

A set of angle-dependent effective cross-section for single inelastic scattering determined by analysis of the REELS with the method described in Tougaard and Chorkendorff[22] was used to form a data matrix, which was analyzed with the TFA method. TFA is usually accomplished in two main steps: principal component analysis (PCA) and target transformation (TT), which are described in the next section. The details can be found in our previous work.[14,23]

Results and discussion

Experimental reflection electron energy loss spectra and effective single inelastic scattering cross-sections

Figure 1 compares REELS for URDIW-cleaned GaAs (row a), GaAs cleaned by Ar^+ sputtering at an incident angle of 7° (row b) and 30° (row c) at various emission angles from 15° to 75° for primary electron beam energies of 3000, 4000, and 4500 eV. All the spectra were normalized at the elastic peaks. The reflected electrons in REELS lose energy as a result of plasmon excitations or single-electron transitions from the valence band or from a core level to the conduction band. There are three main characteristic features in the REELS for GaAs. The bulk-plasmon excitation is at approximately 16.2 eV for URDIW-cleaned GaAs and at approximately 15.8 eV for Ar^+ sputtered GaAs (row b). In addition, a small peak at about 21 eV, which is superimposed on the tail, results from a transition from the Ga 3*d* core level to the conduction band.[24,25] A double bulk-plasmon excitation peak at about 32.4 eV is clearly observed for URDIW-cleaned GaAs and at about 31.6 eV for ion-sputter-cleaned GaAs. The REELS obtained for ion sputtering shows strong surface-plasmon excitation at about 11 eV for high emission angles. The REELS for GaAs cleaned with deionized water shows no strong surface-plasmon excitation peak.

A comparison with the REELS for Ar^+ sputtered GaAs shows that the peak at about 11 eV is slightly smaller for the sample sputtered at a shallow incident angle of 7°. It is known that ion sputtering changes the surface composition of GaAs, and the top surface layer of the sputtered specimen will be Ga rich. To be more specific, XPS analysis with Mg *Kα* X-rays indicated that the composition ratio of

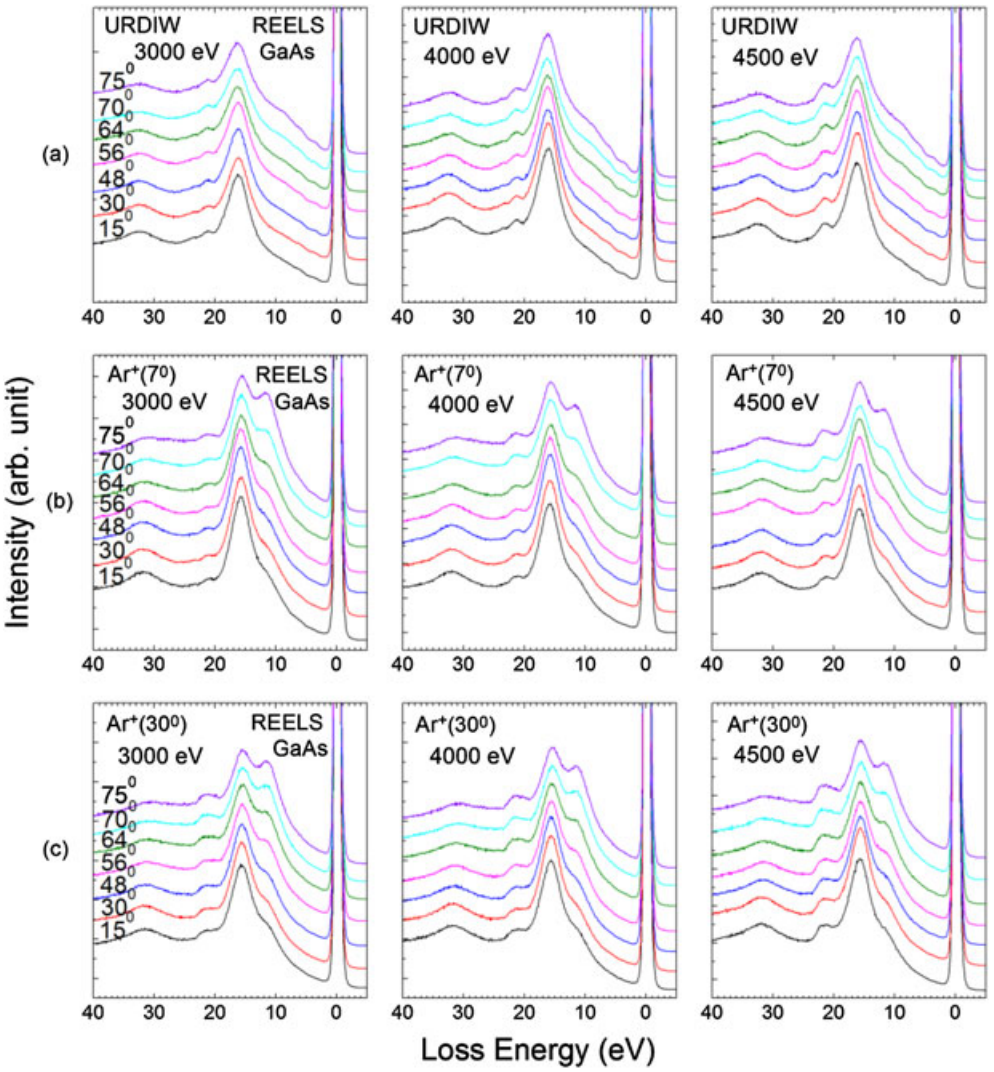

Figure 1. Reflection electron energy loss spectra (REELS) of GaAs at various emission angles from 15° to 75° at primary electron energies of 3000, 4000 and 4500 eV for GaAs cleaned by ultrasonic running deionized water (URDIW) (row a) and GaAs cleaned by Ar^+ sputtering at incident angles of 7° (row b) and 30° (row c).

Ga/As were 1.52 in the normal sputtering condition and 1.40 in the mild sputtering condition. This result shows that the altered surface Ga-rich layer becomes thinner as the ion beam energy and incident angle decrease. So we expect the negative effects of sputter cleaning to be smaller for GaAs cleaned by 1200 eV Ar^+ sputtering at an incident angle of 7°. For URDIW-cleaned GaAs, the ratio of Ga/As was 1.0 (stoichiometric), and the surface oxidation of GaAs was negligible because no chemical shifts of the Ga and As peaks were observed. However, a small amount of oxygen (O 1s peak at 532.3 eV) and carbon residues (C 1s peak at 285.0 eV) remained on the GaAs surface, and the O 1s peak can be assigned to a monolayer of water molecules.[26]

Figure 2 shows the effective cross-section for single inelastic scattering $K(\Delta E)$ multiplied by the IMFP $\lambda(E)$ for URDIW-cleaned GaAs and GaAs cleaned by Ar^+ sputtering at incident angles of 7° and 30°. These $\lambda(E)K(\Delta E)$ distributions were derived from the aforementioned REELS using the QUASES-XS-REELS software,[22,27] which removes the contribution of multiply scattered electrons and provides an effective single inelastic scattering cross-section $K(\Delta E)$. $K(E, \Delta E)$ is the probability that an electron of kinetic energy E will lose energy ΔE per unit energy loss and per unit path length when traveling in a solid. Because multiple-scattering features are removed in the $\lambda(E)K(\Delta E)$ spectra, it is easier to interpret the electronic excitations. From these $\lambda(E)K(\Delta E)$ spectra, we can see that the bulk-plasmon peak position at about 15.6 eV for Ar^+-sputtered GaAs (row *b*) is at a slightly smaller energy than that for URDIW-cleaned GaAs (row *a*) at about 16 eV, which can be compared with the previously measured bulk-plasmon peak of 15.8 eV for single crystalline GaAs.[28] There is a weak hump at 21 eV related to Ga 3*d* core level excitation. The weak structures at about 4 and 6 eV are attributed to interband transitions from the valence band to the conduction band.[29] For URDIW-cleaned GaAs, these $\lambda(E)K(\Delta E)$ spectra show only small variations in the bulk-loss and surface-loss intensities as a function of emission angle and primary beam energy (see row *a* in Fig. 2). The surface-loss peak is very weak, which is probably due to damping caused by a monolayer of adsorbed water molecules. In contrast to this result, the $\lambda(E)K(\Delta E)$ spectra for Ar^+ sputtered GaAs show that the surface-plasmon peak intensity changes continuously with variation in the emission angle for ion sputtering at an incident angle of 30°. However, with ion sputtering at 7°, there is a substantial increase in the surface peak intensity at emission angles larger than 70°. This behavior shows that GaAs cleaned by shallow incident Ar^+

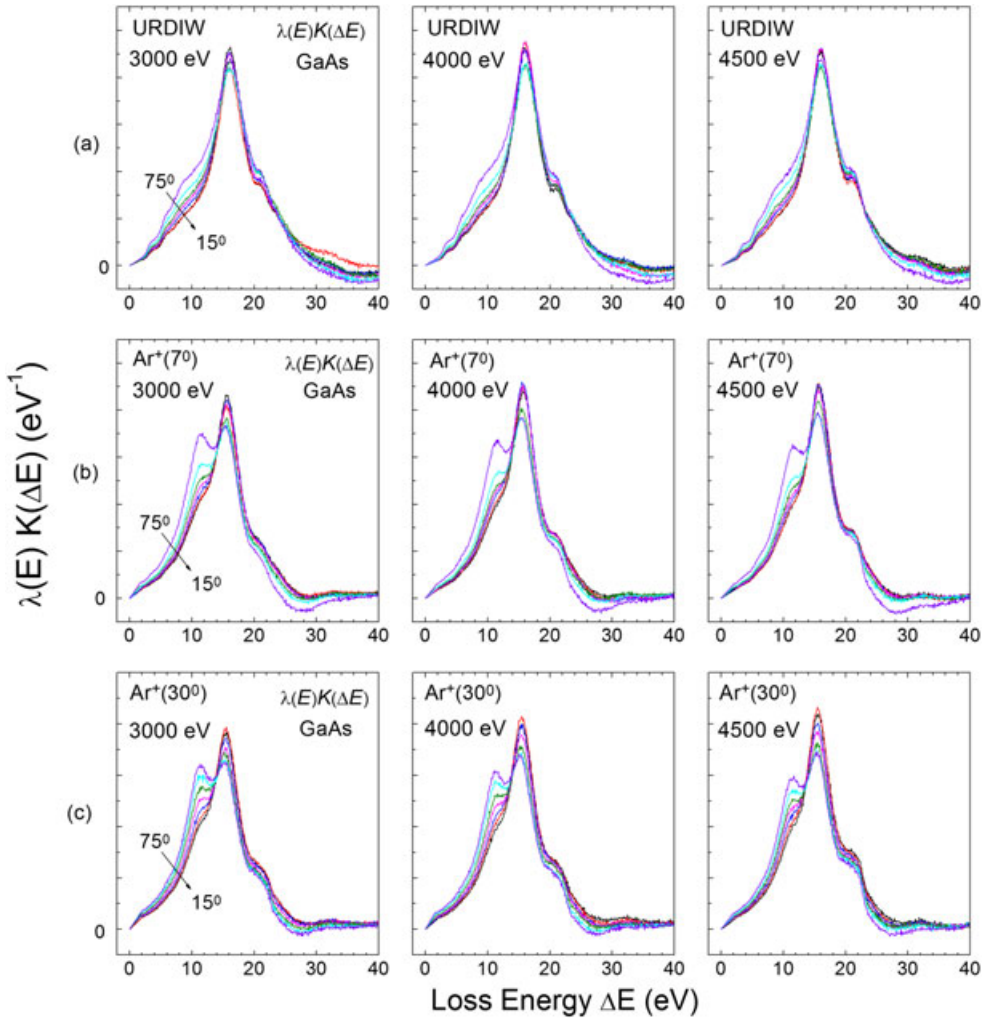

Figure 2. Series of effective cross-sections $\lambda(E)K(\Delta E)$ for single inelastic scattering for GaAs obtained from the corresponding reflection electron energy loss spectra in Fig. 1. The dependence of the cross-sections on the electron emission angles with respect to the surface normal is shown. URDIW, ultrasonic running deionized water.

sputtering has a thinner damaged surface layer and that the shallow-angle and low-energy sputtering conditions are clearly milder and more effective.

Target factor analysis of effective single inelastic scattering cross-sections

The TFA was performed on sets of $\lambda(E)K(\Delta E)$ distributions corresponding to the three cleaning methods to extract the bulk-loss component. In the first PCA step, $\lambda(E)K(\Delta E)$ spectra for different emission angles at the same primary beam energy were placed in a data matrix.[14,23] Figure 3(a) shows the distribution of determined eigenvalues on a logarithmic scale for each data matrix for URDIW-cleaned GaAs. There are seven eigenvalues for each data matrix because we have seven spectra for each energy. To obtain the size of the true factor space, we used the variance $\left(\text{variance}=x_i/\sum_{j=1}^{n}x_j\right)$ to determine the number of main factors.[30] x_i is the ith eigenvalue, and $n=7$ is the total number of eigenvalues. In practice, eigenvectors with large variances are considered to be primary eigenvectors. For example, for the data matrix at 4000 eV, the sum of the first two variances is 0.9998, which suggests that the $\lambda(E)K(\Delta E)$ spectra can be expressed as a linear combination of the first and second abstract factors. Figure 3(b) shows the two main abstract factors of each data matrix. Note that possible electron diffraction effects, which occur for the URDIW-cleaned GaAs, does not disturb the PCA analysis, because this is expected to only influence the relative intensity but not the spectral shape of each of the two factors corresponding to surface and bulk excitations. Figures 3(c, d) and 3(e, f) are the eigenvalues and abstract factors for GaAs cleaned with Ar^+ at incident angles of 7° and 30°, respectively. For all three samples, the results show that the first two eigenvalues are major and that the factor space can therefore be reduced to two dimensions. The two main abstract factors in Fig. 3(b, d, f) contain peaks or troughs at energy loss positions corresponding to the surface-plasmons and bulk-plasmons, and interband transitions. The abstract factors determined from this multivariate statistical analysis are a solution to the problem in the sense that a linear combination of these two factors will give an almost perfect fit to the spectra. However, the abstract factors are an accidental mixture of the corresponding physical factors that correspond to surface and bulk excitations. To determine the physical factors, the two abstract factors are transformed into physically meaningful factors by TT. This transformation was accomplished by rotating the axes of the two abstract factors. The

SURFACE and INTERFACE ANALYSIS

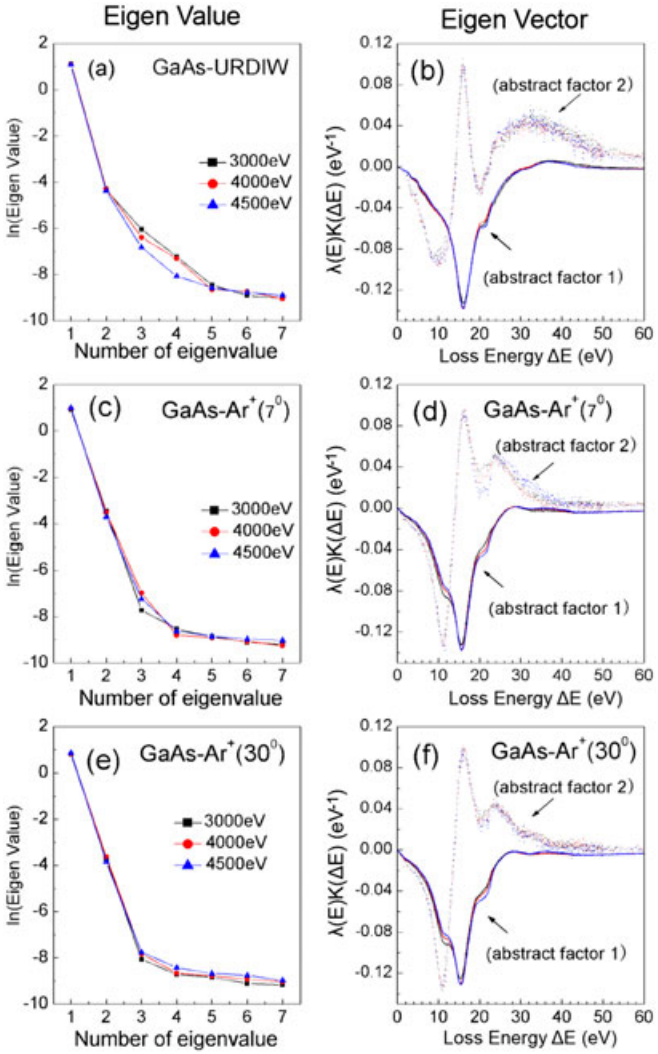

Figure 3. Results of principal component analysis of a series of effective cross-sections for single inelastic scattering in GaAs in Fig. 2. (a) The eigenvalues for data matrices versus eigenvalue number at primary energies of 3000, 4000, and 4500 eV for GaAs cleaned by ultrasonic running deionized water (URDIW) are shown on a logarithmic scale. (b) shows the resulting main two eigenvectors (i.e. abstract factors) corresponding to the first and second eigenvalues in (a). (c) and (d) are the eigenvalues and eigenvectors (i.e. abstract factors), respectively, for GaAs cleaned by Ar^+ with an incident angle of 7°. (e) and (f) are the eigenvalues and eigenvectors (i.e. abstract factors), respectively, for GaAs cleaned by Ar^+ with an incident angle of 30°.

basic abstract factor space determined in PCA is orthogonal. Therefore, a two-dimensional abstract transformation matrix $T = \begin{pmatrix} \cos\theta & -\sin\theta \\ \sin\theta & \cos\theta \end{pmatrix}$, involving an orthogonal rotation angle θ, is first applied. In this TT procedure, we must take advantage of some known information about the materials as criteria for placing important constraints on the rotation of the abstract factor axes to obtain the physical factors. First, we performed an orthogonal rotation to obtain the first physically meaningful real factor corresponding to the bulk-loss component. To determine the orthogonal rotation angle for the bulk-loss component, we utilized the position of the bulk-plasmon loss peak of GaAs, that is to say, the plasmon peak, and the shape of bulk-plasmon fitted with a Lorentzian function on the low-energy side of the bulk-loss component as criteria.[14,23] For instance, for URDIW-cleaned GaAs, the eigenvectors for the data matrix at 4000 eV were rotated 198° to satisfy these criteria. For Ar^+ ion sputtered GaAs, the abstract factor of the data matrix at 4500 eV was rotated 201° for 7° and 203° for 30° sputtering to satisfy these criteria. With this orthogonal rotation, we obtained the bulk-loss component. To determine the other physical factor corresponding to the surface-loss component, we performed an oblique rotation (with rotation angle φ) of one factor axis under the condition that the other factor axis corresponding to the bulk-loss component was fixed. The criterion used for this oblique rotation was that the surface-plasmon loss peak of GaAs was at about 11 eV.

After the coordinate rotation of the two primitive abstract factors, the surface-loss and bulk-loss components were obtained. Figure 4 (a) compares the bulk-loss and surface-loss components derived by TT of the abstract factors for the data matrices at 3000, 4000, and 4500 eV for URDIW-cleaned GaAs. Figure 4(b, c) shows TT results for GaAs cleaned by Ar^+ at incident angles of 7° and 30°, respectively. The surface-loss and bulk-loss components are nearly independent of these primary electron energies. This fact implies

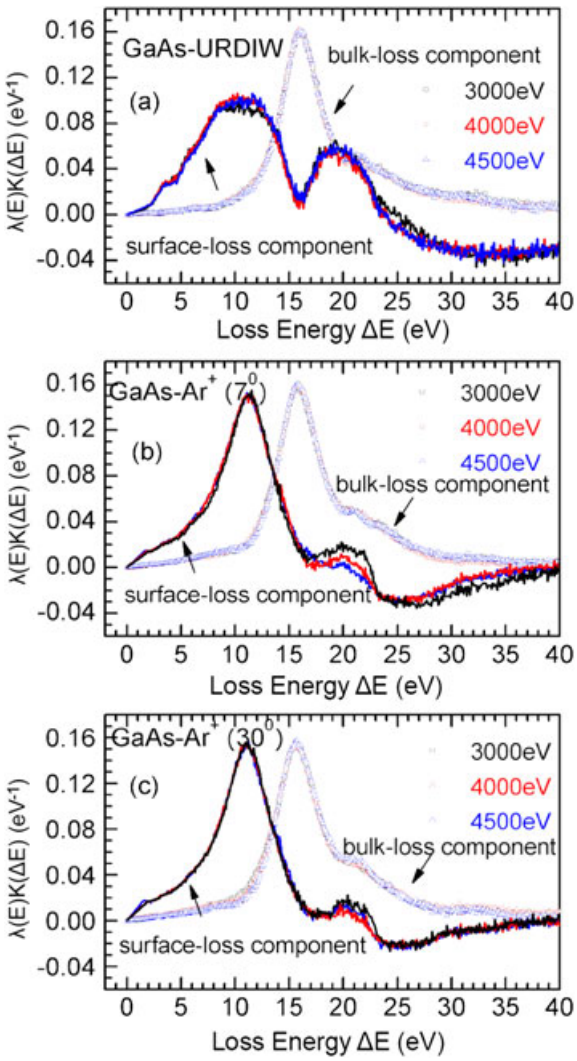

Figure 4. The two most important physical factors (i.e. bulk-loss and 'surface'-loss components) obtained by target transformation of abstract factors for GaAs in Fig. 3(b), (d) and (f). (a) is obtained from Fig. 3(b) for GaAs cleaned with ultrasonic running deionized water. (b) is obtained from Fig. 3(d) for GaAs cleaned with Ar^+ at an incident angle of 7°. (c) is obtained from Fig. 3(f) for GaAs cleaned with Ar^+ at an incident angles of 30°. URDIW, ultrasonic running deionized water.

that the method is reasonable when the matrices are grouped by primary beam energies. As a further test, we found that the original $\lambda(E)K(\Delta E)$ spectra were all well reproduced by a linear combination of these two loss components.

Note that the 'surface-loss' component in Fig. 4 is not a simple surface-loss spectrum (e.g. surface plasmon) and that its shape is not directly related to the bulk-loss spectrum. It consists of all components except the bulk-loss component. This situation means that the 'surface-loss' component originates from energy loss at the altered surface layer and that this component can also be affected by possible contributions from coupling between surface and bulk excitations[12,19] and any errors originating from the approximations in the handling of multiple-scattering components for the procedure applied to determine $\lambda(E)K(\Delta E)$.[22] The observed difference in surface components in Fig. 4 simply shows that the conditions at the surface are very different for the three samples depending on the cleaning methods. In contrast, the bulk loss is practically identical for all three samples. This result shows that the proposed TFA of the REELS procedure for determining the bulk ELF is valid even when the surface layers are very different. As a result, it should be particularly useful for compounds that are hard to clean without destroying the outermost few atomic layers.

As mentioned previously, it is important to use shallow sputter conditions at not too high an energy to reduce the extension of the damaged region and to use rather high (>3000 eV) electron energies to make sure that the electrons spend part of their trajectory in the deep regions beyond the altered surface layer.

Bulk energy loss function and sum rules

The bulk component extracted for $\lambda(E)K(\Delta E)$ is restated as $\lambda(E)K_{\text{bulk}}(\Delta E)$, that is to say the normalized differential inverse IMFP,[31] hereafter. The bulk ELFs of GaAs specimens in the low energy-loss range (typically less than about 100 eV) can be obtained from the bulk-loss component of the TFA analysis. We used an iterative calculation to derive the bulk ELF from $K_{\text{bulk}}(\Delta E)$ using the following relationship:[8]

$$K_{\text{bulk}}(E,\hbar\omega)=\frac{1}{\pi E a_0}\int_{q_-}^{q_+}\frac{dq}{q}\text{Im}\left\{\frac{-1}{\varepsilon(q,\omega)}\right\} \tag{1}$$

where E is the primary electron energy, $\hbar\omega=\Delta E$ and q are the energy loss and momentum transfers in an inelastic scattering event, respectively, and a_0 is the Bohr radius. The bulk ELFs were derived by this iterative procedure where test ELFs lead to good agreement between the normalized $K_{\text{bulk}}(\Delta E)$ calculated from test ELFs on the basis of Eqn (1) and extracted from TFA. In this calculation, the q-dependency in Eqn (1) was treated by the single-pole approximation.[9] Figure 5 (a) shows the resulting normalized bulk ELFs for URDIW-cleaned GaAs and for GaAs cleaned by Ar^+ sputtering at incident angles of 7° and 30°.

To obtain the real ELF for bulk GaAs, we have to determine the scaling or normalizing factor α. For this purpose, we can apply f-sum and Kramers–Kronig (KK)-sum rules[33] for ELFs.[14] However, the ELF from the REELS experiment only covers energy losses up to about 30 eV, because beyond that it has a very small intensity that is comparable with the experimental error. For energy losses larger than 30 eV, we calculated the ELF for a GaAs bulk specimen from the atomic scattering factors for X-rays for Ga and As, which were taken from the database compiled by Henke *et al.*[32]

The scaling factor α is multiplied by the normalized bulk ELF determined from REELS (in the energy loss range less than 30 eV) to obtain the bulk ELF on an absolute scale. The scaling factor α was thus determined by the following f-sum and KK-sum rules.[33]

f-sum rule:

$$\frac{2}{\pi\hbar^2\Omega_p^2}\times\left\{\int_0^{E_x}\alpha\cdot\Delta E\cdot\text{Im}\left\{-1/\varepsilon(\Delta E)_{\text{expr.}}\right\}d(\Delta E)+\int_{E_x}^{\infty}\Delta E\cdot\text{Im}\{-1/\varepsilon(\Delta E)\}_{\text{Henke's}}d(\Delta E)\right\}=Z_{\text{eff}} \tag{2}$$

where $\Omega_p=(4\pi\, n_a e^2/m)^{1/2}$, $n_a=N_a\,\rho/A$ is the density of atoms or molecules, N_a is Avogadro's number, ρ is the bulk density, A is the atomic weight, $\Delta E=\hbar\omega$, and Z_{eff} is the effective number of electrons per molecule contributing to the inelastic scattering, which is 64 for GaAs. E_x is 30 eV, and $\text{Im}\{-1/\varepsilon(\Delta E)\}_{\text{Henke's}}$ is the ELF calculated from Henke's data.

KK-sum rule:

$$\frac{2}{\pi}\times\left\{\int_0^{E_x}\frac{\alpha\cdot\text{Im}\{-1/\varepsilon(\Delta E)\}_{\text{expr.}}}{\Delta E}d(\Delta E)+\int_{E_x}^{\infty}\frac{\text{Im}\{-1/\varepsilon(\Delta E)\}_{\text{Henke's}}}{\Delta E}d(\Delta E)\right\}+\frac{1}{n(0)^2}=1, \tag{3}$$

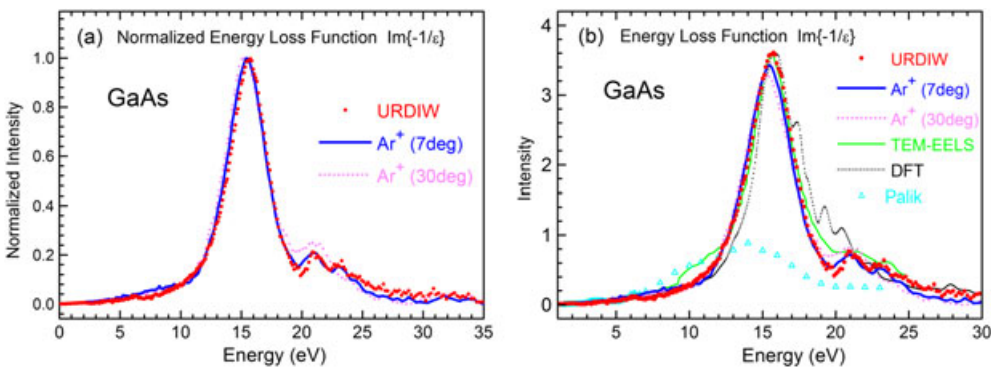

Figure 5. (a) Normalized energy loss functions determined from the bulk-loss components in Fig. 4 for GaAs cleaned with the ultrasonic running deionized water (URDIW) method and GaAs cleaned with Ar^+ at incident angles of 7° and 30°, respectively. (b) Energy loss functions (ELFs) on an absolute scale for GaAs cleaned with Ar^+ at incident angles of 7° and 30°, and with URDIW obtained by applying the constraints of the f-sum and Kramers–Kronig-sum rules to normalized ELFs. (b) also shows reference ELFs: TEM-EELS data (TEM-EELS),[34,35] density function theory calculation results (DFT), and optical data (Palik).[8] TEM-EELS, electron energy loss measurements using transmission electron spectroscopy.

where $n(0) = 3.606$ for GaAs[8] is the refractive index in the low-energy limit. The resulting ELFs are shown in Fig. 5(b). The scaling factor α is determined as the value that gives the smallest average error for both the f-sum and KK-sum errors. The resulting scaling factor was $\alpha = 3.62$ for URDIW-cleaned GaAs. The errors in the f-sum and KK-sum rules are −2.61% and 0.15%, respectively. On the other hand, the scaling factors for GaAs cleaned with Ar^+ at incident angles of 7° and 30° are $\alpha = 3.34$ and 3.33, respectively, and the errors in the f-sum and KK-sum rules are −3.46%, 0.13% and −3.48%, 0.08%, respectively.

In Fig. 5(b), we compare the resulting ELFs with previous ELFs that were obtained by electron energy loss measurements using transmission electron spectroscopy (TEM-EELS),[34,35] by calculation with density function theory (DFT), and by Palik's compiled optical data.[8] The DFT calculations were performed with the WIEN2k code.[36] Details of the DFT calculations will be published elsewhere.

The ELF from Palik's database is very different from the other ELFs in the 10–25 eV energy loss range, and its errors in the f-sum and KK-sum rules are −13% and −37%, respectively. This result is most likely due to the difficulties involved in past optical measurements in the vacuum ultraviolet energy region above 10 eV. The present ELF is in good agreement with ELFs from TEM-EELS except in the 9–12 eV energy region. The DFT calculation does not show any obvious structure in this energy region. We therefore expect this structure to be due to an artifact in the TEM-EELS data, which may be due to the surface conditions and to the treatment of surface excitations in that analysis.

There are doublet structures in the ELF at about 21 and 23 eV for URDIW-cleaned GaAs and shallow-sputter-cleaned GaAs, which are due to interband transitions from the Ga 3*d* core level to the conduction band. This structure is not resolved in the ELF of GaAs sputter cleaned at an incident angle of 30°, which shows a broad peak around 20–25 eV. The thickness of the modified surface layer is larger for the latter sample compared with the sample sputter cleaned at 7° incidence angle, and it is quite probable that the modified layer is larger than the depth reached by the majority of the 4500 eV electrons used in the REELS experiment. We therefore conclude that the doublet peaks at 20–25 eV originate from the bulk of the GaAs specimen. Further evidence for this conclusion can be deduced from the plasmon-peak shifts. It is known that the plasmon peak of amorphous GaAs is lower by 0.3 eV than that of crystalline GaAs.[28] In Fig. 5, the plasmon energy for the GaAs sputter cleaned at an incident angle of 30° is approximately 15.3 eV, for GaAs sputter cleaned at 7° is approximately 15.4 eV, and for URDIW-cleaned GaAs is approximately 15.7 eV. This result also indicates that the amorphous surface layer of the shallow-sputter-cleaned specimen is thinner than the information depth for REELS in our measurements. We conclude that the REELS-TFA method is robust and rather insensitive to variations in the surface condition of the specimen because the method provides almost the same bulk ELF independently of the condition of the top surface layer (or layer altered by surface cleaning) if the probing depth of the REELS electrons is much larger than the thickness of the surface-altered layer. This conclusion is in contrast to other proposed methods based on REELS analysis[9,12] because they require a clean surface layer with the same composition as the bulk.

Optical constants and inelastic mean free paths

The real part $\mathrm{Re}\{-1/\varepsilon\}$ can be calculated from $\mathrm{Im}\{-1/\varepsilon\}$ by the KK transformation,[28] and from this, the real (ε_1) and imaginary part (ε_2) of the complex dielectric function can be determined. We can also obtain the OCs n (E) and k (E) from the following equations:

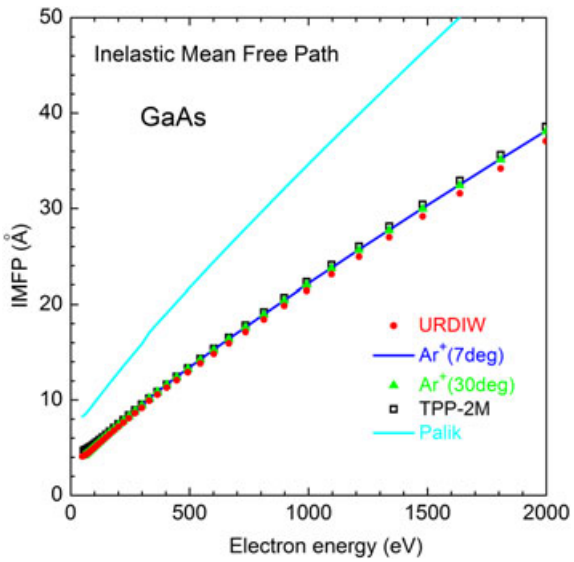

Figure 7. Electron inelastic mean free paths (IMFPs) for GaAs calculated from the ELFs in Fig. 5(b). TPP-2M represents the calculated IMFPs for GaAs with the TPP-2M predictive formula.[15] Note that the IMFP values for Ar^+ sputter cleaning at incident angles of 7° and 30° are practically identical and can hardly be distinguished in the plot. URDIW, ultrasonic running deionized water.

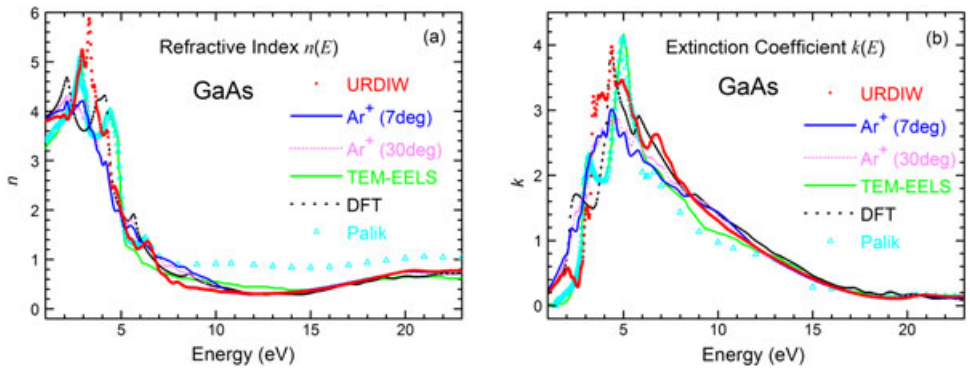

Figure 6. Optical constants for GaAs obtained from Fig. 5(b). (a) Refractive index $n(E)$; (b) extinction coefficient $k(E)$. URDIW, ultrasonic running deionized water; DFT, density function theory; TEM-EELS, electron energy loss measurements using transmission electron spectroscopy.

$$\varepsilon_1 = n^2(E) - k^2(E)$$
$$\varepsilon_2 = 2\, n(E)\, k(E) \quad (4)$$

where $n(E)$ is the refractive index and $k(E)$ is the extinction coefficient at energy E.

Figure 6 shows $n(E)$ and $k(E)$ determined for GaAs with the AR-REELS-TFA method (present work) together with other experimental (TEM-EELS data[35] and Palik's optical data[8]) and theoretical (DFT) values. The $k(E)$ values can be considered as fingerprints of individual electronic transitions. Strong resonant peaks in the $k(E)$ spectra are found at the energies for interband transitions from the valence band to the conduction band at about 4 and 6 eV as mentioned previously. The k (E) value obtained from the TFA for URDIW-cleaned GaAs is in good agreement with the DFT calculation result above 4 eV.

There is a small difference between the OCs at energies below 10 eV for GaAs specimens cleaned by ion sputtering and those cleaned by URDIW. This difference is due to the deviation of the ELFs at small energy losses in the 3–9 eV range as shown in Fig. 5(a). From Figs 5(b) and 6(a, b), we also see that Palik's optical data deviate considerably from the results obtained by other methods above 6 eV. This deviation must be due to technical difficulty in performing optical measurements in this energy region, even though a synchrotron radiation light source was used. In other words, we conclude that our AR-REELS-TFA method is effective in obtaining the ELFs and OCs of GaAs, especially for energies above 4 eV.

We calculated the electron IMFPs of GaAs from the resulting ELFs using the full Penn algorithm[3] in the 50–2000 eV energy region. Figure 7 shows the energy dependence of IMFPs calculated from the obtained ELFs for GaAs cleaned by Ar^+ sputtering and with URDIW cleaning. The IMFPs for GaAs calculated from Palik's optical data and Henke's atomic scattering factors[32] and from the TPP-2M predictive formulas[15] are also shown. This figure shows that all the IMFPs calculated from various ELFs for GaAs are in good agreement except for the IMFPs calculated from Palik's data.

Summary

We have previously demonstrated[14] that TFA of a series of AR-REELS can be used as a method for determining bulk energy-loss functions (ELFs), which by the TFA are separated from the surface-loss structures of REELS. In the present work, we have investigated the robustness of the method to the surface conditions of the sample. To this end, we measured AR-REELS for GaAs specimens at incident electron energies of 3000–4500 eV from samples cleaned by three different methods, which resulted in quite different compositions of the surface layer in the three samples. It was found that the TFA method produced two components that were identified as the bulk ELF and a surface term. The surface term was quite different for the three samples, whereas the bulk ELF was practically identical. This result shows that our method for determining the bulk ELF is largely unaffected by the condition of the outermost surface layers. We therefore conclude that this method is effective in determining the bulk ELF. Our method is expected to be particularly useful for analysis of dielectric properties of compounds and oxides for which it is difficult to produce a clean surface without destroying the structure and composition of the outermost few atomic layers. Previously suggested methods cannot be applied for these surfaces. In this work, we have used the method to determine ELFs and OCs of GaAs from a series of AR-REELS with TFA. The bulk ELFs obtained showed good agreement with results previously obtained with TEM-EELS measurements and DFT calculations. However, we found that Palik's optical ELF data for GaAs deviate considerably from our result above 6 eV. This result is probably due to difficulties in performing optical measurements in this higher energy region even though a synchrotron radiation light source was used. The OCs and IMFPs for GaAs were calculated from the bulk ELFs obtained by the TFA of REELS.

Acknowledgements

This research was supported by Strategic International Cooperative Program promoted by Japan Science and Technology Agency (JST) and partially supported by a Grant-in-Aid for Scientific Research (Proposal No.20510110) from the Japan Society for Promotion of Science (JSPS). Financial support from The Danish Research Council for independent Research – Natural Sciences is acknowledged.

References

[1] R. M. Martin, *Electronic Structure. Basic Theory and Practical Methods*, Cambridge University Press, New York, **2004**.
[2] Z. J. Ding, R. Shimizu, *Surf. Sci.* **1989**, *222*, 313.
[3] D. R. Penn, *Phys. Rev. B.* **1987**, *35*, 482.
[4] S. Tanuma, C. J. Powell, D. R. Penn, *Surf. Interface Anal.* **1988**, *11*, 577.
[5] S. Tanuma, C. J. Powell, D. R. Penn, *J. Appl. Phys.* **2008**, *103*, 063707.
[6] S. Tanuma, C. J. Powell, D. R. Penn, *Surf. Interface Anal.* **1991**, *17*, 927.
[7] S. Tanuma, C. J. Powell, D. R. Penn, *Surf. Interface Anal.* **2011**, *43*, 689.
[8] E. D. Palik, *Handbook of Optical Constants of Solids*, Academic Press, New York, **1985**.
[9] F. Yubero, J. M. Sanz, B. Ramskov, S. Tougaard, *Phys. Rev. B* **1996**, *53*, 9719.
[10] W. S. M. Werner, *Phys. Rev. B* **2006**, *74*, 075421.
[11] T. Nagatomi, S. Tanuma, *Anal. Sci.* **2010**, *26*, 165.
[12] S. Hajati, O. Romanyuk, J. Zemek, S. Tougaard, *Phys. Rev. B.* **2008**, *77*, 155403.
[13] D. Tahir, E. K. Lee, E. H. Choi, S. K. Oh, H. J. Kang, S. Heo, J. G. Chung, J. C. Lee, S. Tougaard, *J. Phys. D: Appl. Phys.* **2010**, *43*, 255301.
[14] H. Jin, H. Shinotsuka, H. Yoshikawa, H. Iwai, S. Tanuma, S. Tougaard, *J. Appl. Phys.* **2010**, *107*, 083709.
[15] S. Tanuma, C. J. Powell, D. R. Penn, *Surf. Interface Anal.* **1994**, *21*, 165.
[16] Y. Hirota, Y. Homma, K. Sugii, *Appl. Phys. Lett.* **1991**, *58*, 2794.
[17] Y. Hirota, Y. Homma, K. Sugii, *Appl. Phys. Lett.* **1991**, *59*, 3410.
[18] Y. Hirota, *J. Appl. Phys.* **1994**, *75*, 1798.
[19] F. Yubero, S. Tougaard, *Surf. Interface Anal.* **1992**, *19*, 269.
[20] H. Jin, H. Yoshikawa, H. Iwai, S. Tanuma, *e-J. Surf. Sci. Nanotech.* **2009**, *7*, 199.
[21] H. Jin, H. Yoshikawa, H. Iwai, S. Tanuma, S. Tougaard, *J. Surf. Anal.* **2009**, *15*, 321.
[22] S. Tougaard, I. Chorkendorff, *Phys. Rev. B.* **1987**, *35*, 6570; information on the QUASES-XS-REELS software can be found at www.Quases.com.
[23] H. Jin, H. Yoshikawa, S. Tanuma, S. Tougaard, *Surf. Interface Anal.* **2010**, *42*, 1076.
[24] M. Krawczyk, A. Jablonski, S. Tougaard, J. Toth, D. Varga, G. Gergely, *Surf. Sci.* **1998**, *402–404*, 491.
[25] H. Luth, G. J. Russell, *Surf. Sci.* **1974**, *45*, 329.
[26] L. Xu, Y. Ma, Y. Zhang, B. Chen, Z. Wu, Z. Jiang, W. Huang, *J. Phys. Chem. C* **2010**, *114*, 17023.
[27] S. Tougaard, J. Kraaer, *Phys. Rev. B.* **1991**, *43*, 1651.
[28] R. F. Egerton, *Electron Energy-Loss Spectroscopy in the Electron Microscopy* (2nd edn), Plenum, New York, **1996**.
[29] R. Ludeke, L. Esaki, *Phys. Rev. Lett.* **1974**, *33*, 653.
[30] E. R. Malinowski, *Factor Analysis in Chemistry* (3rd edn), John Wiley and Sons, New York, **2002**.
[31] D. Briggs, J. T. Grant (Eds.), *Surface Analysis by Auger and X-ray Photoelectrons Spectroscopy*, IM Publications, West Sussex, **2003**, p. 238.
[32] B. L. Henke, E. M. Gullikson, J. C. Davis, *Atom. Data Nucl. Data Tables.* **1993**, *54*, 181.
[33] S. Tanuma, C. J. Powell, D. R. Penn, J. Electron *Spectrosc. Relat. Phenom.* **1993**, *62*, 95.
[34] Y. F. Chen, C. M. Kwei, C. J. Tung, *Phys. Rev. B.* **1993**, *48*, 4373.
[35] C. V. Festenberg, *Z. Physik.* **1969**, *227*, 453.
[36] P. Blaha, K. Schwarz, G. K. H. Madsen, D. Kvasnicka, J. Luitz, *An Augmented Plane Wave Plus Local Orbital Program for Calculating Crystal Properties*,Techn. University Wien, TU Vienna, **2001**.

AIP | Applied Physics Letters

Visualization of hybridization states with atomic resolution using electron energy loss spectroscopy mapping

M. Haruta, K. Kurashima, T. Nagai, H. Komatsu, Y. Shimakawa et al.

Citation: Appl. Phys. Lett. **100**, 163107 (2012); doi: 10.1063/1.4704558
View online: http://dx.doi.org/10.1063/1.4704558
View Table of Contents: http://apl.aip.org/resource/1/APPLAB/v100/i16
Published by the American Institute of Physics.

Visualization of hybridization states with atomic resolution using electron energy loss spectroscopy mapping

M. Haruta,[1] K. Kurashima,[1] T. Nagai,[1] H. Komatsu,[2] Y. Shimakawa,[2] H. Kurata,[2] and K. Kimoto[1]
[1]*National Institute for Materials Science, 1-1 Namiki, Tsukuba, Ibaraki 305-0044, Japan*
[2]*Institute for Chemical Research, Kyoto University, Uji, Kyoto 611-0011, Japan*

(Received 4 January 2012; accepted 3 April 2012; published online 17 April 2012)

Hybridization state mapping with atomic resolution was demonstrated using electron energy loss spectroscopy combined with scanning transmission electron microscopy. The O 2*p* states hybridized with Sn 5*s* and Cu 3*d* in a layered double perovskite La_2CuSnO_6 were individually distinguished by significant contrast differences in the oxygen K-edge energy-loss near-edge structure. The anisotropic oxygen intensity in the distorted CuO_6 octahedron resulting from the Jahn-Teller effect could also be observed. The localized Cu 3*d* hole in the *bc* plane was indirectly imaged in real space using two-dimensional oxygen mapping. © *2012 American Institute of Physics*. [http://dx.doi.org/10.1063/1.4704558]

Transition metal oxides exhibit a variety of physical properties sensitively related to their crystal structures and constituent elements. These properties depend on the energy balances between the Coulomb interactions, bandwidth, exchange interaction, and many other parameters. In particular, the O 2*p* state can strongly hybridize with the cation orbital due to its covalent character and therefore plays an important role in determining the physical properties. A good understanding of the bonding character of oxygen ions at the atomic level in turn provides useful information for material design.

Electron energy loss spectroscopy (EELS) combined with scanning transmission electron microscopy (STEM) is a powerful tool for the investigation of local electronic structure with atomic column resolution.[1,2] Two-dimensional spectrum imaging (SI), in particular, allows us to provide not only elemental mapping[3,4] but also the prospect of bonding maps[5–7] at atomic-column resolution. However, there exists a physical limit on the spatial resolution of the EELS signal due to delocalization of inelastic scattering, which depends on the energy loss value[8,9] and also depends sensitively on the ability to localize the electron probe propagation in the sample.[10] In particular, the delocalization of oxygen K-edge spectra is not so much small as the distance between neighboring oxygen columns. Therefore, the core excitation energy-loss near-edge structure (ELNES) acquired by aligning a fine electron probe along one atomic column has contributions from adjacent columns in addition to the illuminated atomic column weighted according to their relative contributions. Consequently, accurate interpretation of the experimental ELNES spectra using point analysis is complicated due to delocalization. If a fine electron probe were obtained through spherical aberration correction, it would be possible to mainly excite an individual atomic column. Hence, it is expected that two-dimensional oxygen mapping of ELNES would show variation in excitation probability of specific electronic state with position. Mizoguchi *et al.*[11] and Witte *et al.*[12] performed simulations indicating that the O K-ELNES signal would depend on the distribution of the electron probe in the materials and discussed the interactions between the momentum transfer vector and the bond orientation. The pre-peak of the O K-ELNES in the high-temperature cuprate superconductor has been correlated to a local hole concentration arising due to covalent interactions of O 2*p* with the Cu 3*d* state,[13] which shows an anisotropic nature.[11,14]

In the previous work,[15] we have studied the local electronic structure of a transition metal oxide based on point analyses using STEM-EELS. Herein, we describe the two-dimensional distribution of the electronic structure using SI. In particular, we obtain a visualization of the hybridization state with atomic resolution in a double perovskite La_2CuSnO_6 using oxygen K-edge ELNES, revealing the anisotropic oxygen intensity in the distorted CuO_6 octahedron caused by the Jahn-Teller effect. The localized Cu 3*d* hole in the *bc* plane could be indirectly imaged in real space by two-dimensional mapping of the oxygen K-edge ELNES.

As the sample, a layered double perovskite La_2CuSnO_6 film was fabricated using a pulsed laser deposition technique.[16] The La_2CuSnO_6 thin films were grown heteroepitaxially on $SrTiO_3$ (001) substrates. The growth temperature was 670 °C at an oxygen partial pressure of 0.1 Torr, which were previously found to be optimized conditions for fabricating the layered structure.

Figure 1 shows a schematic of the layered crystal structure determined by powder x-ray diffraction analysis.[17] An interesting structural feature is the distortion of the CuO_6 octahedrons by the Jahn–Teller effect of Cu^{2+}. Alternation of the CuO_6 and SnO_6 octahedral layers and buckling of the CuO_2 and SnO_2 sheets induce a monoclinic superstructure with the following lattice parameters: $a = 0.8510$, $b = 0.7815$, $c = 0.7817$ nm, and $\beta = 91.151°$, corresponding closely to $2a_p \times 2a_p \times 2a_p$ (a_p is the lattice parameter for a primitive cubic perovskite). Although there are eight nonequivalent oxygen sites with different atomic coordinates in one unit cell, the nonequivalent oxygen sites can be classified into three groups (O1, O2, and O3) in relation to the nearest-neighbor B site atoms, that is: the O1 atoms binding only to a Sn atom, the O3 atoms binding only to a Cu atom, and the O2 atoms linking both Sn and Cu atoms as shown in Fig. 1.

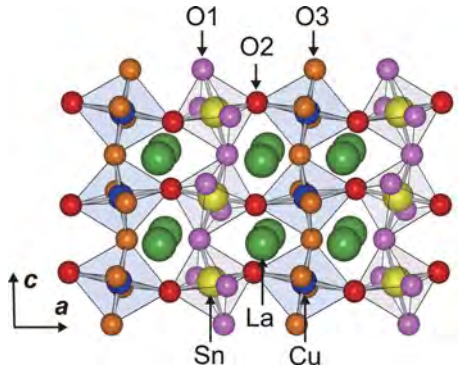

FIG. 1. A layered perovskite structure model of La_2CuSnO_6 along a *b* axis projection.

Cross-sectional samples were thinned down to electron transparency by ion milling. The thickness of the observed area was about 30 nm as estimated by EELS measurements. The high-angle annular dark-field (HAADF) imaging and the SI experiments were carried out using a FEI Titan[3] fitted with an aberration corrector for the probe-forming lens system and an electron energy loss spectrometer (Gatan, Inc., GIF Quantum 966). The SI experiments were performed at 80 keV to improve the limit of the delocalization effect and beam damage.[8,18] The calculated delocalization factor of the O K-edge (532 eV), using the simple formula $0.5\lambda/\theta_E^{3/4}$, where λ is the electron wavelength and θ_E is the characteristic inelastic scattering angle, is approximately 0.15 nm. La_2CuSnO_6 was observed along the *b*-axis projection because of high localization of the electron probe propagation. In this projection, each oxygen column was aligned straight, whereas that one is not arrayed straight in the *c*-axis projection. The convergence semi-angle was 30.5 mrad and the probe current was 130 pA. The inner and outer semi-angles of the HAADF detector were 90 and 200 mrad, respectively. The collection semi-angle in the EELS was 90 mrad. The energy spread of a Schottky emitter was 0.9 eV at full width at half maximum. The SI experiments were performed with a dwell time of 0.1 s/pixel for a 79 × 36 pixel area (2844 spectra) which corresponded to 2.7 × 1.3 nm^2. The specimen drift during the SI experiments was measured and corrected. The total acquisition time including the drift correction was 6 min 50 s. SI datum was processed by principal component analysis (PCA) software (HREM Research Inc., MSA) to reduce the random noise components,[19] in which seven principal components were used for reconstruction of SI datum after the PCA decomposition. All oxygen mappings were obtained by standard integrated signal using the different energy windows after background subtraction based on power-law model. First-principles band structure calculations were performed by a full-potential linear augmented plane wave plus local orbital method using the WIEN2K code.[20] ELNES spectra were calculated using the TELNES.2 package incorporated in the WIEN2K code.[21] The effect of a core hole was taken into account in the calculations by introducing a hole in the oxygen 1*s* state at each nonequivalent oxygen site and by adding an electron to the valence band.

Figure 2(a) shows the experimental O K-ELNES spectrum acquired from the SI analyzed whole area after background subtraction based on the SI datum of La_2CuSnO_6.

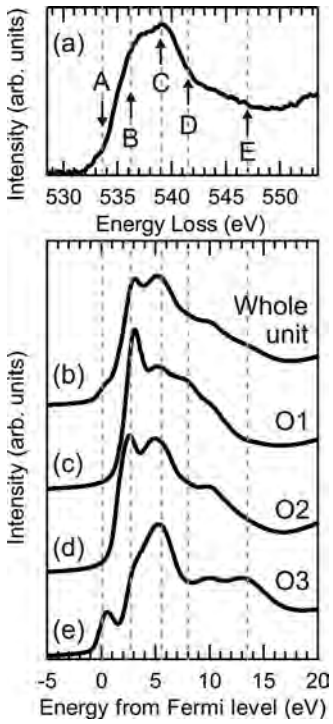

FIG. 2. (a) The experimental O K-ELNES spectrum acquired from the SI analyzed whole area after background subtraction using a power-law model acquired from the SI datum of La_2CuSnO_6. The calculated spectra with the O 1*s* core-hole state over (b) the whole unit cell, and at the (c) O1, (d) O2, and (e) O3 sites. The calculated spectra were averaged by weighting according to the number of sites contained in the unit cell.

Although this spectrum from whole area includes the contributions of all nonequivalent O sites, the individual spectrum in the SI datum has different contributions reflecting the local electronic structure. The simulated ELNES spectra including the core-hole effect is shown in Figs. 2(b)–2(e). The simulated ELNES averaged over the whole unit (Fig. 2(b)) agrees well with the experimental spectrum (Fig. 2(a)). Figures 2(c)–2(e) show three kinds of simulated spectra, which are averaged assuming the above classification of eight nonequivalent oxygen sites as described in Ref. 15. By comparing the spectral features with the partial density of states (PDOSs), the peaks labeled A-E can be attributed to transitions to the unoccupied O 2*p* state hybridized mainly with Cu 3*d*, Sn 5*s*, La 5*d*, Sn 5*p*, and Cu 4*s*/4*p* states, respectively. In the previous research,[15] it was concluded that only the O3 K-ELNES exhibits the pre-peak A, which is attributed to a transition to the unoccupied O 2*p* state hybridized with a Cu 3*d* b_{1g} ($dx^2 - y^2$) hole due to the Jahn-Teller effect.

Figure 3 shows the atomic resolution oxygen mapping discriminated based on differences in the hybridization states, and the simultaneously recorded HAADF-STEM image along the *b*-axis projection. The O mapping consisted of wide energy window (50 eV) from the threshold energy (Fig. 3(b)) shows the slight octahedral rotations of the O sublattice with comparable contrasts for all oxygen sites. In comparison, Figs. 3(c)–3(g) show O mappings constituted of the narrow energy window (1 eV), which are discriminated by differences in the hybridization states using peaks A-E as shown in Fig. 2. These images clearly show different contrasts, reflecting the excitation probability of the particular

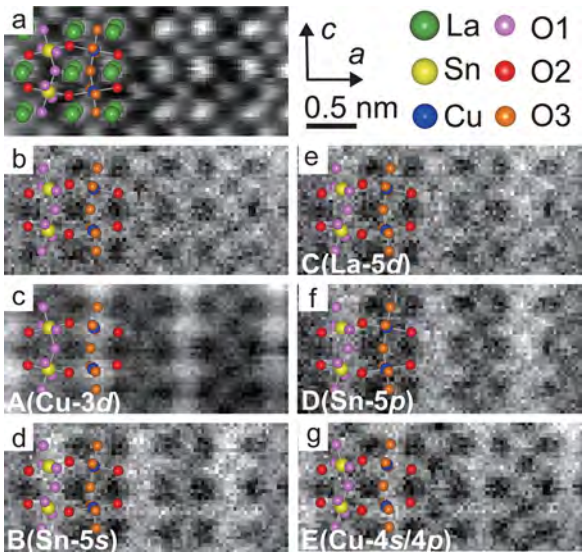

FIG. 3. (a) HAADF-STEM image of the SI analyzed area. (b) Atomic resolution oxygen mapping covering the 50 eV energy window from the threshold energy. Oxygen mappings discriminated in contrast by differences in hybridization states, mainly with (c) Cu 3*d*, (d) Sn 5*s* and (e) La 5*d*, (f) Sn 5*p* and (g) Cu 4*s*/4*p* states corresponding to peaks A to E in Fig. 2, using the 1 eV energy window. The images were carried out in auto contrast levels.

peak at a specific position. These five energy window were selected as observable points of the differences in hybridization states according to above classifications. It should be noted that oxygen atoms hybridized with Cu 3*d* and Sn 5*s* were distinguished by significant differences in contrast (Figs. 3(c) and 3(d)), whereas all oxygen columns show almost comparable contrast in the oxygen mapping using peak C (Fig. 3(e)), which is attributed to hybridization mainly with La 5*d*. For the image obtained using peak D (Fig. 3(f)), corresponding mainly to hybridization with the Sn 5*p* state, a bright contrast identifying the SnO_6 octahedron is observed, while the image obtained using peak E (Fig. 3(g)) shows an increase in the contrast at CuO_6 octahedral sites. The changes of contrast as main hybridization state in oxygen mapping agree well with the correlative relationship between the PDOS and its energy range.

Although Figs 3(c)–3(g) reflect each hybridization state, the oxygen sites that are considered not to hybridize with Cu or Sn still show substantial intensities in the bonding map. Two reasons can be given for this phenomenon related to the following physical limits: those imposed by the nature of the electron scattering and those from the electron energy band structure. In terms of the first effect, the nature of electron scattering means there is a combination of an absorption effect from thermal diffuse scattering (TDS) of the heavier atoms,[22,23] delocalization of inelastic scattering, and electron de-channeling process.[24] It is considered that the latter two factors produce additional intensity depending on probe position because of variety of eight kinds of O K-ELNES.[15] Note that all positions in the present SI datum exhibit an O K-edge signal due to the delocalization effect, even at the La sites. Of course, the intensity of the signal depends on the electron probe position. Hence, the two-dimensional elemental mapping probes the site-dependent subtle differences of the oxygen signal. O columns including heavier B site cations (Cu or Sn) yield a much more significant TDS effect than O-only columns and consequently the EELS signal on the B-site columns is reduced. As shown in Fig. 3(b), a volcano-like structure was observed in the present experiments, which was particularly noticeable on the Sn-O columns in comparison to the Cu-O columns due to the larger atomic number. For the same reason, because the La columns yield the largest TDS, the La sites appear with the darkest contrast in the O mapping, although the O K-edge signal is still apparent for the La sites. In terms of the second effect, the nature of electron energy band structure means the overlapping PDOS between cations in the present energy range. This is because the unoccupied PDOSs of the cations except for Cu 3*d* state are not energetically localized. This effect is particularly conspicuous in the energy range over peak C. Therefore, the present classifications were consistently labeled as main hybridization sate.

Remarkably, the anisotropic mapping of the distorted CuO_6 octahedron caused by the Jahn-Teller effect was observed as significant contrast differences using the pre-peak A (Fig. 3(c)). In other words, the O2 and O3 atomic columns in the CuO_6 octahedron exhibit different contrasts, with the O3 column appearing brighter than the O2 column. In case of the pre-peak mapping, the contributions from O1 and O2 due to the delocalization and electron de-channeling process have no influence, because there is no pre-peak (oxygen signal) in the spectra from O1 and O2 atoms (Fig. 2). In a layered La_2CuSnO_6, the distortion of the CuO_6 octahedron from cubic symmetry due to the Jahn-Teller effect leads to the further crystal field splitting of the t_{2g} and e_g states. In previous research, it was concluded that pre-peak A could be attributed to the hybridization with the unoccupied Cu 3*d* b_{1g} $(dx^2 - y^2)$ state, and that the electron configuration of the ground state should be $(a_{1g})^2(b_{1g})^1$.[15] The b_{1g} orbital in the Cu atom extends only into the *bc* plane. Therefore, the present experimental results demonstrate that an individual localized Cu 3*d* hole in the *bc* plane could be indirectly observed as a hybridization state in real space using oxygen mapping.

In summary, we have visualized oxygen hybridization states with cation orbitals with atomic resolution using the oxygen K-ELNES of a layered double perovskite La_2CuSnO_6. Because the O K-ELNES contains considerable information related to the cation orbital due to its covalent character, the two-dimensional oxygen mapping using STEM-ELNES allows us to investigate not only an elemental distribution but also chemical bonding and the anisotropy of empty states in the cation orbital. SI experiments combined with point analysis with high signal-to-noise ratio can overcome the physical limits arising from delocalization and allow the origins of particular peaks to be determined at atomic resolution as differences in excitation probability. These experimental results indicate the potential for a greater understanding of the anisotropic locations of electron holes in advanced materials, e.g., high-temperature cuprate superconductors at the atomic level.

This work was partly supported by JSPS Fellowships No. 23-51 from the Ministry of Education, Culture, Sports, Science and Technology, Japan. We acknowledge Mr. N. Kawasaki and Dr. Y. Otsuka of TRC for preparing the cross-section samples.

[1]D. A. Muller, T. Sorsch, S. Moccio, F. H. Baumann, K. Evans-Lutterodt, and G. Timp, Nature (London) **399**, 758 (1999).
[2]M. Varela, S. D. Findlay, A. R. Lupini, H. M. Christen, A. Y. Borisevich, N. Dellby, O. L. Krivanek, P. D. Nellist, M. P. Oxley, L. J. Allen, and S. J. Pennycook, Phys. Rev. Lett. **92**, 095502 (2004).
[3]M. Bosman, V. J. Keast, J. L. Garcia-Munoz, A. J. D'Alfonso, S. D. Findlay, and L. J. Allen, Phys. Rev. Lett. **99**, 086102 (2007).
[4]K. Kimoto, T. Asaka, T. Nagai, M. Saito, Y. Matsui, and K. Ishizuka, Nature (London) **450**, 702 (2007).
[5]D. A. Muller, L. F. Kourkoutis, M. Murfitt, J. H. Song, H. Y. Hwang, J. Silcox, N. Dellby, and O. L. Krivanek, Science **319**, 1073 (2008).
[6]L. F. Kourkoutis, in *Proceedings of 17th IMC* (2010), p. 354.
[7]H. Tan, S. Turner, E. Yucelen, J. Verbeeck, and G. V. Tendeloo, Phys. Rev. Lett. **107**, 107602 (2011).
[8]R. F. Egerton, *Electron Energy-Loss Spectroscopy in the Electoron Microscope*, 2nd ed. (Plenum Press, New York, 1996).
[9]D. A. Muller and J. Silcox, Ultramicroscopy **59**, 195 (1995).
[10]K. Kimoto, K. Ishizuka, and Y. Matsui, Micron **39**, 257 (2008).
[11]T. Mizoguchi, J. P. Buban, K. Matsunaga, T. Yamamoto, and Y. Ikuhara, Ultramicroscopy **106**, 92 (2006).
[12]C. Witte, S. D. Findlay, M. P. Oxley, J. J. Rehr, and L. J. Allen, Phys. Rev. B **80**, 184108 (2009).
[13]V. P. Dravid and H. Zhang, Physica C **200**, 349 (1992).
[14]P. E. Batson and M. F. Chisholm, Phys. Rev. B **37**, 635 (1988).
[15]M. Haruta, H. Kurata, H. Komatsu, Y. Shimakawa, and S. Isoda, Phys. Rev. B **80**, 165123 (2009).
[16]A. Masuno, M. Haruta, M. Azuma, H. Kurata, S. Isoda, M. Takano, and Y. Shimakawa, Appl. Phys. Lett. **89**, 211913 (2006).
[17]M. T. Anderson and K. R. Poeppelmeier, Chem. Mater. **3**, 476 (1991).
[18]O. L. Krivanek, N. Dellby, M. F. Murfitt, M. F. Chisholm, T. J. Pennycook, K. Suenaga, and V. Nicolosi, Ultramicroscopy **110**, 935 (2010).
[19]M. Bosman, M. Watanabe, D. T. L. Alexander, and V. J. Keast, Ultramicroscopy **106**, 1024 (2006).
[20]P. Blaha, K. Schwarz, G. K. H. Madsen, D. Kvasnicka, and J. Luitz, *WIEN2k, An Augmented Plane Wave + Local Orbitals Program for Calculating Crystal Properties*, (Vienna University of Technology, Vienna, Austria, 2002).
[21]C. Hébert, J. Luitz, and P. Schattschneider, Micron **34**, 219 (2003).
[22]M. P. Oxley, M. Varela, T. J. Pennycook, K. van Benthem, S. D. Findlay, A. J. D'Alfonso, L. J. Allen, and S. J. Pennycook, Phys. Rev. B **76**, 064303 (2007).
[23]A. J. D'Alfonso, S. D. Findlay, M. P. Oxley, and L. J. Allen, Ultramicroscopy **108**, 677 (2008).
[24]M. Haruta, H. Kurata, H. Komatsu, Y. Shimakawa, and S. Isoda, Ultramicroscopy **109**, 361 (2009).

Spiral-Spin-Driven Ferroelectricity in a Multiferroic Delafossite $AgFeO_2$

Noriki Terada,[1,2,3] Dmitry D. Khalyavin,[2] Pascal Manuel,[2] Yoshihiro Tsujimoto,[1] Kevin Knight,[2] Paolo G. Radaelli,[3] Hiroyuki S. Suzuki,[1] and Hideaki Kitazawa[1]

[1]*National Institute for Materials Science, Sengen 1-2-1, Tsukuba, Ibaraki 305-0047, Japan*
[2]*ISIS Facility, STFC Rutherford Appleton Laboratory, Chilton, Didcot, Oxfordshire, OX11 0QX, United Kingdom*
[3]*Department of Physics, Clarendon Laboratory, University of Oxford, Parks Road, Oxford OX1 3PU, United Kingdom*

(Received 11 June 2012; published 27 August 2012)

We have performed dielectric measurements and neutron diffraction experiments on the delafossite $AgFeO_2$. A ferroelectric polarization $P \simeq 300\ \mu C/m^2$ was observed in a powder sample, below 9 K. The neutron diffraction experiment demonstrated successive magnetostructural phase transitions at $T_{N1} = 15$ K and $T_{N2} = 9$ K. The magnetic structure for 9 K $\leq T \leq$ 15 K is a spin-density wave with a temperature dependent incommensurate modulation $\boldsymbol{k} = (-1, q, \frac{1}{2})$, $q \simeq 0.384$. Below 9 K, the magnetic structure turns into elliptical cycloid with the incommensurate propagation vector $\boldsymbol{k} = (-\frac{1}{2}, q, \frac{1}{2})$, $q \simeq 0.2026$ Based on the deduced magnetic point-group symmetry $m1'$ of the low-temperature polar phase, we conclude that the ferroelectric polarization in $AgFeO_2$ is perpendicular to the monoclinic b axis and is driven by the inverse Dzyaloshinskii-Moriya effect with two orthogonal components $\boldsymbol{p}_1 \propto \boldsymbol{r}_{ij} \times (\boldsymbol{S}_i \times \boldsymbol{S}_j)$ and $\boldsymbol{p}_2 \propto \boldsymbol{S}_i \times \boldsymbol{S}_j$.

DOI: 10.1103/PhysRevLett.109.097203 PACS numbers: 75.80.+q, 75.50.Ee, 77.80.−e

In recent years, magnetoelectric multiferroic materials, which possess (anti)ferromagnetism and ferroelectricity in a single phase, have been the subject of intensive research [1,2]. In such systems, complex magnetic structures stabilized by frustrated exchange interactions between spins break inversion symmetry and induce a ferroelectric polarization. Typical examples of the materials where noncollinear spin ordering induces ferroelectric polarization are $TbMnO_3$ (Refs. [3,4]) and $CoCr_2O_4$ (Ref. [5]) with cycloidal magnetic structures. The induced ferroelectric polarization can be understood in terms of the inverse Dzyaloshinskii-Moriya (DM) effect [6] or spin current mechanism, represented by $\boldsymbol{p} \propto \boldsymbol{r}_{ij} \times (\boldsymbol{S}_i \times \boldsymbol{S}_j)$ (Ref. [7]) where $\boldsymbol{r}_{ij}$ is the vector connecting the nearest spins. On the other hand, the delafossite family, $CuFeO_2$ (Ref. [8]), $CuFe_{1-x}B_xO_2$ [B = Al and Ga (Refs. [9–11])], $CuCrO_2$ (Refs. [12,13]), and $AgCrO_2$ (Ref. [12]), shows ferroelectric polarization induced by the proper screw helical magnetic orderings $\boldsymbol{r}_{ij} || \boldsymbol{S}_i \times \boldsymbol{S}_j$ [14,15]. The magnetic field-induced ferroelectricity in $CuFeO_2$ has been explained by Arima as a combined effect of d-p hybridization and spin-orbit coupling [16].

To further understand the delafossite multiferroic materials, we have studied the magnetodielectric properties of $AgFeO_2$. While $CuFeO_2$ has been extensively investigated as a frustrated magnet [17–19] and a multiferroic material [8–11,14], $AgFeO_2$ has not been studied due to lack of a high-quality sample. Nevertheless, Tsujimoto *et al.*. have recently succeeded in the synthesis under high pressure [20]. Although neutron diffraction measurements were reported recently, no details of the magnetic structure were presented [21].

The crystal structure of $AgFeO_2$, which is shown in Fig. 1(a), belongs to rhombohedral space group $R\bar{3}m$, and has the lattice constants, $a = b = 3.0391(1)$ Å and $c = 18.5899(9)$ Å at room temperature. For later convenience, the monoclinic unit cell stable at low temperature is also depicted in Fig. 1(a). The triangular layers formed by magnetic Fe^{3+} ions (surrounded with distorted oxygen octahedra) are stacked in a rhombohedral sequence and in-between nonmagnetic Ag^{1+} cations are incorporated separating the magnetic layers.

Vasiliev *et al.* [21] and Tsujimoto *et al.* [20] have reported the temperature dependence of the magnetic susceptibility revealing successive phase transitions at ~15 K (T_{N1}) and ~9 K (T_{N2}) [Fig. 2(a)]. In the present study, in order to investigate the microscopic spin structures and dielectric properties of $AgFeO_2$, we have performed neutron diffraction experiments and dielectric measurements using high-quality polycrystalline samples.

Powder specimens of delafossite $AgFeO_2$ were prepared under high pressure as described in Ref. [20]. The electric polarization and dielectric constant were measured using 1.25 mm thickness hardened pellet of polycrystalline $AgFeO_2$ sample covered with an area 19.6 mm^2 of silver paste. The electric polarization was determined by conventional pyroelectric current measurements using a Keithley 6517E electrometer. For the dielectric measurements, we used an Agilent E4980A LCR meter. The neutron powder diffraction measurements were carried out on WISH [22] and HRPD [23] time-of-flight diffractometers at ISIS Facility, United Kingdom. Crystal and magnetic structure refinements were performed using the FULLPROF program [24]. We first refined the data measured on HRPD to get precisely the crystal structure parameters; subsequently,

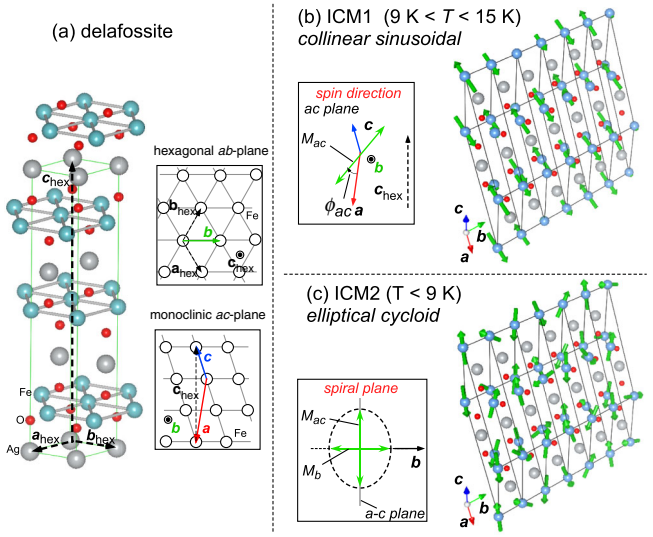

FIG. 1 (color online). (a) The delafossite crystal structure of $AgFeO_2$ with both hexagonal and monoclinic bases. (b) Collinear sinusoidally modulated magnetic structure in ICM1 phase for 9 K $\leq T \leq$ 15 K. (c) Cycloidal structure with elliptical modulation in ICM2 phase for $T \leq 9$ K. The insets are schematic pictures to explain the relationship between these spin directions and crystal axis.

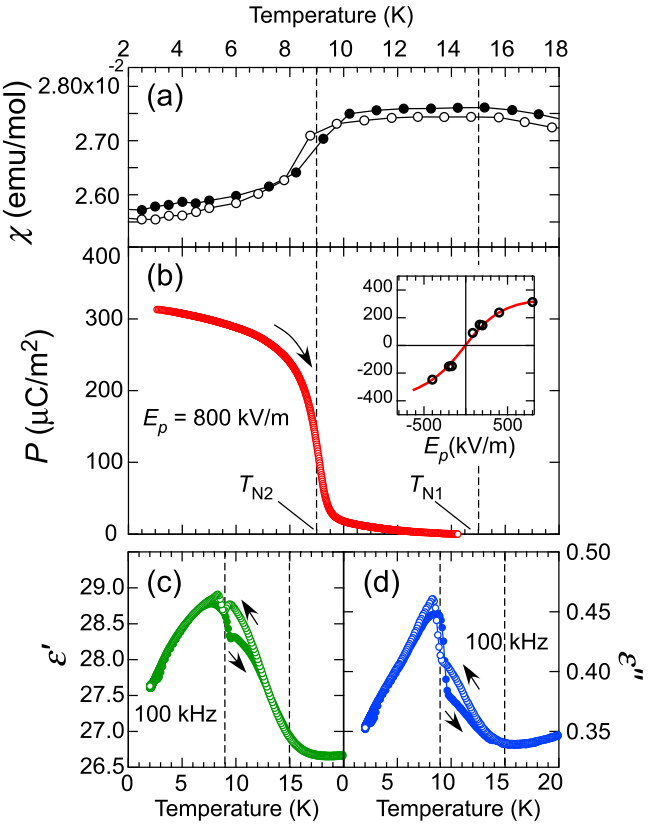

FIG. 2 (color online). (a) Magnetic susceptibility (data taken from Ref. [20]), (b) electric polarization, (c) real and (d) imaginary parts of the dielectric constant of a powder sample of $AgFeO_2$ as a function of temperature. The inset in (b) is the poling electric field dependence of the polarization.

the data measured on WISH were refined to determine the magnetic ordering while the structural parameters were fixed to the values obtained from the HRPD data.

As shown in Fig. 2(b), the electric polarization P appears only below the lower phase transition temperature $T_{N2} = 9$ K. The absolute value of P is 313 $\mu C/m^2$ in the poling electric field, $E_p = 800$ kV/m, which is close to the saturation value [see the inset of Fig. 2(b)]. Since a powder sample was used in the measurements, P is a half of the intrinsic value for a single crystal, namely $P_{\text{intrinsic}} \simeq 600$ $\mu C/m^2$, which is comparable to that of the typical multiferroics [1,8]. The temperature dependence of the real part of the dielectric constant, shown in Fig. 2(c), demonstrates a clear anomaly at T_{N2}, in agreement with the pyroelectric measurements. The imaginary part of the dielectric constant [Fig. 2(d)] corresponding to the energy dissipation, increases with decreasing temperature below $T_{N1} = 15$ K, then exhibits a peak at $T_{N2} = 9$ K, and eventually decreases gradually below 9 K. The relatively large energy dissipation might be caused by the finite correlation lengths in both magnetic phases, which is discussed below.

Based on the HRPD and WISH backscattering data revealing a clear splitting of some nuclear peaks below T_{N1}, a symmetry lowering from the rhombohedral $R\bar{3}m$ down to monoclinic $C2/m$ can be concluded. In addition, a set of magnetic Bragg reflections appears below this temperature (Fig. 3), which can be indexed by the incommensurate propagation vector $\boldsymbol{k} = (-1, q, \frac{1}{2})$ with $q \simeq 0.384$, referring to the monoclinic cell shown in Fig. 1(a). The wave number q depends on temperature and cooling or heating process, as shown in the inset of Figs. 3 and 4(b). Note that the $\boldsymbol{k}$ in the monoclinic setting corresponds to the $(q', q', \frac{3}{2})$ with $q' \simeq 0.192$ in the hexagonal cell, which is almost identical to that found in the partially disordered state of $CuFeO_2$ [25]. The width of the magnetic peaks in the ICM1 phase is slightly wider than the instrumental resolution width depicted by the horizontal bar in the inset of Fig. 3. As shown in Fig. 4(c), the correlation length is about 200–600 Å (65–200 sites), and significantly depends on temperature.

Below $T_{N2} = 9$ K (ICM2 phase), a set of new magnetic reflections indexed by the propagation vector $\boldsymbol{k} = (-\frac{1}{2}, q, \frac{1}{2})$ with $q \simeq 0.206$ appears [Figs. 3 and 4(a)]. At $T = 9$ K, the reflections from both ICM1 and ICM2 phases coexist upon heating or cooling processes, indicating a first order phase transition. The propagation vector in the ICM2 phase also slightly depends on temperature, and does not lock in any commensurate value even at the lowest measured temperature 5 K [Fig. 4(b)]. As shown in Fig. 4(c), the correlation length remains finite ~500 Å (~ 165 sites) at the lowest temperature, as evidenced by the peak width, which is wider than the resolution limit (inset of Fig. 3).

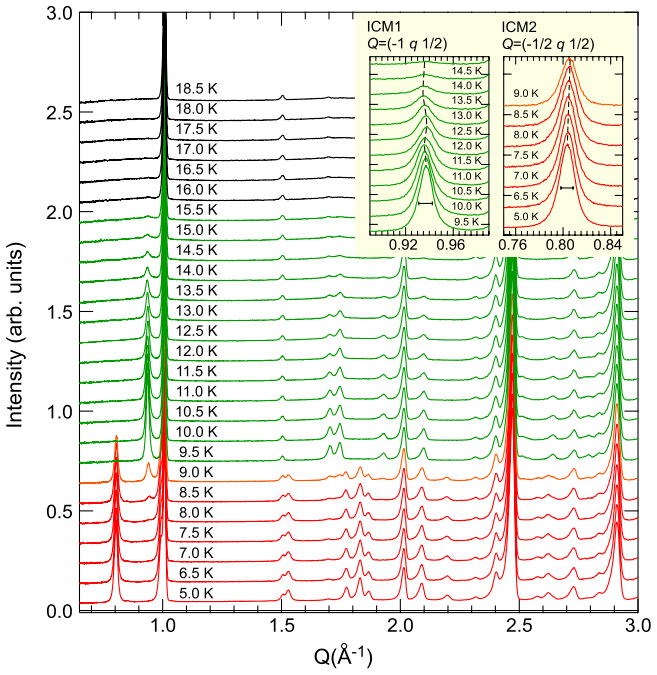

FIG. 3 (color online). Temperature dependence of the neutron powder diffraction profiles of $AgFeO_2$. The inset shows the expansions of profiles in low-Q regions in ICM1 and ICM2 phase. The data were taken on heating process on WISH. The horizontal bars denote the experimental resolution at each position.

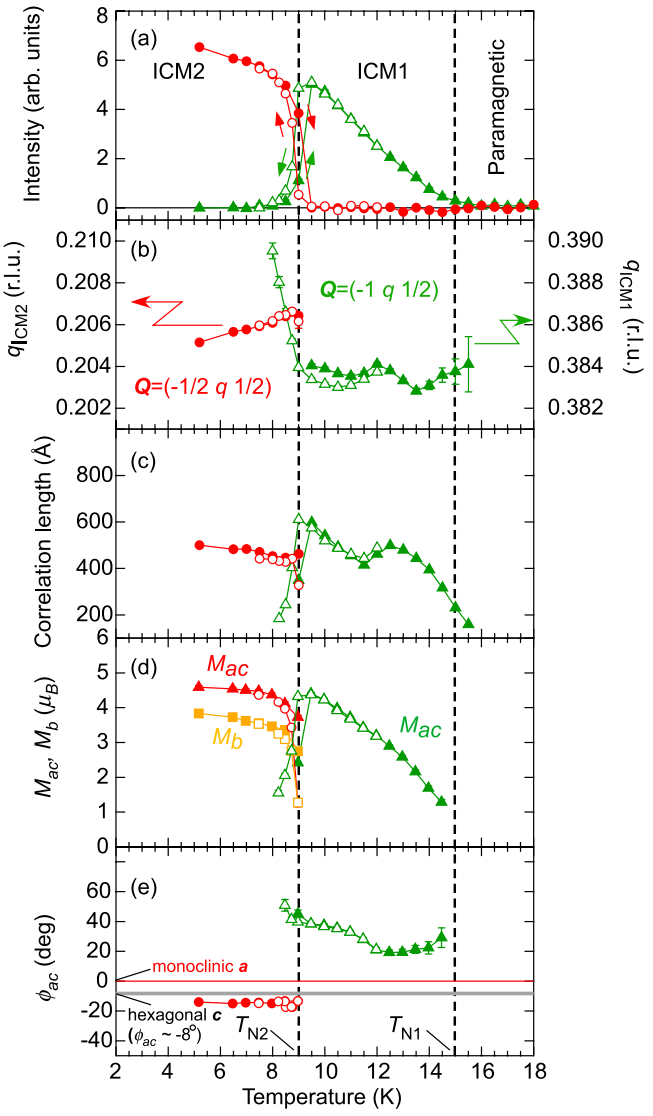

FIG. 4 (color online). Temperature dependence of (a) the integrated intensity of the magnetic Bragg reflections, (b) the propagation wave numbers, (c) the correlation lengths for $(-1, q, \frac{1}{2})$ and $(-\frac{1}{2}, q, \frac{1}{2})$. Temperature dependence of (d) the magnetic momentum components, M_{ac} and M_b, and (e) the angle between the spin direction projected into ac plane and the crystal a axis ϕ_{ac}. Closed and open symbols denote data measured with heating and cooling processes, respectively.

For the ICM1 phase with $\boldsymbol{k} = (-1, q, \frac{1}{2})$, we successfully refined the diffraction data using the monoclinic $C2/m$ space group for the nuclear scattering and the collinear sinusoidally modulated spin structure [Fig. 1(b)] for the magnetic scattering. The quality of the refinement is demonstrated in Fig. 5(a). The symmetry of the magnetic phase preserves the structural point group and contains time inversion as a separate element due to the incommensurate nature of the spin ordering. Thus, the magnetic point group in the ICM1 phases is the centro-symmetric $2/m1'$ in agreement with the lack of the polarization in the dielectric measurements (Fig. 2). The tilt angle of the spin-density plane from the a axis toward the c axis ϕ_{ac} depends significantly on temperature, $20^\circ \leq \phi_{ac} \leq 50^\circ$, as illustrated in Fig. 4(e). These spin directions are considerably different from $\phi'_{ac} \simeq 10^\circ$ in $CuFeO_2$ [26], implying that A-site cation (Cu^{1+} or Ag^{1+}) plays an important role in determining the magnetic anisotropy in these systems, as suggested in a recent x-ray absorption spectroscopy study [27].

For the ICM2 phase with $\boldsymbol{k} = (-\frac{1}{2}, q, \frac{1}{2})$, the magnetic contribution to the diffraction data [Fig. 5(b)] can be refined in the model with the noncollinear cycloidal spin arrangement [Fig. 1(c)]. The cycloid is elliptically modulated with the spin components in the ac plane and along the b axis being $M_{ac} = 4.56(4)\mu_B$ and $M_b = 3.81(5)\mu_B$, respectively, at $T = 5$ K. The angle between the elliptical axis (perpendicular to b) and a axis in the ac plane is $\phi_{ac} = -14.6(8)^\circ$, which is very close to the c direction of the hexagonal cell [see thick solid line in Fig. 4(e)]. The cycloidal magnetic ordering breaks the inversion symmetry but preserves the mirror plane perpendicular to the b axis. Therefore, the magnetic point group in the ICM2 phase is the polar $m1'$, which is consistent with the polarization measurements (Fig. 2). The obtained results clearly demonstrate the difference in the magnetic ground stats of $AgFeO_2$ and $CuFeO_2$. The latter compound exhibits commensurate $\boldsymbol{k} = (-1, 1/2, 1/2)$ magnetic ordering with collinear $\uparrow\uparrow\downarrow\downarrow$ spin arrangement along hexagonal [110]

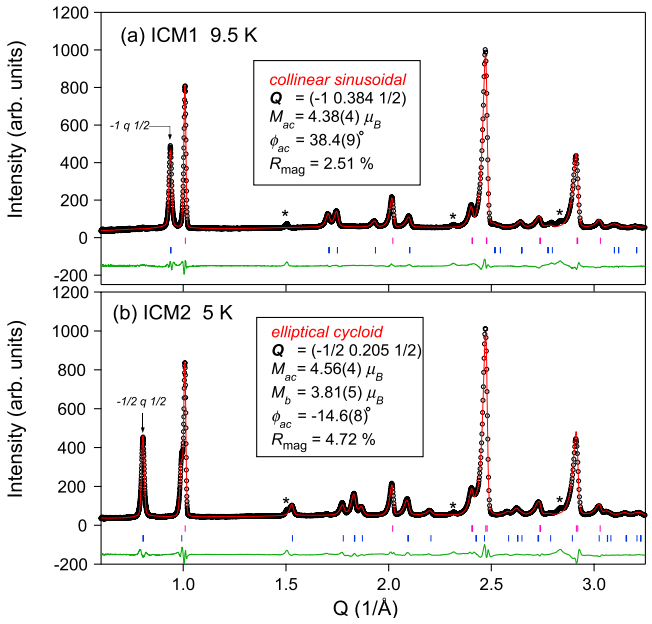

FIG. 5 (color online). Typical results of the magnetic structural refinement for the experimental data measured with WISH at (a) 9.5 and (b) 5 K. The vertical bars indicate magnetic and nuclear (upper row) Bragg peaks, and the stars indicate the reflection from a small amount impurity contained in the sample. The refined parameters and reliability factors are written in these insets.

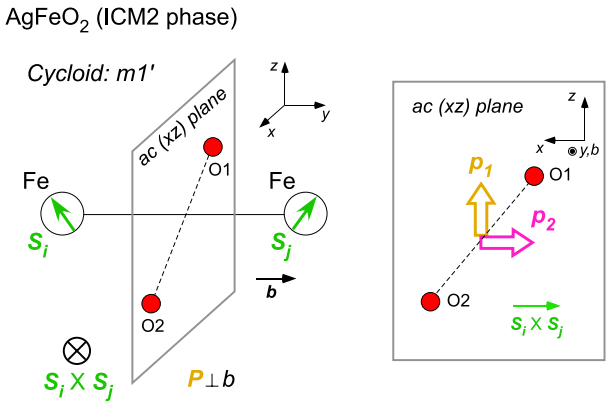

FIG. 6 (color online). (left) Illustration of two spins in the cycloidal structure with two oxygen atoms in $AgFeO_2$. (right) Directions of two possible electric dipole moments in the ac plane $\boldsymbol{p}_1 \propto \boldsymbol{r}_{ij} \times (\boldsymbol{S}_i \times \boldsymbol{S}_j)$ and $\boldsymbol{p}_2 \propto \boldsymbol{S}_i \times \boldsymbol{S}_j$. x, y, and z is (anti)parallel to $\boldsymbol{S}_i \times \boldsymbol{S}_j$, parallel to b, and perpendicular to them, respectively.

direction [28]. Thus, the nonmagnetic A-site cation plays a crucial role in the delafossite ferrites not only for the magnetic anisotropy but also for the exchange interactions.

Let us discuss the direction of $\boldsymbol{P}$ in the ICM2 phase based on the deduced magnetic point-group symmetry and recent theoretical works. The $m1'$ symmetry restricts the polarization direction to be parallel to the mirror plane ($\boldsymbol{P} \perp b$). Considering the well-known theory of inverse DM effect [6] or spin current mechanism [7], represented by $\boldsymbol{p} \propto \boldsymbol{r}_{ij} \times (\boldsymbol{S}_i \times \boldsymbol{S}_j) (\equiv \boldsymbol{p}_1)$, $\boldsymbol{P}$ is expected to be perpendicular to both $\boldsymbol{r}_{ij}$ and $\boldsymbol{S}_i \times \boldsymbol{S}_j$, i.e., along the z axis in Fig. 6 (this direction is very close to the hexagonal c axis). However, an additional contribution to the polarization $\boldsymbol{p}_2 \propto \boldsymbol{S}_i \times \boldsymbol{S}_j$ is also expected by symmetry since the mixed product $\boldsymbol{p}_2 \cdot \boldsymbol{S}_i \times \boldsymbol{S}_j$ is invariant under all symmetry operations of $C2/m1'$. Kaplan and Mahanti have shown that this additional term $\boldsymbol{p}_2$ contributes to macroscopic polarization in both cycloidal and proper screw helical cases unless mirror plane containing $\boldsymbol{r}_{ij}$ or twofold rotation axis perpendicular to $\boldsymbol{r}_{ij}$ exist [29]. Since $\boldsymbol{p}_2$ is perpendicular to $\boldsymbol{p}_1$ (see Fig. 6), the direction of the macroscopic polarization in $AgFeO_2$ should not be restricted by the well-known formula [2,6,7]. Although the mechanism causing the appearance of $\boldsymbol{P}$ is the inverse DM effect, its direction is given by the sum of the two components $\boldsymbol{p}_1 + \boldsymbol{p}_2$. It should be pointed out here that the $\boldsymbol{p}_2$ component parallel to $\boldsymbol{S}_i \times \boldsymbol{S}_j$ is also applicable for other delafossite compounds ABO_2 (A = Cu, Ag, B = Fe, Cr) where the spin ordering breaks the threefold and inversion symmetry [8–13]. Finally, we should mention that the calculations based on the spin-dependent d-p hybridization mechanism [16] also yield $\boldsymbol{P} \perp b$.

In conclusion, a ferroelectric polarization $P \simeq 300\ \mu\mathrm{C/m^2}$ was observed in a polycrystalline sample of delafossite $AgFeO_2$ below $T_{N2} = 9$ K. The appearance of the polarization is related to cycloidal spin ordering with the incommensurate propagation vector $\boldsymbol{k} = (-\frac{1}{2}, q, \frac{1}{2})$, with $q \simeq 0.206$, resulting in the polar magnetic point-group $m1'$. Above T_{N2}, the spins are ordered into spin-density wave with the modulation vector $\boldsymbol{k} = (-1, q, \frac{1}{2})$, with $q \simeq 0.384$ and nonpolar point-group symmetry $2/m1'$. The polar magnetic ground state of $AgFeO_2$ is drastically different from the nonpolar commensurate state of $CuFeO_2$, testifying the crucial role of the nonmagnetic A-site cation. The induced macroscopic polarization can be understood in terms of the inverse Dzyaloshinskii-Moriya effect with two orthogonal components $\boldsymbol{p}_1 \propto \boldsymbol{r}_{ij} \times (\boldsymbol{S}_i \times \boldsymbol{S}_j)$ and $\boldsymbol{p}_2 \propto \boldsymbol{S}_i \times \boldsymbol{S}_j$.

The authors wish to thank T. Nakajima for useful discussion and T. Yamaguchi for technical support in dielectric measurements. The images shown in Fig. 1 were depicted using the software VESTA [30] developed by K. Monma. This work is supported by an international collaboration research program, "Young Researcher Overseas Visits Program for Vitalizing Brain Circulation" of JSPS. N. T. is supported by the JSPS Postdoctoral Fellowships for Research Abroad.

[1] T. Kimura, T. Goto, H. Shintani, K. Ishizaka, T. Arima, and Y. Tokura, Nature (London) **426**, 55 (2003).
[2] S.-W. Cheong and M. Mostovoy, Nature Mater. **6**, 13 (2007).

[3] M. Kenzelmann, A. B. Harris, S. Jonas, C. Broholm, J. Schefer, S. B. Kim, C. L. Zhang, S.-W. Cheong, O. P. Vajk, and J. W. Lynn, Phys. Rev. Lett. **95**, 087206 (2005).
[4] T. Arima, A. Tokunaga, T. Goto, H. Kimura, Y. Noda, and Y. Tokura, Phys. Rev. Lett. **96**, 097202 (2006).
[5] Y. Yamasaki, S. Miyasaka, Y. Kaneko, J.-P. He, T. Arima, and Y. Tokura, Phys. Rev. Lett. **96**, 207204 (2006).
[6] I. A. Sergienko and E. Dagotto, Phys. Rev. B **73**, 094434 (2006).
[7] H. Katsura, N. Nagaosa, and A. V. Balatsky, Phys. Rev. Lett. **95**, 057205 (2005).
[8] T. Kimura, J. C. Lashley, and A. P. Ramirez, Phys. Rev. B **73**, 220401(R) (2006).
[9] S. Kanetsuki, S. Mitsuda, T. Nakajima, D. Anazawa, H. A. Katori, and K. Prokes, J. Phys. Condens. Matter **19**, 145244 (2007).
[10] S. Seki, Y. Yamasaki, Y. Shiomi, S. Iguchi, Y. Onose, and Y. Tokura, Phys. Rev. B **75**, 100403(R) (2007).
[11] N. Terada, T. Nakajima, S. Mitsuda, H. Kitazawa, K. Kaneko, and N. Metoki, Phys. Rev. B **78**, 014101 (2008).
[12] S. Seki, Y. Onose, and Y. Tokura, Phys. Rev. Lett. **101**, 067204 (2008).
[13] K. Kimura, H. Nakamura, K. Ohgushi, and T. Kimura, Phys. Rev. B **78**, 140401(R) (2008).
[14] T. Nakajima, S. Mitsuda, K. Takahashi, M. Yamano, K. Masuda, H. Yamazaki, K. Prokes, K. Kiefer, S. Gerischer, N. Terada, H. Kitazawa, M. Matsuda, K. Kakurai, H. Kimura, Y. Noda, M. Soda, M. Matsuura, and K. Hirota, Phys. Rev. B **79**, 214423 (2009).
[15] M. Soda, K. Kimura, T. Kimura, M. Matsuura, and K. Hirota, J. Phys. Soc. Jpn. **78**, 124703 (2009).
[16] T. Arima, J. Phys. Soc. Jpn. **76**, 073702 (2007).
[17] M. Mekata, N. Yaguchi, T. Takagi, T. Sugino, S. Mitsuda, H. Yoshizawa, N. Hosoito, and T. Shinjo, J. Phys. Soc. Jpn. **62**, 4474 (1993).
[18] S. Mitsuda, M. Mase, K. Prokes, H. Kitazawa, and H. A. Katori, J. Phys. Soc. Jpn. **69**, 3513 (2000).
[19] O. A. Petrenko, G. Balakrishnan, M. R. Lees, D. M. Paul, and A. Hoser, Phys. Rev. B **62**, 8983 (2000).
[20] Y. Tsujimoto *et al.* (unpublished).
[21] A. Vasiliev, O. Volkova, I. Presniakov, A. Baranov, G. Demazeau, J.-M. Broto, M. Millot, N. Leps, R. Klingeler, B. Büchner, M. B. Stone, and A. Zheludev, J. Phys. Condens. Matter **22**, 016007 (2010).
[22] L. C. Chapon, P. Manuel, P. G. Radaelli, C. Benson, L. Perrott, S. Ansell, N. J. Rhodes, D. Raspino, D. Duxbury, E. Spill, and J. Norris, Neutron News **22**, 22 (2011).
[23] R. M. Ibberson, W. I. F. David, and K. S. Knight, Rutherford Appleton Laboratory, Chilton, Didcot, England Report No. RAL-92-031, 1992.
[24] J. Rodriguez-Carvajal, Physica (Amsterdam) **192B**, 55 (1993).
[25] S. Mitsuda, N. Kasahara, T. Uno, and M. Mase, J. Phys. Soc. Jpn. **67**, 4026 (1998).
[26] N. Terada, T. Kawasaki, S. Mitsuda, H. Kimura, and Y. Noda, J. Phys. Soc. Jpn. **74**, 1561 (2005).
[27] M. Malvestuto, F. Bondino, E. Magnano, T. T. A. Lummen, P. H. M. van Loosdrecht, and F. Parmigiani, Phys. Rev. B **83**, 134422 (2011).
[28] F. Ye, Y. Ren, Q. Huang, J. A. Fernandez-Baca, P. Dai, J. W. Lynn, and T. Kimura, Phys. Rev. B **73**, 220404(R) (2006).
[29] T. A. Kaplan and S. D. Mahanti, Phys. Rev. B **83**, 174432 (2011).
[30] K. Momma and F. Izumi, J. Appl. Crystallogr. **41**, 653 (2008).

Soft Matter

Cite this: *Soft Matter*, 2012, **8**, 7351

www.rsc.org/softmatter

COMMUNICATION

Swelling in spin-coated methylcellulose ultra-thin films: effect on film structure, surface topography, and temperature-response property

Vallerie Ann Innis-Samson†[a] and Kenji Sakurai*[ab]

Received 8th March 2012, Accepted 10th May 2012
DOI: 10.1039/c2sm25544h

Methylcellulose (MC) thin films on a Si substrate, with a thickness of ~200 Å (near the radius of gyration R_g of the polymer), were exposed to a saturated water vapor condition to study the moisture absorption and swelling behavior *in situ* and the changes in the film surface topography, structure and temperature-response nature after such swelling. *In situ* visual observation of the MC thin films showed a color change with the swelling to as much as a factor of 5 from the original dry thickness. After removal of the film under saturated water vapor condition, X-ray reflectivity measurements revealed no change in the film thickness and surface/interface roughness of the film which means that the film is robust and retains its original film structure. Surface topography images by AFM showed roughening of the film texture due to water cavities on the film surface. The presence of cavities is indicative of the slow relaxation process of the polymer chains relative to the transport time of the water vapor molecules. Temperature-dependent contact angle measurements of the swelled films showed a loss in the hydrophilic-to-hydrophobic switching property of the MC film surface.

1. Introduction

The swelling characteristics of the methylcellulose (MC) polymer and several cellulose ethers have been much studied in the bulk solution case mainly due to their hydration properties and swelling of the polymer chains for use in drug delivery.[1–3] In the ultra-thin film case (sizes comparable to the radius of gyration, R_g, of the polymer), the film's swelling property has not been explored which can be of importance for future device applications of this thermoresponsive polymer such as thermal sensors and nanoswitches or even for nano-scale drug delivery systems.[4] Moisture absorption and the accompanying swelling are important for polymer thin film industries like microelectronics, adhesives and coatings as water absorption can lead to degradation of the dielectric properties, corrosion or delamination.[5,6] In the same way, moisture absorption and swelling can have detrimental effects on the temperature-response property which has not yet been studied in the ultra-thin film case even for other temperature-responsive polymers.

Equilibrium swelling in micron-thick methylcellulose hydrogels has been reported elsewhere.[7,8] However, such bulk polymer properties may be different from the equilibrium structural and dynamical behaviors of the polymer chains close to the substrate or at some interface as has been observed in the dependence of the glass transition temperature on the thickness,[9–13] rheological properties[14] or chain mobility close to the substrate[15,16] for other polymer systems.

In this work, we visually observed the swelling behavior of methylcellulose thin films, with a thickness close to the radius of gyration, R_g, of the polymer (~200 Å), in a saturated water vapor environment for 2 hours. By X-ray reflectivity (XRR) we were able to measure the change in film thickness and surface/interface roughness before and after removal of the film under the vapor environment. This is to determine whether the polymer thin film retained the water vapor molecules absorbed since methylcellulose is known to be hygroscopic. Atomic force microscopy (AFM) measurements showed the angstrom scale changes in the surface topography of the films after swelling. Our previous work showed that annealing at or above the glass transition temperature of the MC thin film contributed to a loss in the temperature-response mechanism (hydrophilic-to-hydrophobic switch) of the film surface.[17] We also studied whether swelling can have an effect on the hydrophilic-to-hydrophobic switching mechanism by measuring the temperature-dependent contact angle of the MC surface for the as-prepared and the swelled films.

To the best of our knowledge, this work is the first in reporting the swelling behavior of methylcellulose in ultra-thin film geometry and how the swelling would affect the thermo-responsive nature of the film.

2. Experimental

Analytical grade methylcellulose (MC) polymer powder (molecular weight: 40 000 g mol^{-1}) from Sigma-Aldrich was used without further purification. A 0.5% aqueous solution of the polymer was prepared *via* hot water dispersion and cold-water dissolution. 60–80 μl of the solution was pippetted onto pre-cleaned Si (1 0 0) substrates (size: 15 mm × 15 mm) and spin-coated at a final speed of 5000 rpm for 30 seconds. The Si substrates were cleaned by sequential ultrasonication for 5–10 minutes in soap solution, distilled water and acetone

[a] *University of Tsukuba, Tennodai 1-1-1, Tsukuba, Ibaraki, Japan. E-mail: sakurai@yuhgiri.nims.go.jp*
[b] *National Institute for Materials Science (NIMS), Sengen 1-2-1, Tsukuba, Ibaraki, Japan*
† Present address: National Institute for Materials Science (NIMS), Sengen 1-2-1, Tsukuba, Ibaraki, Japan.

followed by heated ultrasonication (55 °C) in 1–2% nitric acid solution for 30 minutes and then washed with ultra-pure distilled water. This procedure was repeated 2–3 times until the Si surface was sufficiently hydrophilic (water covers the entire surface with washing). After spin-coating, the films were dried in a vacuum oven (Shimadzu AS ONE AV0-250N with vacuum <1 torr) at 105 °C for 1 hour to remove excess solvent.

Swelling observation

The MC thin films were placed in a transparent container (11 cm × 8 cm × 3 cm) with enough water to set the environment at the saturated water vapor condition at a room temperature of 23 °C or a relative humidity (RH) of 100%. The film was put on a pedestal to avoid direct contact with liquid water which can dissolve the film entirely. Direct visual observation of the swelling phenomenon was recorded by an ordinary digital camera for 2 hours.

After observing the swelling, the thin films were taken out of the container to ambient atmosphere (RH ≈ 40–50% at room temperature of 23 °C) and AFM observation or X-ray reflectivity measurements were immediately done (no drying process, "naturally" or in an oven, was performed).

Atomic force microscopy

Atomic force microscopy (AFM) observations were made using a Shimadzu SPM9500-J3 scanning probe microscope. Topography images were obtained in the tapping mode at constant force using AC mode micro-cantilever tips (Olympus, Japan) with an average resonant frequency of 70 kHz and an average spring constant of 2 N m^{-1} according to the manufacturer's specifications. The images were analyzed using the built-in software of the Shimadzu AFM.

X-Ray reflectivity (XRR)

XRR measurements were performed using a home-built X-ray reflectometer with a $\theta - 2\theta$ geometry and Cu as the target. The incident X-ray energy used was Cu-Kα_1 monochromatic X-rays operated at 8.04 keV (λ = 1.54 Å). Data fitting for the specular reflectivity measurements was performed by the WMUREX software.[18] From the XRR results, the thickness, density and surface/interface roughness of the thin film can be determined.

Contact angle measurements

Static sessile drop contact angle measurements in air (ambient temperature: 25 °C), with water as a probe, on the MC surfaces were performed on a contact-angle set-up which consisted of: (i) a home-built Peltier-controlled heating stage which can vary the surface temperature at a precision of 0.01 °C; (ii) a Musashi Engineering's SMP digital plunger system to automatically dispense the test liquid onto the sample surface with high precision (±0.1 μl); and (iii) an ordinary web camera. A volume of 4 μl of the test liquid was deposited onto the surface for each measurement. With the Peltier-controlled heating stage, temperature-dependent contact angle measurements were done by heating up the samples to the desired temperature (from 20 °C to 75 °C) and then equilibrating at the desired temperature for 5 minutes for the sample surface to have the same temperature as the heating device and dropping the test liquid onto the heated sample surface. Four to five measurements per temperature were performed on different samples.

3. Results and discussion

Images of the swelling behavior of the MC thin film with a thickness of around 200 Å in saturated water vapor are shown in Fig. 1 with increasing time inside the container under the saturated vapor condition from $t = 0$ min, when the film is placed inside the container. The films we studied were only subjected to saturated water vapor for 2 hours as we suppose that such a time span is enough for the ultra-thin film to achieve equilibrium condition. The initial color of the film in ambient atmosphere is transparent brown. The color of the film changes to a deep dark brown, in this case at $t = 20$ min. The change in color is not instantaneous for such ultra-thin films and one possible reason is the saturation of the water vapor inside the container. When placing the film inside the container, the container is not readily in a saturated condition. However, it must be noted that the change in color is instantaneous for the relatively thicker films that we have studied with a thickness of ~600 Å. This means that the greatly confined geometry of the thinner polymer film hinders its ability to swell due to its strong interaction with the substrate. Confined geometry in this case is due to the film thickness being less than the radius of gyration (R_g) of the polymer. For the MC polymer that we used, the radius of gyration is ~240 Å. Due to such confined geometry, there is a significant contribution of the interfacial effect (strong polymer substrate interaction) to the film properties. The inability to swell which is related to the decrease in the diffusivity of the water molecules into the film is attributed to the coupling of the water mobility within the polymer film to the local chain motion, which has been found to be retarded in thin films.[19]

The change in color of the film during the swelling observation from transparent brown to deep brown after 20 minutes signifies a change in film thickness. From deep brown, the film will further thicken to a blue color. The film thickness of the swelled film was estimated from a prior film thickness measurement, by X-ray reflectivity, using as-prepared MC films fabricated at different spin-coating parameters which showed different film colors. These films are shown in Fig. 2. As shown in Fig. 2c, the dark brown colored film has a thickness of around 800 Å while the blue-colored film in Fig. 2d has a thickness of around 1100 Å. Thus, the dark brown color exhibited during swelling of the film in Fig. 1b–d means a thickness change to around 800 Å. The blue color exhibited, with continuous swelling, in Fig. 1e and f represents a thickness change to around 1000 Å. Therefore. we were able to estimate the film thickness change during the swelling observation from such previous experiments of MC films with different film colors. We tried to measure directly the film thickness change with white light interferometry as used by ref. 20 to characterize film thickening in polymer layers with swelling in a vapor environment. However, in our case the film is so thin (250 Å) that the optical path of the traveling light is not long enough to observe a sufficient number of spectrum extrema in the reflectance spectrum. Nevertheless, we would try other techniques in the future to obtain a more quantitative description of the film thickening.

When a dry polymer film is exposed to a solvent, the solvent molecules enter into the porous structure of the polymer and diffuse into the entire accessible volume. The solvent molecules are physically or chemically adsorbed on the surface as well as absorbed into the pores and the available free volume. In the case of MC, it is soluble in

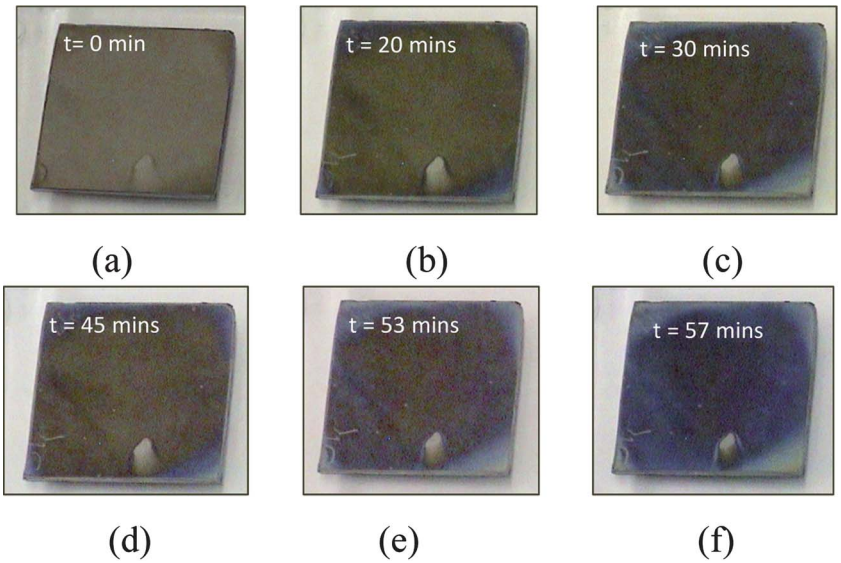

Fig. 1 Time-dependent visual observations of swelling in an MC thin film under a saturated water vapor condition showing the cyclic swelling and deswelling. (a) $t = 0$ min (transparent brown); (b) $t = 20$ min (dark brown); (c) $t = 30$ min (dark brown at the center, blue at the edges); (d) $t = 45$ min (dark brown); (e) $t = 53$ min (dark brown and blue); and (f) $t = 57$ min (dark blue). Initial film thickness is 200 Å, the deep brown color suggests that the film thickness is ~800 Å and the blue color ~1000 Å.

water and there is a strong attractive interaction between the polymer chains and water vapor molecules. This results in a net repulsive interaction between polymer segments and will lead to swelling of the polymer chains which gives rise to the film thickening that we can directly observe. S. Harms *et al.*[21] in a recent work with another temperature-responsive polymer system concluded that the thinner the polymer film, the stronger is the response to swelling; in their case as much as a factor of 6.5 thickening was observed. They attributed such a strong response to an increase in free volume as measured by positron annihilation lifetime spectroscopy (PALS). The increase in free volume observed with decrease in film thickness can be attributed to the additional degrees of freedom near the free surface[21] for ultra-thin films which allows the polymer chains to adapt a more open chain conformation as compared to the bulk. This is the reason why, in our case, we can observe a thickening of around a factor of 5 during swelling for the MC thin films.

The excess absorption of the water vapor molecules during swelling can lead to changes in the film structure (*e.g.* thickness) and its surface–interface morphology. Such changes might be retained in the film even after removal under the saturated water vapor condition. Methylcellulose is known to be hygroscopic and it can retain the water molecules absorbed inside its film structure (pores and free volume) and the diffusion of water vapor molecules in and out of the film can change the surface/interface roughness. Such changes to the MC film were determined after removal of the film under the saturated water vapor condition.

The XRR profile of the MC film was taken in ambient atmosphere after the films were removed under the saturated water vapor condition. Fig. 3a shows an insignificant change of the XRR profile of the film after swelling as compared to that before swelling. The thickness of the film, which is reflected in the period of the oscillation fringes, is the same for both conditions. The roughness of the film along the depth or rms roughness, as shown by the amplitude of the oscillations, also shows no significant change.

The parameters derived from data fitting of the XRR profile of Fig. 3a and two other samples, before and after swelling, are shown in Table 1. The surface and interface (polymer and substrate) roughness of the films after swelling showed very small changes (maximum of 2.5 Å) compared to the roughness values before swelling. The same is true for the thickness values. This means that even with the film swelling to a factor of 5 compared to its initial film thickness, the film retains its original structure and deswelling is complete when the film is removed from the saturated water vapor condition.

We have studied the relative expansion of MC thin films after swelling for 2 hours for different film thicknesses over a narrow thickness range (120–300 Å) to see whether water vapor molecule

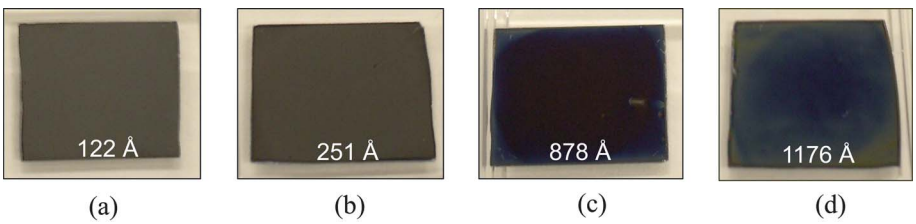

Fig. 2 As-prepared MC thin films fabricated with different film thicknesses showing the different colors of the film with increasing film thickness: (a) 122 Å; (b) 251 Å; (c) 878 Å and (d) 1176 Å.

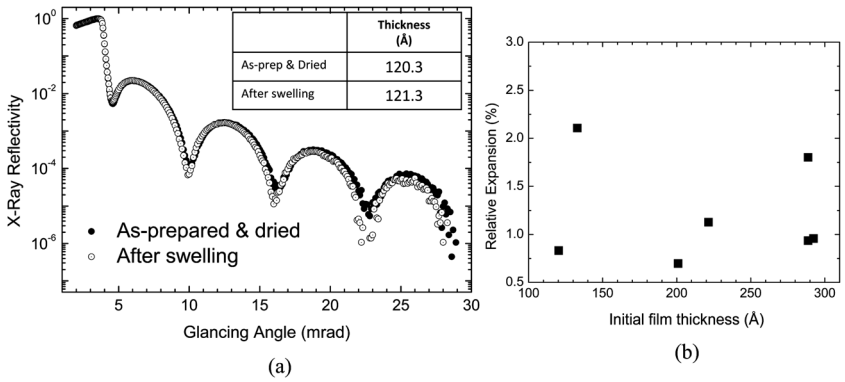

Fig. 3 (a) X-ray reflectivity profile of an MC film before swelling and after removal of the film under the saturated water vapor condition (measurements were done in ambient atmosphere). Film thickness (period of oscillation fringes) and the surface–interface roughness (amplitude of oscillations) reveal no significant change in the film structure after swelling in water vapor. (b) Relative expansion of MC films of various thickness after subjecting to saturated water vapor for 2 hours.

Table 1 Layer thickness d, surface roughness σ_{surf} and interface (polymer–Si substrate) roughness σ_{int} parameters from the XRR profiles of MC thin films before and after swelling for 2 hours

	Before swelling (as-prepared and dried)			After swelling		
Sample	d (Å)	σ_{surf} (Å)	σ_{int} (Å)	d (Å)	σ_{surf} (Å)	σ_{int} (Å)
1	120.3	2.9	5.6	121.3	2.9	3.9
2	221.5	5.5	6.9	224.0	5.2	6.9
3	288.7	3.8	7.2	291.4	5.0	4.7

retention in the film structure depends on the thickness. No thickness dependence was observed though as shown in Fig. 3b and the very low relative expansion observed can only be attributed to instrumental resolution or systematic errors.

Temperature-dependent contact angle measurements were made on as-prepared and swelled films after removal in the humid environment to determine how the hydrophobic switch property can change after swelling. As-prepared, *i.e.*, with no heat/swelling treatments, MC thin films show a characteristic hydrophilic-to-hydrophobic switching in the surface property when the test liquid water is dropped at film temperatures around the bulk lower critical solution temperature of ~70 °C as seen in Fig. 4. The change in surface property with heating in the presence of water is due to surface reconstruction of the functional moieties (–OH and $–CH_3$) to achieve an equilibrium state with the contact medium.[17] However, for the films swelled in water vapor, the surface became more hydrophobic at all temperatures (contact angle ≈ 80°) and the hydrophilic-to-hydrophobic switch has been lost after the films were taken out of the humid environment.

We have also observed such a loss in the hydrophobic switching with annealing of the MC film near the glass transition temperature.[17] Our explanation for these changes in the surface property with annealing is surface reorganization during annealing to lower the surface energy which leads to less polar surfaces. During the annealing process near the bulk T_g, the polymer molecules on the surface are free to move towards an energetically favorable configuration to minimize the polymer/air interfacial tension, that is the polar components buried in the bulk and the nonpolar components sticking out of the surface, creating a more hydrophobic conformation. In the case of the MC film inside the water vapor environment, surface reorganization would occur due to the attractive interaction force between water and the –OH moiety of the polymer,[22] with water being a good solvent for MC. This means that the surface would be populated with the –OH moiety making it more hydrophilic. We were not able to confirm this *in situ* because of the difficulty in measuring the contact angle while in the saturated water vapor environment box. But previous time-dependent contact angle measurements done in as-prepared films using liquid water showed a slowly decreasing contact angle (from 40° to 27°) on the MC surface due to such a solvation effect. Therefore, we expect that such a surface configuration change is possible under the water vapor environment.

However, upon removal of the polymer film in the saturated water vapor environment and then measuring the contact angle at temperatures below 70 °C, the surface was neither hydrophilic (its surface configuration in the humid environment), nor did it return to the as-prepared film surface configuration in air with a contact angle of around 40° at low temperatures. Instead the film became hydrophobic at all temperatures. In the as-prepared film, heat greater than 70 °C is required to switch to a hydrophobic state and normal

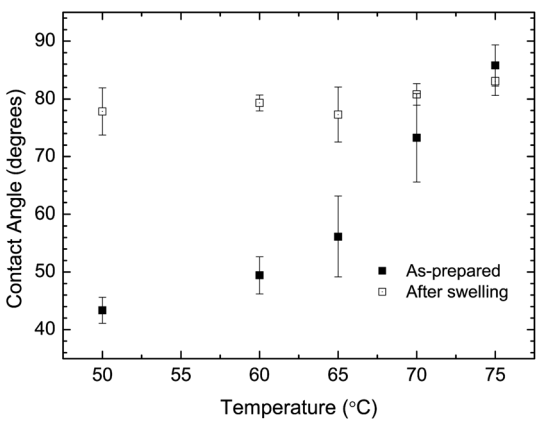

Fig. 4 Temperature-dependent contact angle measurements of MC films before and after removal of the film under the saturated water vapor condition.

exposure to air cannot result in a hydrophobic surface. Therefore, the hydrophobicity change after the swelling of the film might not be due to surface reorganization.

The possible reason for the increase in the contact angle of the swelled samples and the surface morphology and structural information were determined by AFM. XRR can only give information on the out-of-plane roughness indirectly. By AFM, we directly observed how the surface of the film changed after removal under the saturated vapor condition. The surface topography of the films was examined before and after the swelling as shown in Fig. 5. For the as-prepared MC films, the surface was almost flat with the rms roughness (out-of-plane roughness) of the film at ~3 Å as measured by AFM. After the swelling, the surface topography changed but the rms roughness was only ~5 Å. (Normal Si wafer rms roughness is between 3 Å and 5 Å.) Water droplet cavities can be observed in the swelled polymer film where water droplets condensed onto the polymer surface. With the water droplet cavities, the "texture" of the surface was significantly affected according to the Hurst parameter of the surfaces as measured by AFM. The Hurst parameter h is restricted to the range $0 < h \leq 1$ and defines the fractal box dimension $D = 3 - h$ of the surface/interface.[23] Small values of h correspond to extremely jagged surfaces while values close to unity appear to have "smooth" hills and valleys. The as-prepared film has $h = 0.96$ while the swelled film has $h = 0.64$. The presence of the water cavities is due to the slow relaxation or motion of the polymer chains to completely homogenize the penetrant's (water vapor) environment.[24] This leads the water vapor molecules to sit in holes or irregular cavities with very different intrinsic diffusional mobilities. The different texture of the surface introduced by the water cavities might be one of the reasons for the hydrophobic surface observed on the MC film at all temperatures. Further experiments by other techniques (*e.g.* XPCS and FTIR) need to be done, however, to understand more the surface state of the MC film as other parameters (*e.g.* chemical configuration of the polymer, conformational state of macromolecules, surface configuration, and energy level of surface-state electrons) can also influence such a loss in the hydrophobic switching property with temperature.

Subjecting therefore the MC surface to a high humidity environment can be destructive to its temperature-sensitive properties. On the other hand, this result also showed that by saturated water vapor swelling, the MC surface can be made more hydrophobic at all temperatures. This can be used to improve the hydrophobicity of the MC surface for packaging or coating applications.

4. Conclusion

We have studied the moisture absorption and swelling of spin-coated MC thin films on a Si substrate, with thickness near the radius of gyration of the polymer, and have observed that the "confined geometry" of the film leads to a non-instantaneous reaction of the film upon exposure to water vapor molecules. This can be due to decreased diffusivity of the water molecules inside the film and a stronger polymer–substrate interaction which hinders the swelling of the polymer chains. Even with the film swelling to as much as a factor of 5 from its original thickness *in situ*, there is no retention of the absorbed water molecules after removal of the film under the saturated vapor condition and the film retains its original film structure. Temperature-dependent contact angle measurements showed a loss in the hydrophobic switching property of the MC film, with the film becoming hydrophobic at all temperatures. Surface

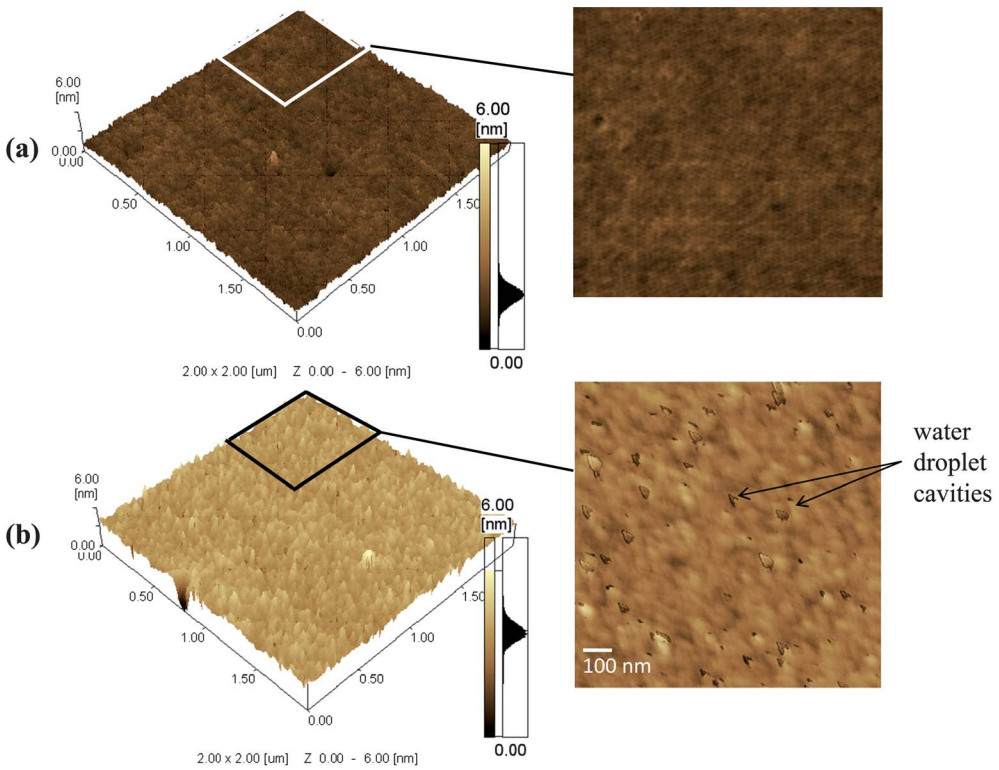

Fig. 5 3D view of the surface topography by AFM of: (a) as-prepared MC film and (b) MC film after 2 hours of swelling in water vapor. The inset of each image is an enlarged portion in the top view direction for the square area indicated.

topography images reveal the presence of water cavities in the film after annealing which leads to roughening of the film's texture. Thus, the change in surface property of the MC film after annealing can be attributed to changes in the surface morphology of the swelled films.

References

1 S. R. Parakh, A. V. Gothoskar and M. T. Karad, *Pharm. Technol.*, 2003, 40–48.
2 D. A. Alderman, *Int. J. Pharm. Technol. Prod. Manuf.*, 1984, **5**, 1–9.
3 Y. Lin, J. Sun, G. Jiang, J. Zan and F. Ding, *Chin. J. Chem. Eng.*, 2007, **15**(4), 566–572.
4 I. H. Kim, J. H. Park, I. W. Cheong and J. H. Kim, *J. Controlled Release*, 2003, **89**, 225–233.
5 B. D. Vogt, C. L. Soles, H.-J. Lee, E. K. Lin and W. Wu, *Langmuir*, 2004, **20**, 1453–1458.
6 L. Quercia, F. Loffredo, M. Bombace, I. Nasti and G. di Francia, *Sens. Actuators, B*, 2005, **111–112**, 166–170.
7 F. Debeaufort, A. Voilley and P. Meares, *J. Membr. Sci.*, 1994, **91**, 125–133.
8 N. Vasquez, R. Cruz, A. Castillo, A. M. Martinez and A. B. Cepeda, *Revisita Mexicana de Ingenieria Quimica*, 2007, **6**(3), 337–345.
9 W. J. Orts, J. H. van Zanten, W. L. Wu and S. K. Satija, *Phys. Rev. Lett.*, 1993, **71**, 867–870.
10 J. A. Forrest, K. Dalnoki-Veress, J. R. Stevens and J. R. Dutcher, *Phys. Rev. Lett.*, 1996, **77**, 2002–2005.
11 J. L. Keddie, R. A. L. Jones and R. A. Cory, *Faraday Discuss.*, 1994, **98**, 219.
12 W. E. Wallace, J. H. van Zanten and W. L. Wu, *Phys. Rev. E: Stat. Phys., Plasmas, Fluids, Relat. Interdiscip. Top.*, 1996, **52**, R3329–R3332.
13 M. Auobouy, *Phys. Rev. E: Stat. Phys., Plasmas, Fluids, Relat. Interdiscip. Top.*, 1997, **56**, 3370–3377.
14 H. W. Hu and S. Granick, *Science*, 1992, **258**, 1339–1342.
15 E. K. Lin, W. L. Wu and S. K. Satija, *Macromolecules*, 1997, **30**, 7224–7231.
16 E. K. Lin, R. Kolb, S. K. Satija and W. L. Wu, *Macromolecules*, 1999, **32**, 3753–3757.
17 V. A. I. Samson and K. Sakurai, *J. Phys.: Condens. Matter*, 2011, **23**(43), 435010.
18 (*a*) K. Sakurai and A. Iida, *Jpn. J. Appl. Phys.*, 1992, **31**, L113; (*b*) K. Sakurai and A. Iida, *Adv. X-Ray Anal.*, 1992, **35**, 813.
19 C. L. Soles, J. F. Douglas, W. L. Wu and R. M. Dimeo, *Macromolecules*, 2003, **36**(2), 373–379.
20 D. Goustouridis, K. Manoli, S. Chatzandroulis, M. Sanopoulou and I. Raptis, *Sens. Actuators, B*, 2005, **111–112**, 549–554.
21 S. Harms, K. Rätzke, F. Faupel, W. Egger, L. Ravello, A. Lachewsky, W. Wang and P. Müller-Buschbaum, *Macromol. Rapid Commun.*, 2010, **31**, 1364–1367.
22 T. Yasuda, T. Okuno, K. Tsuji and H. Yasuda, *Langmuir*, 1996, **12**, 1391–1394.
23 B. B. Mandelbrot, *The Fractal Geometry of Nature*, W.H. Freeman, New York, 1982.
24 H. L. Frisch, *Polym. Eng. Sci.*, 1980, **29**(1), 2–13.

Addition and correction

Note from RSC Publishing

This article was originally published with incorrect page numbers. This is the corrected, final version.

The Royal Society of Chemistry apologises for these errors and any consequent inconvenience to authors and readers.